Voluntary Driven, Velocity Controlled Tremor Suppression

by

Gil Herrnstadt

B.Sc., Technion – Israel Institute of Technology, 2006

Thesis Submitted in Partial Fulfillment of the
Requirements for the Degree of
Doctor of Philosophy

in the
School of Engineering Science
Faculty of Applied Science

SIMON FRASER UNIVERSITY
Spring 2018

Approval

Name:	**Gil Herrnstadt**
Degree:	**Doctor of Philosophy (Engineering Science)**
Title:	**Voluntary driven, velocity controlled tremor suppression**
Examining Committee:	**Chair:** Rodney Vaughan Professor
	Carlo Menon Senior Supervisor Professor
	Martin McKeown Supervisor Professor Department of Neurology, Faculty of Medicine University of British Columbia
	Edward Park Supervisor Professor
	Ryan D'Arcy Internal Examiner Professor
	Eduardo Rocon External Examiner Tenure Researcher Spanish National Research Council
Date Defended/Approved:	December 15, 2017

Ethics Statement

The author, whose name appears on the title page of this work, has obtained, for the research described in this work, either:

a. human research ethics approval from the Simon Fraser University Office of Research Ethics

or

b. advance approval of the animal care protocol from the University Animal Care Committee of Simon Fraser University

or has conducted the research

c. as a co-investigator, collaborator, or research assistant in a research project approved in advance.

A copy of the approval letter has been filed with the Theses Office of the University Library at the time of submission of this thesis or project.

The original application for approval and letter of approval are filed with the relevant offices. Inquiries may be directed to those authorities.

Simon Fraser University Library
Burnaby, British Columbia, Canada

Update Spring 2016

Abstract

The standard course of treatment for pathological tremor mainly involves pharmacotherapy. However, treatment can be challenging as individual responses to therapy vary widely. Individuals with a disabling or medication refractory tremor, may have the option for one of several surgical procedures. Essential Tremor (ET) and Parkinson's Disease (PD) are considered to be among the most pervasive of tremor related disorders. Overall pathological tremor prevalence statistics range from 2% to well over 10% in the elderly. Up to 60% of those affected by tremor experience disability in their Activities of Daily Living (ADL) and more than a quarter struggle to find relief through conventional treatments. There is, therefore, a persuasive case for alternative therapies for individuals with pathological tremor. This thesis proposes a tremor suppression approach to track the intentional motion. Typically tremor suppression methods estimate the tremor component and produce a counteracting signal. The suggested approach instead predicts the voluntary motion component via force information, while the tremor signal is regarded as a motion disturbance and consequently rejected. The approach is demonstrated in a modular form for flexibility in implementation. The suppression approach, involving an admittance and speed controlled feedbacks, was evaluated experimentally with a benchtop tremor simulation system. Parametric stability and controller tuning were demonstrated, and response time performance specifications were achieved. Spectral analysis results show a 99.8% tremor power reduction; the power reduction related to the voluntary movement was instead negligible (0.18%). A robotic orthosis was subsequently developed to validate the approach for the suppression of pathologic elbow tremor. Two types of robotically simulated human inputs were evaluated in addition to employing orthosis gravity compensation. Finally, nine participants with either ET or PD were recruited and performed computerized pursuit tracking tasks with the orthosis. The mean tremor power reduction was 94.4%; significantly higher than typically achieved with pharmacotherapy. Importantly, the effect to the voluntary motion was limited to only 6.6%. When mechanically suppressing tremor, there is a risk of preventing the individual with tremor from performing volitional movements. An important contribution of this work involves the explicit treatment of the impact to the volitional motion.

Keywords: tremor; movement disorders; orthosis; assistive robot; tremor suppression; robot control

Acknowledgements

I would like to express my gratitude to my senior supervisor, Carlo Menon, for his support and guidance throughout my PhD.

I would also like to thank the members of the MENRVA lab for their help and friendship. Their company certainly made the journey more enjoyable.

Finally, I would like to thank my spouse, Susanne Kim, for the unwavering support and for tolerating the long hours of work.

Table of Contents

Approval ii
Ethics Statement iii
Abstract iv
Acknowledgements v
Table of Contents vii
List of Tables x
List of Figures xi
List of Acronyms xiv

Chapter 1. Introduction 1
1.1. Motivation 1
1.2. Goal and Objectives 2
1.3. Outline of Thesis 2

Chapter 2. Physiological and Pathological Tremor 4
2.1. Etiology 4
2.2. Clinical Features and Statistics 8
2.3. Tremor Suppression Solutions 11
2.3.1. Research 11
2.3.2. Commercial Systems 15

Chapter 3. A Voluntary Driven Tremor Suppression Approach 16
3.1. Suppression Approach 16
3.1.1. Background 16
3.1.2. Voluntary-Driven Motion with Speed-Controlled Tremor Rejection 16
Fundamental Assumptions 17
3.1.3. Signal Filtering 18
3.1.4. Impedance and Admittance Control 19
Impedance control for Tremor Suppression 21
3.2. Suggested Data Processing and Outcomes 22
3.2.1. Spectral Analysis 22
3.2.2. Temporal Analysis 23
3.3. Suggested Implementation 23
3.3.1. Controller Scheme 23
3.3.2. Kalman Filter 26
Background 26
Model Implementation 28
3.3.3. Filter Comparison 29
3.4. Summary and Conclusion 30
3.5. Related Publications 31

Chapter 4. Tremor Suppression Approach Validation via a Hardware Simulator 32
4.1. Benchtop Validation System 32
4.1.1. Background 32
4.1.2. Validation Mechanism 32
4.2. Stability and Performance Analysis 34
4.2.1. Feedback Stability 34
Internal Feedback System 37
External Feedback System 38
4.2.2. Controller Tuning 39
4.2.3. Step Response 40
4.3. Experimental Results 41
4.4. Discussion 46
4.5. Limitations and Conclusion 50
4.6. Related Publications 51

Chapter 5. An Elbow Orthosis for Speed Controlled Voluntary Driven Tremor Suppression 52
5.1. Introduction 52
5.2. Orthosis System 53
5.3. Orthosis Control 54
5.4. Experimental Procedure 56
5.5. Experimental Results 58
5.5.1. Velocity Based 58
5.5.2. Torque Based 60
5.6. Discussion 67
5.7. Summary and Conclusion 70
5.8. Related Publications 71

Chapter 6. Following Elbow Volitional Movement With a Suppression Orthosis: Tests With Individuals With Pathological Tremor 72
6.1. Introduction 72
6.2. System Implementation 72
6.2.1. Suppression Approach and Elbow Orthoses 72
6.2.2. Changes Relative to Previous Controller Implementation 73
ABPF 75
6.3. Participant Selection and Experimental Protocol 77
6.3.1. Individuals with Tremor 77
6.3.2. Healthy Individuals 81
6.4. Data Processing and Expected Outcomes 82
6.4.1. Spectral Analysis 82
6.4.2. Temporal Analysis 83
6.4.3. Data Selection and Processing 85
6.5. Results 86
6.5.1. Tremor Motion Component 86
6.5.2. Voluntary Motion Component 88

6.5.3. Motion Errors of Healthy Individuals 94
6.6. Discussion 95
6.7. Summary and Conclusion 101
6.8. Related Publications 102

Chapter 7. Conclusion and Future Work 103
7.1. Summary and Conclusion 103
7.2. Thesis Scientific Contributions 105
7.2.1. Refereed Journal Papers 105
7.2.2. Refereed Conference Papers 105
7.2.3. Abstract Refereed Conference Papers 106
7.3. Other Scientific Contributions 106
7.3.1. Refereed Journal Papers 106
7.3.2. Refereed Conference Papers 106
7.3.3. Abstract Refereed Conference Papers 107
7.4. Future Work 107

References 110

List of Tables

Table 4.1 Simulation Systems Review 50
Table 5.1 Orthosis system specifications. 54
Table 6.1 ABPF comparison 76
Table 6.2 Participant Data 78
Table 6.3 Protocol Summary 80
Table 6.4 Healthy Participant Data 82
Table 6.5 Tremor Suppression (%) with TSO in Off Mode 88

List of Figures

Figure 2.1 Central nervous system connectivity [10] 5
Figure 2.2 Tremor activation conditions [4], [31] 9
Figure 2.3 Tremor classification based on syndrome, frequency and activation condition [4] 10
Figure 3.1 Suppression approach elements and flow. 17
Figure 3.2 General position-based impedance control diagram [115]. 20
Figure 3.3 General admittance control diagram. 21
Figure 3.4 Admittance control diagram. 24
Figure 3.5 Tremor suppression approach control diagram. The approach includes an inner speed control, a state feedback loop and an external PID force loop. 25
Figure 3.6 Plant with process and measurement noise. 26
Figure 3.7 Kalman filter and a low-pass filter comparison. 29
Figure 4.1 Tremor Simulation Device (TSD). The Driving Motor (DM) represents the human input, and the Suppressing Motor (SM) and the torque sensor represent the suppression system. 34
Figure 4.2 Detailed plant G(s) diagram (encircled in dotted line) describing a BLDC motor with a gearbox. The suppression system consists of the plant G(s) and a force sensor H(s). 35
Figure 4.3 Suppression system control diagram. The block diagram is similar to that of Figure 3.5 but organized to facilitate derivation of the TF from the human input to the velocity output. 36
Figure 4.4 Step response of the system in Figure 3.5. The blue dashed and red solid lines are the DM velocity input and TSD response respectively. The black line with circles is the TSD interaction force. The rise time and delay time are 200 and 220 ms respectively. The Settling time (within 8%) is 1.06 s. 41
Figure 4.5 Tremor data of person et05 [150] A) Linear acceleration data B) PSD C) Angular velocity and its zero-phase filtering. 42
Figure 4.6 Basic admittance control implementation. The TSD is controlled as in Figure 3.4. A) The input velocity produced by the DM when disengaged from the SM (blue dashed line) and output velocity of the TSD when engaged with the DM (red solid line). B) The measured interaction force (red solid line) and desired force (blue dashed line). 43
Figure 4.7 Tremor suppression approach implementation. The TSD is controlled as in Fig. 3 A) Suppression-off (blue solid line), its zero-phase filtering (black dashed line) and suppression-on velocity (red solid line). B) The interaction force (red solid line) and desired force (blue solid line) 45
Figure 4.8 PSD of the velocity signal. A clear difference can be observed between the suppression-off case (blue solid line) and the suppression-on case (red dashed line). 46

Figure 5.1 Orthosis system. A) The orthosis simulation system connected to the DM. P1 and P2 indicate the two passive wrist joints. B) The orthosis donned. 54
Figure 5.2 Orthosis control diagram. The controller includes a force feedback, with an inner speed controller and state feedback, as well as a gravity compensation loop. 56
Figure 5.3 ET patient data (et02). A) Linear acceleration. B) PSD. A first harmonic tremor frequency is observed at 4.3 Hz. 59
Figure 5.4 Velocity driven case suppression velocity and force tracking results. A) Velocity tracking B) Interaction force. 59
Figure 5.5 Velocity based input, PSD of suppression-on and -off cases. 60
Figure 5.6 PD patient (park05) data. A) Linear acceleration. B) PSD. A first harmonic tremor frequency is observed at 4.5 Hz. 61
Figure 5.7 Torque driven case suppression velocity and force tracking results. A) Velocity tracking B) Interaction force. 61
Figure 5.8 Phase response of open loop torque (red lines) and velocity (blue lines) driven motor. The marked black squares and the vertical dashed line indicate the 0.8 Hz frequency intersection with the phase lines. 66
Figure 5.9 Torque based input, PSD of suppression-on and -off cases. 67
Figure 6.1 (a) TSO components and TSO donned. (b) MO components and MO donned. 73
Figure 6.2 Control structure employed during testing with indivduals with tremor. 74
Figure 6.3 Adaptive Band Pass Filter Block Diagram [108]. 75
Figure 6.4 Computer interface and illustrative pursuit target profiles (a) Graphical interface as seen by the study participants on a computer screen. The outlined circle indicates the position of the target on the screen. The dashed blue arrow is added for illustration of the target (vertical) motion direction. The filled orange circle indicates the participant's elbow cursor position. (b) Example of a sinusoid (top) and a pseudo-random (bottom) target position profiles. Target position and Next random target indicate the current target position and the random target position goal. Target velocity indicates the current target velcity. The zero degree angle refers to the fully extended elbow position as well as to the cursors being located at the bottom of the graphical interface window. 80
Figure 6.5 Tremor motion related measures. (a) Tremor power change in *Tasks 1-2*. Square and plus markers indicate the values from Task 1 and Task 2 respectively. (b) Tremor power change in *Task 3*. (c) *Task 3* MO tremor fundamental frequency calculated based on PSD. The dotted horizontal lines in a-c indicate the participants' mean. The legend on the right refers to both b and c. The sine slow (ss), sine fast (sf), random slow (rs) and random fast (rf) motion cases are represented with outlined circle, filled circle, outlined diamond, and filled diamond shape markers, respectively. 87
Figure 6.6 Participant T06 sine target tasks (a) slow and (b) fast sinusoid target tasks. For both subfigures a and b, the subplots from top to bottom are position tracking (zero degree angle refers to a fully extended elbow

position), velocity tracking, interaction torque, and PSD. TSO and MO refer to the Tremor Suppression Orthosis and Measurement Orthosis; Target refers to the target profile; fMO is the zero phase LPF of the MO; Fm is the measured torque and Fe is the estimated torque. 89

Figure 6.7 Participant T06 pseudo-random target tasks. (a) slow and (b) fast pseudo-random target tasks. For both subfigures a and b, the subplots from top to bottom are position tracking (zero degree angle refers to a fully extended elbow position), velocity tracking, interaction torque, and PSD. Random target is the next random target position goal indicated by the solid green square wave line; TSO and MO refer to the Tremor Suppression Orthosis and Measurement Orthosis; Target refers to the target profile; fMO is the zero phase LPF of the MO; Fm is the measured torque and Fe is the estimated torque. 90

Figure 6.8 Task 3 voluntary motion related measures. (a) Voluntary component power change for the MO, i.e. $PCPMO_{v,PTarget_v}$ and the TSO, i.e. $PCPTSO_{v,PTarget_v}$. Zero value is indicated by the horizontal dashed line. (b) Voluntary position pursuit tracking RMSE for the fMO and the TSO. (c) Voluntary velocity pursuit tracking RMSE for the fMO and the TSO. (d) Voluntary interaction torque RMS recorded with the TSO. For plots a-d, the sine slow (ss), sine fast (sf), random slow (rs) and random fast (rf) motion profiles are represented with outlined circle, filled circle, outlined diamond and filled diamond shapes, respectively. 92

Figure 6.9 Tremor, Voluntary and TETRAS Relations. (a) Tremor power change (reduction) vs the voluntary components power change difference (between TSO and MO). Circle and cross marker shapes indicate negative and positive voluntary power change differences, respectively. (b) Tremor power change vs tremor severity (TETRAS) for the nine participants. (c) Voluntary power change difference vs position RMSE difference (TSO-fMO). (d) Voluntary power change difference vs velocity RMSE difference (TSO-fMO). 94

Figure 6.10 MO Voluntary motion related measures for healthy individuals. (a) Position pursuit tracking RMSE. (b) Velocity pursuit tracking RMSE. The dotted horizontal lines in a and b indicate the participants' mean. For plots a and b, the sine slow (ss), sine fast (sf), random slow (rs) and random fast (rf) motion profiles are represented with an outlined circle, a filled circle, an outlined diamond and a filled diamond shape respectively. 95

List of Acronyms

ABPF	Adaptive Band-Pass Filter
ADL	Activities of Daily Living
BLDC	Brushless DC
CNS	Central Nervous System
DBS	Deep Brain Stimulation
DC	Direct Current
DM	Driving Motor
DOF	Degrees Of Freedom
EMG	Electromyography
EOG	Electrooculography
ET	Essential Tremor
FES	Functional Electrical Stimulation
fMO	Zero-phase LPF Measurement Orthosis
KF	Kalman Filter
LPF	Low Pass Filter
MEG	Magnetoencephalography
MO	Measurement Orthosis
ODE	Ordinary Differential Equation
PD	Parkinson’s Disease
PI	Proportional-Integral
PID	Proportional-Integral-Derivative
PR	Power Reduction
PSD	Power Spectral Density
RMS	Root Mean Square
RMSE	Root Mean Square Error
ROM	Range of Motion
rTMS	repetitive Transcranial Magnetic Stimulation
SD	Standard Deviation
SFU	Simon Fraser University
SM	Suppression Motor
SNR	Signal to Noise Ratio
TACS	Transcranial Alternating Current Stimulation

tDCS	transcranial Direct Current Stimulation
TETRAS	The Essential Tremor Rating Assessment Scale
TF	Transfer Function
TSD	Tremor Simulation Device
TSO	Tremor Suppression Orthosis
UPDRS	Unified Parkinson's Disease Rating Scale
WFLC	Weighted-frequency Fourier Linear Combiner

Chapter 1. Introduction

Pathological tremor in humans is a widely recognized phenomenon. Many people may be familiar with the condition through well-known personalities (e.g. Michael Jay Fox, Muhammad Ali and Katharine Hepburn), leaders and politicians (e.g. John Adams and Pierre Trudeau), or just through family and friends. Pathological tremor is a neurologically based movement disorder; it is a relatively common condition, with prevalence on par or exceeding many other recognizable neurological conditions [1]–[3].

Manifestation of physiological tremor is evident in all humans and is in fact a normal occurrence. In contrast pathological tremor is an abnormal condition that can result in an increase in amplitude as well as in modification of the tremor frequency. Pathological tremor has been defined as an “involuntary, rhythmic, oscillatory movement produced by either synchronous or alternating contractions of antagonist muscles” [4], [5].

1.1. Motivation

Human tremor is thought to superimpose over the intended motion and thus corrupt the planned activity. In particular, when a person attempts to interface with the surrounding world, the tremorous motion can obstruct and diminish the resulting motion accuracy and stability. Thus, cancelation of human tremor is desirable.

There are two primary scenarios that commonly require attenuation or removal of tremor. The first is in individuals suffering from a neurological disorder resulting in a “rhythmic, roughly sinusoidal involuntary movement” [6], referred to as pathological tremor. Individuals suffering from pathological tremor may benefit from mechanical attenuation of the involuntary movements [7]. Medical robots and orthoses have been suggested for this purpose, and can be donned on the limbs and apply resistive forces, either distally or to a specific joint, that reduce the tremor. The second scenario is when a person is required to perform a task involving high accuracy, which may be difficult to achieve due to the normal physiological tremor, with a consistent level of performance. Achieving high precision and reliability in such a scenario may be difficult without an intermediate system interfacing between the hands and the target object to be

manipulated, such as in medical procedures [8]. Often an electromechanical system (e.g. a teleoperation system) is used to interface between the human and the surrounding world in order to attenuate even small (normal) levels of tremor that are present [9].

1.2. Goal and Objectives

The overall goal of this thesis is to propose an effective tremor suppression approach. An effective approach in this context refers to one that removes the tremorous motion while creating minimum obstruction to the intentional motion component. The conceived approach could be used in multiple scenarios requiring the attenuation of undesired tremor movements. Typical applications range from medical assistive devices to fine motion teleoperation devices.

The following objectives were defined as stepping stones towards achieving the research goal:

1. Propose a novel tremor suppression approach.
2. Validate the proposed approach via a hardware simulator.
3. Design a tremor suppression orthosis implemented with the proposed approach.
4. Test the suppression approach and orthosis on individuals with tremor.

1.3. Outline of Thesis

This work aims to develop a tremor suppression solution. As such, the thesis begins with a background on tremor. From **Chapter 3** to **Chapter 6**, a tremor suppression solution is proposed and demonstrated first in simulations and finally with individuals with tremor. The thesis is structured as follows:

Chapter 2 provides, in essence, a literature review of etiology, clinical aspects, and prevalence and statistics of tremor; finally tremor solutions in research and industry are reviewed. The etiology section touches on the physiology and mechanisms of tremor, the neuronal structure, and related muscle synergies. The clinical features and statistics section talks about types of tremor, their activation conditions, and unique

characteristics such as typical tremor frequency. The chapter concludes with a review of tremor suppression solution in research and industry involving a variety of technologies.

Chapter **3** introduces the suggested suppression approach in a generic and modular fashion. The approach motivation and novel features are described. Specific modules of the approach are reviewed with respect to the literature and state of the art. Furthermore, the chapter delves into a possible controller implementation for application purposes with mathematical modeling.

In **Chapter 4**, a benchtop system is developed for the simultaneous simulation and suppression of tremor. The benchtop mechanism is introduced, followed by a parametric stability and performance analysis. Simulation is performed using a tremor signal recorded from an individual with tremor as input, and results are presented. A discussion of the simulation system and its results ensues including identified limitations.

Chapter 5 involves the development of an elbow orthosis and its implementation with the proposed suppression approach and controller, similar to that presented in **Chapter 3** and **Chapter 4**. Experimental results are obtained by simulations with a tremor input. Importantly, two types of tremor inputs are considered, namely velocity and torque based tremor signals. Differences in the results between the two input signals are discussed analytically and qualitatively.

In **Chapter 6**, the orthosis developed in **Chapter 5** is employed in a pilot clinical study involving participants with tremor. The study participants performed functional as well as pursuit tracking tasks. Healthy participants' data was also collected to be used as reference for the tremor participants' data. Participant selection and protocol details are provided. Uniquely, detailed results are provided not only with regard to the tremor suppression but also in relation to the voluntary motion and how it is affected by the proposed solution.

Chapter 7 concludes with a summary of the thesis objectives. Each objective is reviewed with respect to the work completed in the thesis and supported by quantitative data. A list of peer reviewed contributions is provided. Finally, possible future work is proposed.

Chapter 2.

Physiological and Pathological Tremor

2.1. Etiology

Pathologic tremors are generally thought to emerge from Central Nervous System (CNS) and peripheral nervous system disorders. The physiologies of different pathologies, however, differ and the specific neurophysiological pathways have proven to be elusive [10], [11].

The cerebellum is a major brain structure within the posterior fossa, with its anterior part connected to the brain stem [12]. The cerebellum contributes to the regulation of motions, for example by comparing actual to desired movements, and to feedforward control [13]; it is also likely to be a center of oscillatory processes associated with tremor, exhibiting frequencies compatible with tremor [14]. However, the cerebellum is not solely responsible, as the entire central motor network is thought to be involved in tremor generation, including but not limited to the cortex, basal ganglia, and thalamus [11].

A representation of central and peripheral nervous system loops connectivity is provided in **Figure 2.1** [10]. Peripheral connections include reflex loops that interface muscle with the spinal cord and back. Higher level connections to the spinal cord, brain stem, and brain are considered central loops. Central oscillators in humans give out rhythmic motor commands. There exist normal as well as pathologic central oscillators.

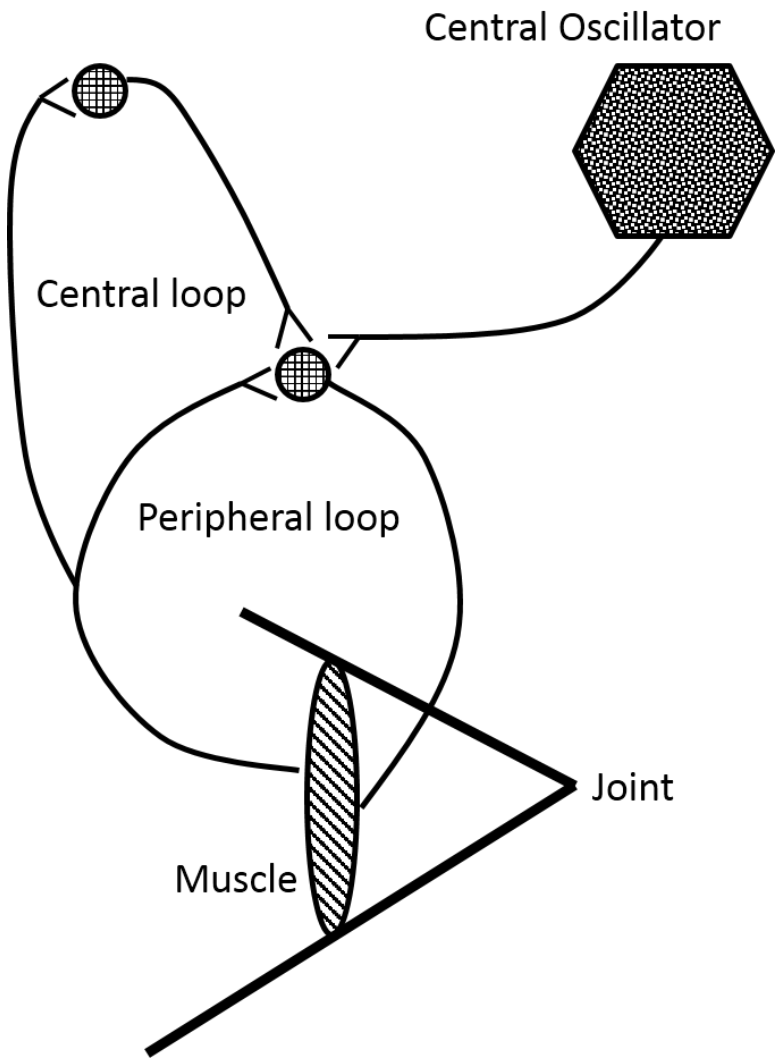

Figure 2.1 Central nervous system connectivity [10]

A variety of sensing and stimulation modalities have been used to investigate the involvement of the Cerebellum in tremor including Electromyography (EMG), Magnetoencephalography (MEG), repetitive Transcranial Magnetic Stimulation (rTMS), Electroencephalography (EEG), Magnetic Resonance Imaging (MRI), functional MRI, Voxel-Based Morphometry (VBM), Magnetic Resonance Spectroscopy (MRS), Diffusion Tensor Imaging (DTI), Positron Emission Tomography (PET) and Single-Photon Emission Computed Tomography (SPECT). Many of the above methods offer evidence of cerebellar dysfunction associated with tremor. Recent studies including tissue based ones have also highlighted clinical and neuropathological evidence linking the cerebellum to Essential Tremor (ET) [11], [14]–[17].

In bidding to understand the mechanisms behind physiological tremor, early works have hypothesised a connection to an oscillatory process in the stretch reflex loop [18]. Stein et al. have distinguished between two different mechanistic sources of (physiological) tremor, namely mechanical and reflex oscillations [19]. The former is purely mechanical in nature and arises from the interaction between muscles and load. Mechanical tremor tends to decay over time. The latter arises from high gain in reflex pathways that connect muscles to the CNS. Furthermore, when the frequencies of the mechanical and reflex tremors are close, the two may mutually entrain to a single frequency tremor referred to as mechanical-reflex tremor [10]. Both mechanical and mechanical-reflex oscillations frequencies tend to inversely depend on the load such that higher load is associated to a lower motion frequency and vice versa [20].

Mechanical properties of the limb contribute to the tremor frequency through the following relation

$$f = \frac{1}{2\pi}\sqrt{\frac{K}{I}} \tag{1}$$

Equation **(1)** models the joint physiology as a mass-spring mechanical system where K, I, and f are the spring stiffness, mass inertia, and resonant frequency respectively. Upper limb typical unloaded resonant frequencies are around 25-27 Hz at the finger, 9 Hz at the wrist and 2 Hz at the elbow. If forces or loads are applied different resonant frequencies may result.

As mentioned, central oscillators are another contributing factor of both normal and pathologic tremors, with frequencies typically in the range of 8-12 Hz [10], [21] they are unique in that they operate independently of peripheral input [20]. In contrast, mechanical and reflex tremors are generally influenced by a mechanical or nerve perturbation (peripheral input) that can result in a frequency or phase shift of the tremorous motion. In order to distinguish between tremors arising from mechanical, mechanical-reflex or central oscillators many studies have incorporated accelerometry and EMG data while weighing the affected body part and utilizing a spectral analysis [10], [22]. Weighing the human body part can affect the inertia. As mentioned, the frequency of mechanical and reflex tremors decreases with increased body part inertia.

In contrast, central oscillator tremor will tend to remain unchanged. Consequently, it is possible to separate tremor into its constituent driving components, which in turn can help distinguish between tremor pathologies. Overview of different mechanistic origins of physiologic and pathologic tremor is provided in a review paper by McAuley et al. [21] and in [6], [10], [23] respectively.

To summarise, four outcomes may generally be observed, when measured using EMG and accelerometry, and with inertial loading applied to the human arm [24]. Note the aforementioned is true for both physiological and pathological tremor.

1. Accelerometer data shows oscillations, and EMG data shows no oscillations. Tremor frequency decreases when a load is attached according to **(1)**. This behaviour represents normal tremor due to mechanical resonance with little contribution from reflex loops or a central oscillator.

2. Both the accelerometry and EMG data show a tremorous signal that decreases by more than 1 Hz with inertial loading. The condition represents motor unit entrainment by the mechanical and mechanical-reflex resonant frequency, essentially dictating the EMG tremor frequency. The condition is typical of enhanced physiological tremor.

3. In the unloaded case the same frequency is observed for the accelerometry and EMG. In the loaded case two frequencies are observed, a mechanical-reflex resonant lower frequency component and a higher motor unit frequency driven by a central oscillator. The central oscillator component frequency is unaffected by loading.

4. The same frequency is observed in the accelerometry and EMG for both the loaded and unloaded cases. A frequency decrease of less than 1 Hz is seen with the inertial loading. The condition represents a dominant central oscillator with minor effect by mechanical-reflex resonant oscillations.

An active research topic in motor control is that of modularity, also known as motor primitives or muscle synergies. The basic premise of muscle synergies suggests the nervous system flexibly controls groups of muscles rather than isolated muscles when performing a variety of motor tasks [25]. Across different tasks as well as similar tasks, but different conditions, the CNS may modulate the timing and/or activity of the same group of muscles [26]. Thus, a control dimensional space may be achieved using synergies that is reduced relative to the variables (muscles or joints) dimensional space. Motor primitives have been identified in the muscular (e.g. through EMG), kinematic, and

neural substrate level. It has been hypothesized that the modularity of synergies simplifies movement generation and motor learning [27].

Neurological disorders (e.g. stroke and spinal cord injury) can affect muscle synergy movement repeatability as well as the flexibility with which the movement can be executed under different conditions [26]. Evidence relating pathological tremor to muscle synergies is limited. It has been suggested, however, that cortical and subcortical disorganization exists in some diseases (e.g. Parkinson's disease) resulting in abnormal synergies [26]. It is also conceivable that loss of inhibition, as is suggested to be the case for hand dystonia [28], [29], is related to pathologic synergy seen in tremor. A tremor compensatory mechanism, involving synergy of upper inter-limb joints, resulted in reduced fingertip physiological tremor as shown by Morrison et al. [30]. However, this compensatory mechanics was primarily associated to higher frequencies, which account for a small portion of the tremor power [31]. In a later study by Carignan et al. no such compensatory mechanism was observed in the critical lower frequencies of physiological tremor [32]. Nevertheless, a relationship between upper limb segments, distal to the shoulder and mechanically driven by it, was observed in lower frequencies whereby little or no phase existed between the different limb segments.

2.2. Clinical Features and Statistics

A variety of pathological tremor conditions have been identified by the medical community that include more than ten subtypes of tremor [5], [6], [23], [33]. The proposal of the Movement Disorder society for the clinical classification of tremors [4] was one of the first comprehensive studies summarizing clinical features for the classifications of tremor. The proposed classification, among other factors, considers and defines the activation conditions during which tremor may be observed as shown in **Figure 2.2**.

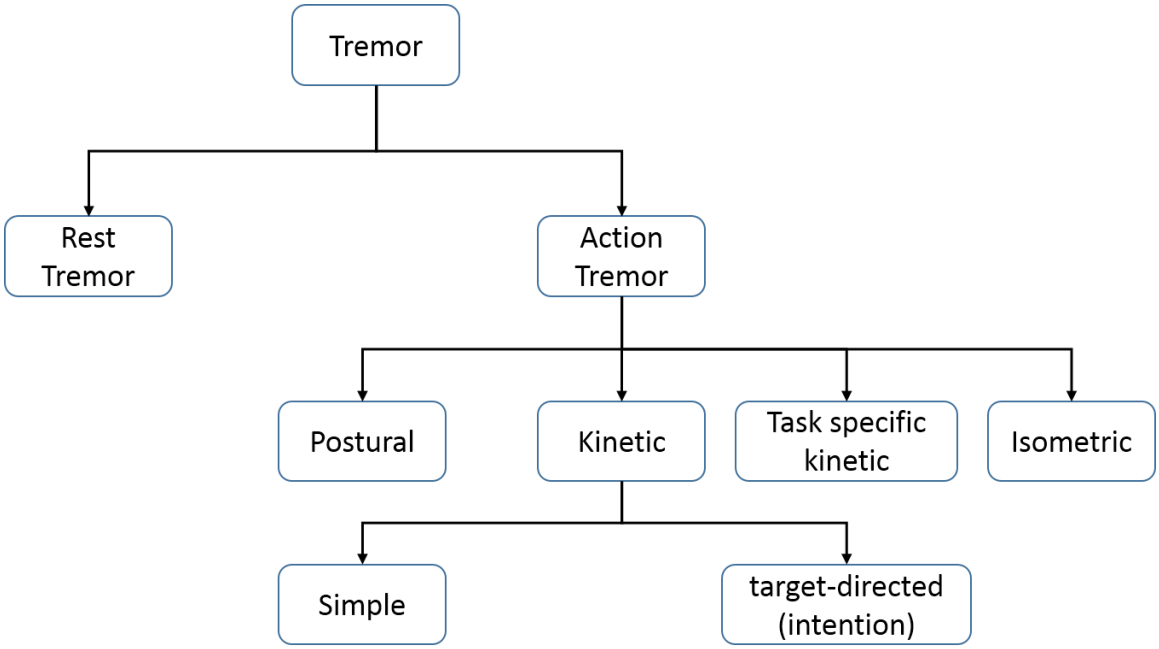

Figure 2.2 Tremor activation conditions [4], [33]

In addition to the conditions under which tremor is activated (**Figure 2.2**), factors such as tone and rigidity, topography (part of the body being affected), frequency, medical history and scale rating should be taken into account in the classification of tremor [4]. Using these different factors a variety of clinical disorders are defined. A list of defined tremor disorders, their frequency and activation conditions are shown in **Figure 2.3**.

Rating scales have also been proposed for resting tremor (the Unified Parkinson's Disease Rating Scale (UPDRS)) [34], [35], and for action tremor [36]–[40].

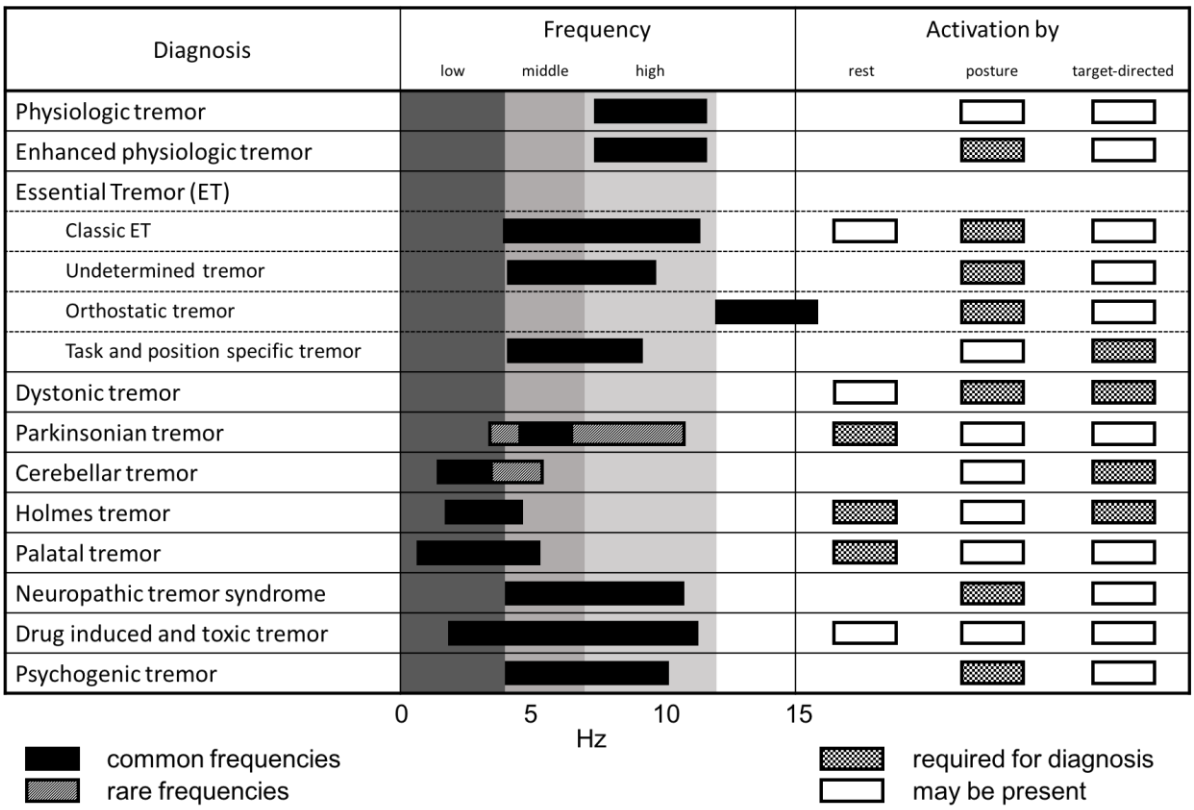

Figure 2.3 Tremor classification based frequency and activation condition [4]

Among movement disorders known to affect humans, pathological tremor is highly prevalent [23]; some estimates show it to affect above 10% of the elderly population [41]–[44]. Tremor often affects the upper extremities [33], and can adversely impact the ability to perform basic tasks. Additionally, social discomfort is a common grievance with tremor patients [45]. Disability in Activities of Daily Living (ADL) is experienced in more than 60% of upper limb tremor patients [7], [46].

Of the above diagnosed conditions (**Figure 2.3**) ET and Parkinsonian Disease (PD) are by far the more common [11], [23], and often occur together [6]. ET prevalence has been estimated at 4% of people aged 40 years or older, with an increase in incidence with age. PD overall prevalence has been estimated at 1.6% [42], [47], [48]. Essential tremor is characterized by an involuntary oscillatory frequency component of 4-12 Hz, inversely related to age [1], whereas Parkinson's disease tremor frequency is typically between 3-5 Hz. A high frequency form of a Parkinson's disease action tremor has oscillations between 5-10 Hz [6]. The conditions are progressive, and the greatest oscillations amplitude is typically observed at distal joints. ET and PD often appear at the upper limbs, and slightly asymmetrically [33], [49]. ET is often bilateral, while PD is often

unilateral and commonly involves Bradykinesia [5]. No known cure is available and treatments primarily consist of pharmacotherapy on a trial-and-error basis, however surgery and Deep Brain Stimulation (DBS), typically reserved for severe and medication resistant patients [50], also account for therapeutic alternatives [7], [46], [51], [52]. Other surgical procedures include γ knife radiosurgery (invasive), and Magnetic Resonance-Guided Focused Ultrasound (MRgFUS) (noninvasive) [53], [54]. Specifically, MRgFUS is a non-invasive thalamotomy procedure that has been demonstrated to reduce tremor [55]. Risks for the procedure include intracerebral hemorrhage and other potential neurologic impairments [56]. Comprehensive clinical trials are currently underway to validate the MR-guided focused ultrasound approach. Both ET and PD are central neurogenic driven tremors [23]. Therefore, with regard to the electrophysiologic measure outcomes due to the effects of inertial loading (mentioned in section 2.1) advanced ET and PD have typically outcome 4, while mild ET has outcomes 2 and 3 [10].

As mentioned previously medications comprise the primary course of therapy, however are commonly precluded due to their poor effectiveness or significant side effects in 30% or more of the cases [50], [57]. When beneficial, the tremor reduction due to medication is estimated between 39% and 68%, dependent on the specific medication [23]. Instead, DBS effectiveness is estimated at 90%. However, about 20% of patients undergoing unilateral DBS experience side effects, and about 30% of patients undergoing bilateral thalamic DBS experience complications [6].

Therefore, there is a need for continued investigation of novel treatments in order to enhance efficacy while minimizing side effects and risks. Wearable robotic devices may provide a solution for some patients. The main challenge for electromechanical orthoses is to offer an effective suppression as defined in section **1.2**; namely, the orthosis should resist the tremor component while allowing the intentional motion to be carried out unhindered.

2.3. Tremor Suppression Solutions

2.3.1. Research

Over the past few decades, a variety of mechanical based solutions have been proposed for lessening patients' tremors, and in so doing assisting them in their ADL.

Devices for tremor suppression can be categorized as passive or active. There are benefits and drawbacks to both methods. Passive systems tend to be simpler to implement, however the suppressive force may affect not only the tremorous but also the voluntary motion. Active systems tend to involve higher complexity and power consumption yet with a potential to offer better performance. Likewise, tremor suppression devices can be categorized as ambulatory, typically as wearable devices, or non-ambulatory [7], [58]. Non-ambulatory devices can nevertheless serve users in their ADL (e.g. by being connected to a wheelchair). More typically, non-ambulatory devices are grounded (e.g. connected to a table) for use in a home or a clinic.

Early investigations into biomechanically suppressing tremor resulted in devices that were predominantly non ambulatory [59], [60]; these devices additionally relied on damping forces. One of the first published devices to tackle pathological tremor was a joystick with viscous damping for improved wheelchair control accuracy [59]. Another device, named CEDO, utilizing magnetic particle brakes, delivered velocity proportional resistive forces in three Degrees of Freedom (DOF), moving in a horizontal plane. It was assembled on a wheelchair and attached with a brace to the subject's forearm [60], [61]. Further, a wrist flexion/extension viscous friction orthosis was designed for tremor suppression by Kotovsky et al. [62]. The device acted passively to dampen the tremor, though its dimensions were relatively small such that it was mobile and could fit beneath a garment.

Several wearable (ambulatory) active devices have also been suggested since, that target the upper limbs and assist the wrist and elbow joints [63]–[65], utilizing controlled dampers and electric motors. A similar device to that developed by Kotovsky et al. but with an active suppression, employing Magneto-Rheological Fluids was developed by Loureiro et al. [63]. The WOTAS orthosis developed by Rocon et al. was composed with DC motors spanning 3 DOF for the elbow, forearm and wrist [64]. Passive and active control strategies were suggested utilizing kinematic data with an impedance controller or a notch filter respectively. A second parallel force feedback loop aimed at reducing the obstruction to the voluntary motion. The WOTAS is among the most significant works utilizing force sensor data.

Other tremor solutions involving force feedback include a work by Ohara et al. who designed a meal-assist stationary robot with an adaptive force band-stop filter [66].

Research using force data in tremor suppression applications is scarce, and generally only exploits the force for the purpose of recording and validation [67], [68]. EMG sensors have also been suggested for suppression applications and can be considered analogous to a force transducer as they provide a measure of the user's applied force [69]. Kiguchi et al. implemented an EMG based control strategy with a 7 DOF exoskeleton [67]. Ando et al. demonstrated an EMG voluntary component estimation, tested with a normal and a tremor patient [65]. A 1 DOF elbow device, actuated with a DC motor, was presented but not involved in the patient testing. Classification accuracy can however be an inhibiting factor for EMG based solutions, in particular, when considering accessibility to muscle signals specific to a motion such as pronation and supination.

Functional Electrical Stimulation (FES), soft actuators and smart wearable garments based on conducting polymer polypyrrole, piezoelectric fibre composites and polymer films, for tremor suppression have been suggested by several research groups as an alternative to systems with rigid components and actuators [70]–[75]. EMG and FES technologies complement each other. As such, EMG sensors are often utilized in conjunction with FES. Recognized limitations for FES include muscles redundancy and coupling involved in the activations of joints, surface electrodes hardware limitation in accessing specific muscles, as well as muscle fatigue.

Recently, several non-invasive brain stimulation techniques have been proposed and tested with individuals with tremor. Two such techniques include repetitive Transcranial Magnetic Stimulation (rTMS) and transcranial Direct Current Stimulation (tDCS) [76]. rTMS stimulates cortical neurons by generating a magnetic field with induction coils. rTMS therapy has been applied to several movement disorders including PD, levodopa-induced dyskinesia, Dystonia, Tourette's syndrome, Chorea, ET, and cortical tremor [77]. Specifically for ET, both a reduction in tremor amplitude and functional disability were observed when applying bilateral rTMS to the posterior cerebellar cortex for a period of 5 days [78]. Another study involving one participant receiving invasive motor cortex stimulation with rTMS showed improvement in hand tremor [79]. There are few sham controlled studies applying tDCS for movement disorders [80]. One recent double blind, crossover, and placebo controlled study with 10 ET participants involved applying inhibitory tDCS to the cerebellum through surface electrodes [81]. No short or long terms benefits were observed. Another similar non-

invasive method to tDCS is Transcranial Alternating Current Stimulation (TACS). In a study by Brittain et al. TACS was applied to PD patients [82]. A mean tremor amplitude reduction of 42% was obtained. The system can adjust online to tremor parameters such as frequency and phase by probing the tremor circuit.

Impedance control strategies for tremor suppression have been suggested by multiple researchers [64], [83], [84]. The impedance control approach attempts to modify the human machine frequency response such that higher impedance is present at the tremor frequencies [84]. Often, the impedance tremor suppression approach uses a human-machine model of stiffness, damping, and mass properties that are modified to achieve a desired frequency response [83], [85]. An early work by Pledgie et al. used a feedback controller to modify the parameters of a linear second-order mass, damping and stiffness system, used to model the human robotic coupling [83]. Hashemi et al. developed a similar concept called a tuned vibration absorber having 2 DOF (shoulder and elbow). The approach was tested with a simulated tremor for a single DOF vibration absorber [86]. The passive strategy by Rocon et al. was also based on impedance control [64]. A recent work by Taheri et al. presented the development of a human arm simulator and proposed a torque estimation method relying on kinematic signals [68], [87]. An adaptive disturbance rejection algorithm estimated the involuntary motion torque and applied an opposite force to cancel the tremorous motion. Their work requires a human-machine model. The main drawback of impedance control involves sensitivity to inaccuracies in the human machine model parameters or changes to thereof over time.

It is not uncommon to assess tremor suppression methods by performing simulations, either numerical or experimental [65], [67], [68], [86]–[89] and obtaining access (with ethics consent) to patients once simulations have yielded optimal results. Several FES systems belong to this group [72], [90], [91]. Comparatively higher values for attenuation have been reported [72], though the system was not tested with tremor participants. Simulations can promote verification of the suppression approach by promoting tuning and debugging of the suppression system and thus improving its performance. Furthermore, recordings from patients can be used to simulate the tremor profile helping to bridge the gap between simulations and testing with subjects.

Physiological tremor, a normal occurrence of human tremor, has also been targeted in several applications. Teleoperation devices such as surgical robots are a

class of machines with a human interface designed to provide enhanced performance by the removal of human physiological tremor [8], [92]–[94].

The tremor reduction effectiveness of the reviewed suppression solutions varies significantly from around 40% to above 90%. It should be noted that even when attenuation levels were stated for the tremorous motion, the influence to the voluntary motion was seldom reported.

2.3.2. Commercial Systems

In contrast to the aforementioned investigative devices, a limited number of devices, including the Neater Eater, Handy-1, Winsford Feeder, MIT-manus, the My Spoon, Readi-Steadi glove, and Liftware spoon, offering passive and active pathological tremor cancelation have become commercially available [95]–[103] and are for the most part non-ambulatory in nature. Another device currently being developed [104] is purported to use gyroscopes for the tremor suppression.

Several robotic microsurgical systems like the ZEUS and Da Vinci robotic surgical systems, that decrease normal human tremor transferred to the end effector in order to increase surgical accuracy, have also become commercially available [8].

Chapter 3.

A Voluntary Driven Tremor Suppression Approach

3.1. Suppression Approach

3.1.1. Background

Typically active-based suppression approaches attempt to estimate and isolate the involuntary motion component (tremor) in order to subsequently suppress it [7]. This work proposes instead to only estimate the intentional movement and reject any disturbance that interferes with such an intended movement. Furthermore, this work makes use of a force transducer signal to perform the voluntary and tremor components separation, different from most approaches primarily relying on inertial sensors. By designing the control feedback such that motions other than the voluntary are rejected, the tremor component is attenuated.

3.1.2. Voluntary-Driven Motion with Speed-Controlled Tremor Rejection

In this section, the approach proposed in order to achieve attenuation of a tremor signal superimposed over a voluntary signal is described. The presented approach deals primarily with the voluntary motion. The block diagram in **Figure 3.1** illustrates a breakdown and flow of the elements involved in the suppression approach implementation. The suppression approach is illustrated in a generic and modular form such that each block may be interchangeably implemented with a variety of alternative modules. A force[1] sensor is used to detect the interaction force between a human and the suppression system. A filtering algorithm then decomposes the force sensor signal into voluntary and tremor components. The sensed voluntary force is responsible for driving the mechanical suppression system (e.g. a robotic orthosis) using a mechanical admittance controller [105]. The voluntary force component is subsequently translated into a velocity signal commanding the actuator of the suppression system. An internal

[1] Force may be represented as measured force, torque, EMG or other equivalent sensing method.

feedback loop is incorporated to track the commanded velocity and reject disturbances such as the human tremor. A brief review of each module is provided next.

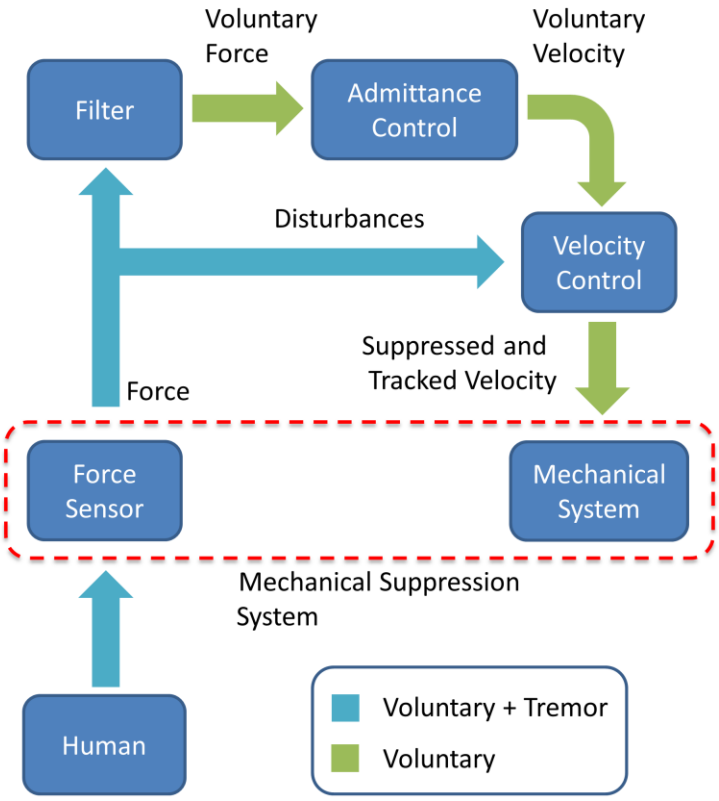

Figure 3.1 Suppression approach elements and flow.

Fundamental Assumptions

The following two assumptions are fundamental to the success of most tremor suppression approaches and specifically to the one proposed in this work:

1. Voluntary frequencies are assumed below 2 Hz while tremor frequencies above 3 Hz. Thus, voluntary and tremor motions occupy different frequency bands. This notion is widely supported in the literature.

2. Tremor and volitional motions are superimposed and thus can be dealt with independently.

3.1.3. Signal Filtering

Distinguishing the tremor and voluntary components from a recorded signal is a fundamental step in tremor applications, whether for diagnosis or treatment. Online signal decomposition in particular poses a greater challenge than an offline computation. Strategies ranging from linear filtering to stochastic estimators have been employed. Gonzalez et al. designed an optimal digital filter offline through pursuit tracking tasks [94]. Ando et al. used a second order Low Pass Filter (LPF) applied to an EMG tremorous signal to be passed on to a neural network, intended to control an elbow device [65]. Verstappen et al. used a high pass filter to separate the tremor component before passing it to a repetitive control loop using an FES system [106]. Another recent work utilized a tremor estimator in the form of a high pass filter [107]. The filter resulted in a significant phase shift, which was corrected prior to being applied to the suppressive actuator. The inherent phase shift of linear filters is considered their main limitation [7].

Another tremor estimation method is the Weighted-frequency Fourier Linear Combiner (WFLC) – an adaptive noise canceler. The WFLC adaptively models (with zero-phase lag) a tremor signal by tracking its frequency, amplitude and phase [92], [93]. For best performance pre-filtering with a high pass filter is recommended. Several variations of the WFLC method have been subsequently proposed (BMFLC and ASBMFLC), that can adaptively adjust the frequency bandwidth for the tremor estimation [108], [109]. A different approach, the Adaptive Band-Pass Filter (ABPF), was proposed by Popovic et al. and compared favorably to the WFLC [110].

The Kalman Filter (KF) is a stochastic estimator, based on a Bayesian model, traditionally employed in navigation (e.g. satellite) and ballistic tracking [111]. The KF has been utilized for tremor suppression in several studies. Rocon et al. have implemented a KF to track the voluntary motion and by subtracting it from the total motion, obtain an estimation of the tremor [64], [112]. The tremor signal was used to control a 3 DOF upper arm orthosis. Additionally g-h and Benedict–Bordner filters were employed. The main difference between the above filters is the method of weights selection [113]. Widjaja et al. have also implemented the KF, fusing information from accelerometer and EMG data, to obtain a single joint (1 DOF) estimate of the tremor angle to be used in diagnosis, classification and FES applications [69]. Other studies involving KF focused on online estimation of the tremor and voluntary signals. Veluvolu

et al., in their study, combined the KF with the BMFLC algorithm to estimate the tremor motion where the KF replaced the standard LMS algorithm used to adapt the BMFLC weights [114]. Bo et al. implemented the EKF with the tremor motion modeled as an autoregressive process while the voluntary motion was modeled as an autoregressive moving-average model [115]. Tatinati et al. also employed an autoregressive model and used KF to estimate the model coefficients [116].

3.1.4. Impedance and Admittance Control

Force control aims to regulate the robot motion and applied force based on some defined control goal [117]. Impedance and admittance control strategies generally fall under the umbrella of force controllers along with stiffness, hybrid position/force and explicit force controllers. Force controllers are beneficial in robotic applications that require interacting with an environment such as cutting and grinding tasks, typical for industrial settings, or when dealing with environmental uncertainties by regulating the permissible contact forces [118], [119]. In contrast, implementing a purely position based control approach for a robot-environment interaction requires a very precise knowledge of the robot model and environment geometry. Since, in practice, modeling errors are difficult to avoid, small position errors can lead to large interaction forces. Sensed variables in force control may include position, velocity, acceleration and force. Impedance and admittance control methods are reciprocal and are often employed in human robot interaction to provide movement resistance or assistance [120]–[122].

Mechanical Impedance [117] is defined as

$$Z_m(s) = \frac{F(s)}{\dot{X}(s)} \tag{2}$$

where $F(s)$ is the applied force, and $\dot{X}(s)$ is the resultant velocity. The equation in (2) describes a frequency dependent relation between the input velocity and output force. A mechanical impedance controller regulates the robot dynamics such that the environment experiences a desired impedance. In its simple form, the impedance controller generates a desired resistance force based on motion errors. Notably for an impedance controller, the environment is assumed to be an admittance [118]. A linear case for the impedance in (2) is commonly represented as follows:

$$sZ_m(s) = Ms^2 + Ds + K \tag{3}$$

where M, D, K are the inertia, damping and stiffness matrices. The manipulator impedance can thus be specified through the selection of the matrices. A general (position-based) impedance control structure is shown in **Figure 3.2**, however, other representations have been suggested in the literature [123]. The parameters F, K_E, X_F, X_D, X_I, J, and N are the environment contact force, net stiffness of the sensors and environment, force feedback trajectory, desired trajectory, resultant impedance trajectory, robot Jacobian, and nonlinear feedforward compensation. K_P, K_V are position and velocity control gains. The dashed area in **Figure 3.2** encloses the proportional-deriviative position feedback loop that enforces the tracking of X_I by the end effector position X. Therefore, the manipulator can realize the target impedance.

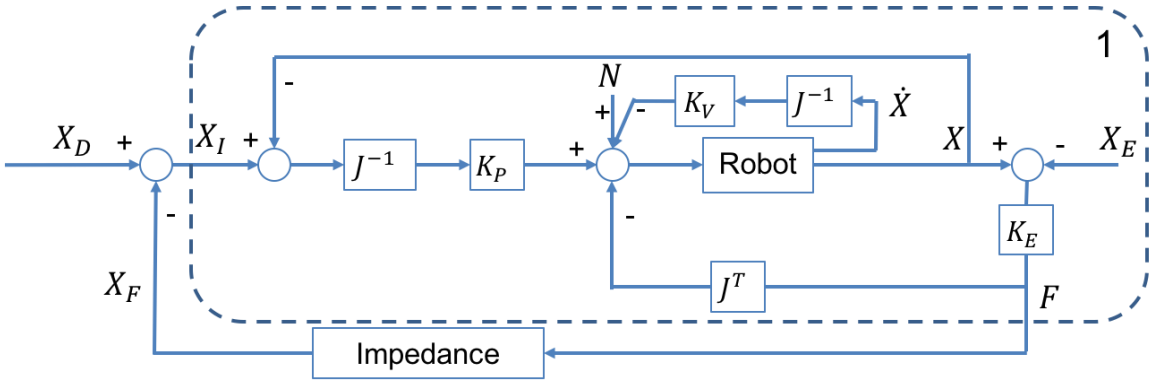

Figure 3.2 General position-based impedance control diagram [117]**.**

Mechanical admittance is defined as

$$A_m(s) = \frac{\dot{X}(s)}{F(s)} \tag{4}$$

Equation (4) is the inverse of (2). Admittance control focuses on force tracking which results in a robot trajectory that provides a compliant motion relative to the constraining environment. An admittance controller is suitable for tasks in which the robot motion is to be guided by the environment [118]. Notably for an admittance controller, the environment is assumed to be an impedance.

A common admittance control structure is shown in **Figure 3.3**. The parameters F_D, F_E, X_C, and X_D are the desired contact force, the contact force error, the commanded trajectory, and the desired trajectory respectively. Block 1 is the same inner position controller as in **Figure 3.2**. Admittance control is often depicted as a particular case of explicit force control that includes an internal position or velocity feedback [124], [125].

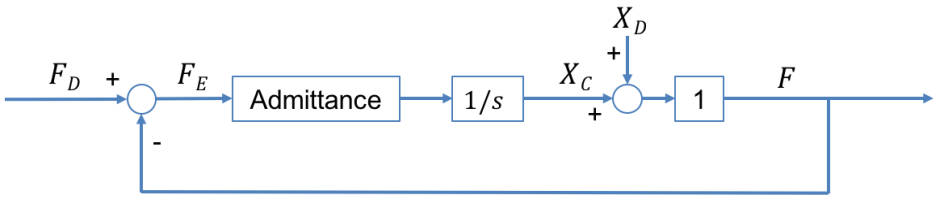

Figure 3.3 General admittance control diagram [117]**.**

Impedance control for Tremor Suppression

At its foundation, impedance control provides a frequency dependent relation between motion and a force (i.e. of a limb). Two impedance approaches have typically been employed in the literature. The first involved modification of the biomechanical characteristics of the system (robot and limb) to achieve a desired frequency response and consequently attenuation of motions in the tremor frequency range [83], [86]. The second approach involved defining an impedance relationship specifically for the tremor component, between motion and force [64], [68]. It has been shown by several researchers that loading of the tremorous body part (externally or internally) can cause changes to tremor properties such as amplitude and frequency [60], [126]–[128]. In turn, the desired impedance relationship (in the second approach mentioned above) between the motion and force may be altered, thus compromising the effectiveness of an impedance controller.

Adaptive control strategies may help mitigate impedance changes to successfully attenuate tremor, though these may only effectively account for internal loading (i.e. muscle activation) while external loading may not be known and thus still affect performance. To the authors best knowledge adaptive impedance control has yet to be investigated for the application of tremor suppression. Taheri et al. in their recent work suggested a tremor suppression controller designed to attenuate tremor near the tremor fundamental frequency. The controller adapted online to the tremor frequency [68]. Nonetheless, the stiffness, damping, and mass impedance properties did not adaptively update.

Some works unrelated to tremor have investigated adaptive impedance controllers. The idea behind adaptive impedance control is to maintain consistent system performance in the presence of robot or environment parameter uncertainty [117]. Learning impedance control has been researched in manipulator control, typically for industrial applications [129]. Investigations involving rehabilitation devices have also been carried out. Hussain et al. developed a control scheme whereby the robot assistance is adapted based on the level of disability or participation expressed by the user [130]. Adaptive impedance has been considered for prosthetic devices in order to achieve more natural capabilities, similar to the human limbs [131]. For the application of tremor suppression, biological feedback, such as EMG, may be used to guide the learning of the impedance control law. In the same vein as in the work by Hussain et al. [130], a change in muscle participation or in the combination of muscles used for a given task may require a change of the controlled impedance.

As mentioned previously, most tremor suppression methods model the tremor signal and generate a corresponding suppressing command. An impedance-controlled system that models the tremor motion-force relationship may therefore experience fluctuation in the suppression performance due to the impedance variability. In contrast, the method proposed in this work only models the voluntary motion. Therefore, variability in the limb impedance is not expected to affect the attenuation performance.

3.2. Suggested Data Processing and Outcomes

3.2.1. Spectral Analysis

The main analysis tool for the spectral domain involved the Power Spectral Density (PSD). The PSD describes the power in the signal per unit of frequency [132]. Integrating the PSD over a range of frequencies results in the total power in the signal for the respective frequency range, which can be expressed as P_s^f where s designates the signal and f designates either the tremor (t) or the voluntary (v) frequency range for the signal power calculation. A comparison of the total power can be performed between two signals (e.g. with and without the tremor suppression), and can be referred to as the power change. The power change calculation was defined as follows:

$$PC\left(P_{s1}^{f}, P_{s2}^{f}\right) = \frac{P_{s1}^{f} - P_{s2}^{f}}{P_{s2}^{f}} \times 100 \quad (5)$$

where P_{s1}^{f} and P_{s2}^{f} are the power in the first signal (e.g. measured with the suppression system) and the power in the second signal (e.g. measured without the suppression system), respectively. Throughout this work, a negative power change value indicates a power reduction while a positive value indicates a power increase relative to the signal $s2$.

The spectral analysis can be used for both the tremor and voluntary motion components. Voluntary motions are typically considered to have a frequency spectra below 2 Hz [133], [7], as such, the 0-2 Hz frequency range is appropriate for the calculation of P_{TSO}^{v} and P_{MO}^{v}. The range for tremor may include frequencies above the voluntary, e.g. from 2 to 10 Hz, typical for ET and PD [6].

3.2.2. Temporal Analysis

Time domain data processing mainly relates to the intentional motion component. The evaluation should involve knowledge of the intentional motion trajectory in order to make a comparison with the measured motion resulting from the tremor suppression system. A Root Mean Square (RMS) error can be calculated between the desired (intentional) and actual motions.

3.3. Suggested Implementation

3.3.1. Controller Scheme

As a first step in constructing the proposed suppression approach, we consider a motion of a healthy person, composed of a voluntary component only. The control goal is set to track a desired zero force (or torque) $f_d = 0$, i.e. to minimize the measured interaction force between the person and the mechanical suppression device. Under these conditions the suppression system would track the human movement while being transparent [134]. Transparency is typically defined in teleoperation systems as a match between the impedance perceived by the operator on the master and that of the

environment at the slave [135], [136]. By analogy, the suppression system can be considered the master device, while a virtual, rather than a physical, system may be considered for the slave. It is then assumed the slave experiences zero environment impedance such that the master (suppression system in this case) delivers zero impedance to the user.

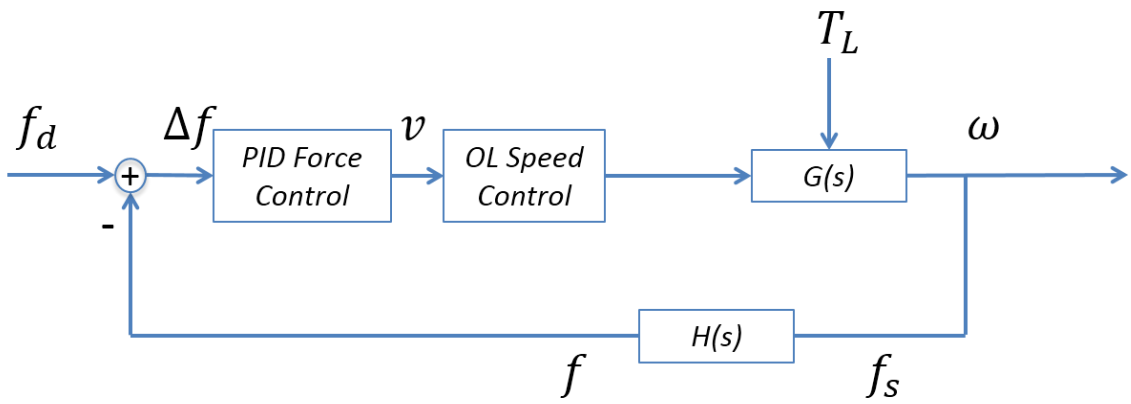

Figure 3.4 Admittance control diagram.

The admittance control structure employed is shown in **Figure 3.4** depicting the force feedback loop. A Proportional-Integral-Derivative (PID) was used as an admittance controller [137]. $G(s)$ is the actuator with gearing model, and $H(s)$ is the force sensor. Together $G(s)$ and $H(s)$ represent the suppression system. It should be noted that in the proposed approach the input force applied by the human (T_L) is regarded as a disturbance to the system.

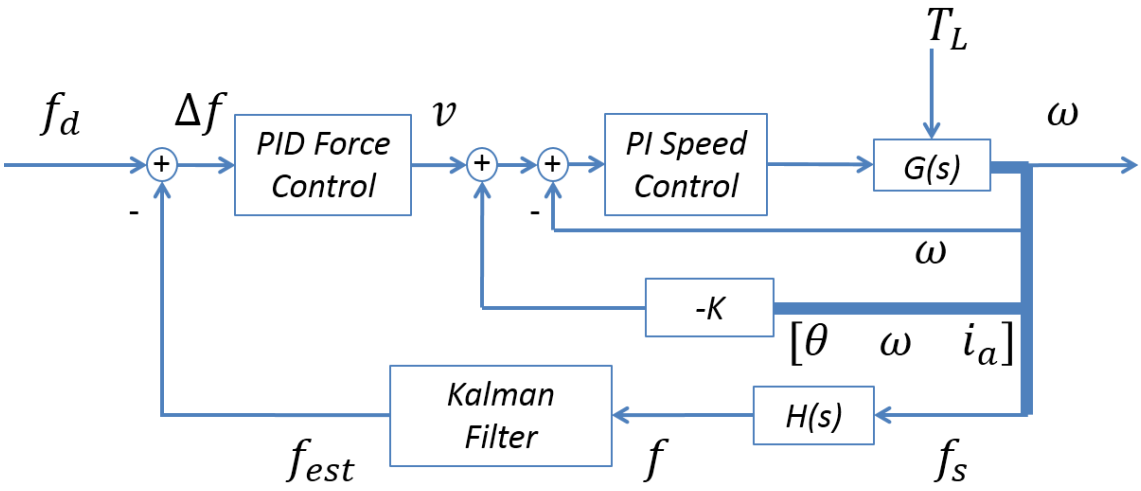

Figure 3.5 **Tremor suppression approach control diagram. The approach includes an inner speed control, a state feedback loop and an external PID force loop.**

As previously mentioned, the control goal was to reduce the interaction force (f) such that the suppression system follows the arm volitional movement (i.e. $f_d=0$). For a healthy person the sensed force signal is associated with the voluntary motion. However for a person with tremor, the movement and thus the force profile is composed of both an intentional and a tremorous component. Therefore, an estimation of the voluntary component from the force sensor signal is required (see the "Filter" block in **Figure 3.1**).

In our implementation shown in **Figure 3.5**, the Kalman Filter (KF), a commonly used stochastic estimator, was employed to separate the voluntary and tremor force components. The KF is used as an observer for the force signal, considering the tremor as noise. The estimated intentional component is then fed back to the force control loop and the force controller outputs a command representing the voluntary velocity to the suppression system. In the case where the voluntary motion alone is present, the output of the filter should simply be the voluntary force with no distortion (i.e. $\Delta f = -f$ for the diagram shown in **Figure 3.5**). The complete tremor suppression control approach is an extension to the control diagram in **Figure 3.4**, as shown in **Figure 3.5**.

For a healthy person, in **Figure 3.4** the PID output represents an input to the mechanical suppression system based on the intentional motion. However, with tremor present, the suppression system would be exposed to the forces associated with the involuntary motion, exerted by the high frequency component. These forces can cause the suppression system to deviate from the intended motion profile. Therefore, for the

approach to perform successfully, the tremor forces must be absorbed without impact to the system voluntary motion. An inner velocity controller, in **Figure 3.5**, helps to reject the disturbances introduced by the tremorous component. The implemented tremor suppression control scheme is then composed of an outer PID force controller fed by the negative voluntary force from the KF output, a state feedback, and an inner velocity Proportional-Integral (PI) controller that acts to reject the tremor forces applied to the suppression system. The state feedback was used to increase the voluntary component gain and improve the velocity tracking.

3.3.2. Kalman Filter

Background

A system with noise as shown in **Figure 3.6** can be described as a discrete stochastic dynamical system as follows:

$$x_{k+1} = Ax_k + Bu_k + Ew_k \tag{6}$$

$$y_k = Cx_k + v_k \tag{7}$$

where x_k, u_k, y_k are the state, control input, and output respectively. A, B, E and C are matrices of appropriate dimensions that can be time variant (here the time index has been omitted for legibility). w_k, v_k are the process and measurement noises respectively.

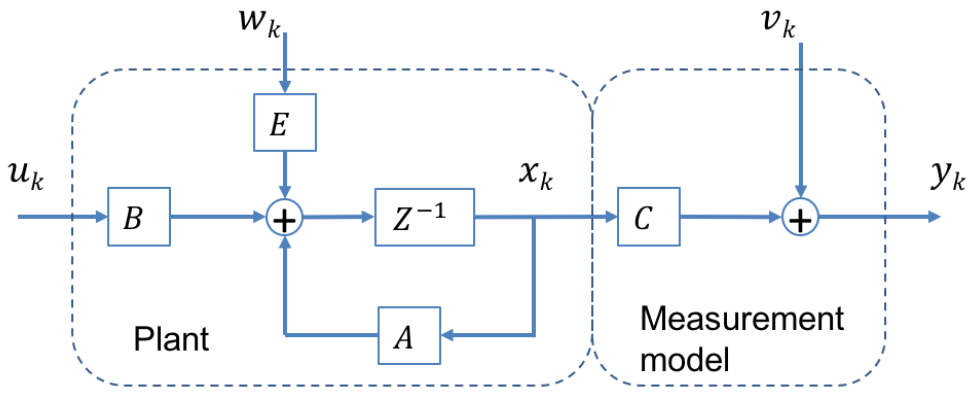

Figure 3.6 Plant with process and measurement noise [138]**.**

It is assumed the process and measurement noise are stationary zero mean white noise processes. Furthermore, the initial state x_0 is assumed to have a zero mean and be uncorrelated with w_k and v_k. The process and measurement noise covariance and cross-covariance can be expressed as follows:

$$E\begin{bmatrix} w_k \\ v_k \end{bmatrix}\begin{bmatrix} w_k \\ v_k \end{bmatrix}^T \triangleq \begin{bmatrix} Q_k & S_k \\ S_k & R_k \end{bmatrix}\delta_{kj} \tag{8}$$

Where Q_k, R_k, S_k, and δ_{kj} are the process noise covariance, measurement noise covariance, noise cross-covariance, and the Kronecker delta. E indicates the expected value.

A common formulation of the KF involves an iterative two-step algorithm with a time update and a measurement update (also called the predictor–corrector formulation) [138].

Time update:

$$P_{k+1}^{-} = A_k P_k A_k^T + E_k Q_k E_k^T \tag{9}$$

$$x_{k+1}^{-} = A_k \hat{x}_k + B_k u_k \tag{10}$$

Measurement update:

$$R_{e,k+1} = R_{k+1} + C_{k+1} P_{k+1}^{-} C_{k+1}^T \tag{11}$$

$$K_{k+1} = P_{k+1}^{-} C_{k+1}^T R_{e,k+1}^{-1} \tag{12}$$

$$P_{k+1} = (I - K_{k+1} C_{k+1}) P_{k+1}^{-} \tag{13}$$

$$\hat{x}_{k+1} = \hat{x}_{k+1}^{-} + K_{k+1}(y_{k+1} - C_{k+1} x_{k+1}^{-}) \tag{14}$$

where $R_{e,k+1}$ is the innovation covariance. The innovation is defined as $e_{k+1} = y_{k+1} - C_{k+1} x_{k+1}^{-}$. K_{k+1} is the Kalman gain. $\hat{x}_{k+1}^{-}$ and P_{k+1}^{-} are the a priori state estimate and error covariance. $\hat{x}_{k+1}$ and P_{k+1} are the a posteriori state estimate and error covariance.

Is it assumed initial conditions $\hat{x}_0$ and P_0 are given. Often a further assumption is made stating that $S_k = 0$, i.e. the w_k and v_k are uncorrelated. It should be noted there are different formulations of the same algorithm in terms of how the state error covariance is expressed [138]**,** [139].

Model Implementation

In order to implement the KF, the interaction force signal dynamical model was used as described in the following evolution equations:

$$D_{k+1} = D_k + T(\tilde{u}_k + \tilde{d}_k) \tag{15}$$

$$M_{k+1} = M_k + TD_k + \frac{1}{2}T^2(\tilde{u}_k + \tilde{m}_k) \tag{16}$$

where the parameters M_k and D_k represent the k^{th} measured torque and its first derivative ($D_k = \frac{dM_k}{dt}$), and $\tilde{u}_k$ is the input to the dynamic model with Nm/s^2 units (different from T_L). T is the sampling time, and $\tilde{m}_k$ and $\tilde{d}_k$ express the measured force and the force-derivative noises respectively and have units of Nm/s^2. Expressing the system in matrix notation results in a multiple input single output linear system. The matrix form of the state and measurement equations is as given in (6) and (7) where the corresponding vectors and matrices are defined as

$$X_k = \begin{bmatrix} M_k \\ D_k \end{bmatrix}, w_k = \begin{bmatrix} \tilde{m}_k \\ \tilde{d}_k \end{bmatrix}, u_k = \begin{bmatrix} \tilde{u}_k \\ \tilde{u}_k \end{bmatrix}$$

$$A = \begin{bmatrix} 1 & t \\ 0 & 1 \end{bmatrix}, B = E = \begin{bmatrix} t^2/2 & 0 \\ 0 & t \end{bmatrix} \tag{17}$$

$$C = [1 \quad 0]$$

It should be noted that the interaction force is affected by the human applied force to the suppression system. Therefore, the KF model input u_k is considered unknown and does not contribute to the signal estimate (excluded from the time update step). The process and measurement noise parameter values and the initial state estimation $\hat{x}_0$ and state

error covariance matrix P_0 are defined below, with the assumption that $\tilde{m}_k$ and $\tilde{d}_k$ are uncorrelated.

$$w = \begin{bmatrix} 0.002 \\ 0.2 \end{bmatrix}$$

$$v = 0.01 \tag{18}$$

$$P_0 = BQB^T$$

$$\hat{x}_0 = \begin{bmatrix} 0 \\ 0 \end{bmatrix}$$

3.3.3. Filter Comparison

To demonstrate the feasibility of utilizing alternative filters in the 'Filter' block of **Figure 3.1**, an offline comparison between a KF and a LPF is shown in **Figure 3.7**. A 1st order Chebyshev filter with cut-off frequency of 2 Hz and 0.1 dB ripple was considered as a measure of comparison. The difference between each filter (LPF and KF) and the voluntary component was calculated and an RMS was applied to the error. A PSD was also calculated for each filter, and the total signal power (in the 2-6 Hz band) was obtained. The error RMS for the LPF and the KF were 0.21 and 0.13 rad/s respectively. The signal power reduction, relative to the total signal, for the LPF and the KF are 92.1% and 94.8% respectively. The LPF relatively small performance loss in relation to the KF suggests a LPF could be used successfully with the proposed suppression approach. Another work comparing between a LPF and the BMFLC with KF in [114] demonstrates superior performance to the latter filtering method.

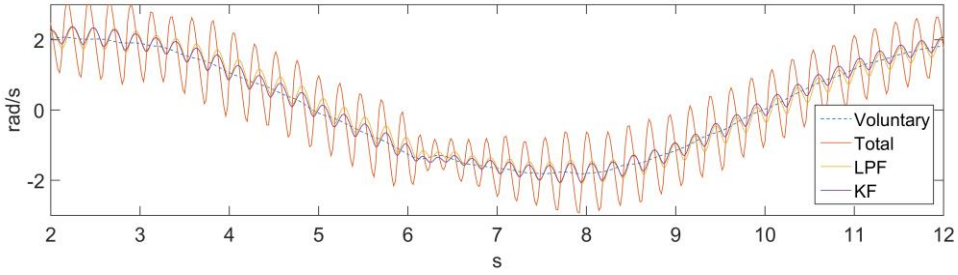

Figure 3.7 Kalman filter and a low-pass filter comparison.

3.4. Summary and Conclusion

A benefit of the proposed approach is that it avoids assumptions with regard to prior knowledge of the human musculoskeletal system parameters. In contrast, impedance control strategies for tremor suppression commonly rely on such information [83], [86], [68]. The controller used can be tuned successfully with no information concerning the mechanical properties of the human body part being affected. Tremor suppression approaches that estimate the tremor component often perform further computations to update the tremor signal estimation. Additional computations include modelling the tremor frequency and amplitude online [66], [68]. One such algorithm is the WFLC, which fits a sine wave to a tremor signal [140], [64]. Thus, the potential to avoid explicit processing of the tremor component is considered an additional benefit of the approach suggested here.

Most commonly, tremor suppression methods process primarily kinematic data in the control approach in order to establish the required attenuating signal. A motivation to using primarily admittance control in this work emerges from a realization concerning a potential limitation of kinematic control suppression algorithms. Namely, if a position (or velocity) controlled suppression is successful, then the reduced tremor motion would mean the signals based on which the algorithm performs the computations (e.g. position or velocity) also become reduced. A decrease in the signal amplitude can lead to smaller Signal to Noise Ratio (SNR) between a position or a velocity signal and any existing noise. Therefore, some restriction in implementation seems inherent to kinematic control based approaches, which can affect performance. Signal conditioning, such as filtering and amplification, have been used to mitigate signal degradation, and increase the SNR [68]. While the suppression of tremor signals leads to reduced motion signals, it also leads to more of the force associated with the tremor motion to be applied to, and absorbed by, the suppression system. Thus, in an admittance control approach, greater suppression of tremor leads to an increase in the force reading between the human and the suppression system, and consequently to an increase in the SNR of the force signal used in the control scheme.

3.5. Related Publications

G. Herrnstadt and C. Menon, “Admittance based voluntary driven motion with speed controlled tremor rejection,” *IEEE/ASME Trans. Mechatronics*, pp. 1–1, 2016.

Chapter 4.

Tremor Suppression Approach Validation via a Hardware Simulator

4.1. Benchtop Validation System

4.1.1. Background

Since in this line of research simulation systems are indicated and frequently employed [68], [86], [87], [88], [109], as they allow verification of the approaches prior to obtaining access to persons with tremor, a benchtop Tremor Simulation Device (TSD) was developed specifically to validate the proposed approach.

The TSD consists of two motors, which respectively simulate the motion of a human joint and the suppressing action of a mechanical suppression system. A parametric stability analysis of the proposed tremor-suppression strategy is presented. A motion profile recorded from a person with tremor is used as human input in the TSD to experimentally validate the proposed tremor rejection strategy.

In section 4.1.2 a benchtop simulator that was developed specifically to validate the proposed approach is presented. Parametric stability is demonstrated for a generic tremor suppression simulator in section 4.2, and also covers the controller tuning and an experimental analyses of the system via a step response. Results of the performed tests, using the benchtop device, are presented and discussed in Sections **4.3** and 4.4, with conclusions and limitations provided in section 4.5.

4.1.2. Validation Mechanism

We developed the TSD to evaluate the suppression approach. The TSD offers the opportunity to perform tuning and debugging before considering a specific system configuration to be tested with participants. The TSD, shown in **Figure 4.1**, is composed of two DC motors connected in-line with a torque sensor. A coupling is used to interface the components. The Driving Motor (DM) represents the person's generated input containing a low frequency motion, corresponding to the intentional component, and

superimposed by a higher frequency motion corresponding to the tremor component. The Suppression Motor (SM) and the torque sensor represent a generic suppressing robotic system.

The DM used in the TSD was a Brushless DC (BLDC) motor (Maxon EC 45 flat P/N 339287). A gearbox with a ratio of 18:1 was attached to the DM (Maxon Spur Gearhead GS 45 A P/N 301175). The DM assembled setup could generate up to 1.6 Nm of continuous torque. The DM was controlled in open-loop mode (velocity controller) in order to appreciate the effect of the suppression system. A commercial embedded controller (ESCON Module 50/5 P/N 438725) was used for this purpose. The SM was a BLDC motor (Maxon EC 45 flat P/N 339286). A gearbox with a ratio of 26:1 was attached to the SM (Maxon Spur Gearhead GS 45 A P/N 301173). The SM assembled setup generated up to 1.8 Nm of continuous torque. The SM was controlled using an embedded controller unit (ESCON Module 50/5 P/N 438725). A torque sensor (Transducer Techniques, TRT-100) was connected directly between the motors enabling the measurement of the interaction forces, equivalent to the forces between a human and a tremor suppression system. An amplifier and conditioning unit was used to acquire the torque sensor signal (Transducer Techniques, TM0-1).

The TSD controller implementation was developed in NI LabVIEW environment and operated at a sampling rate of 50 Hz ($dt = 0.02\ s$), using a data acquisition device (NI USB-6341).

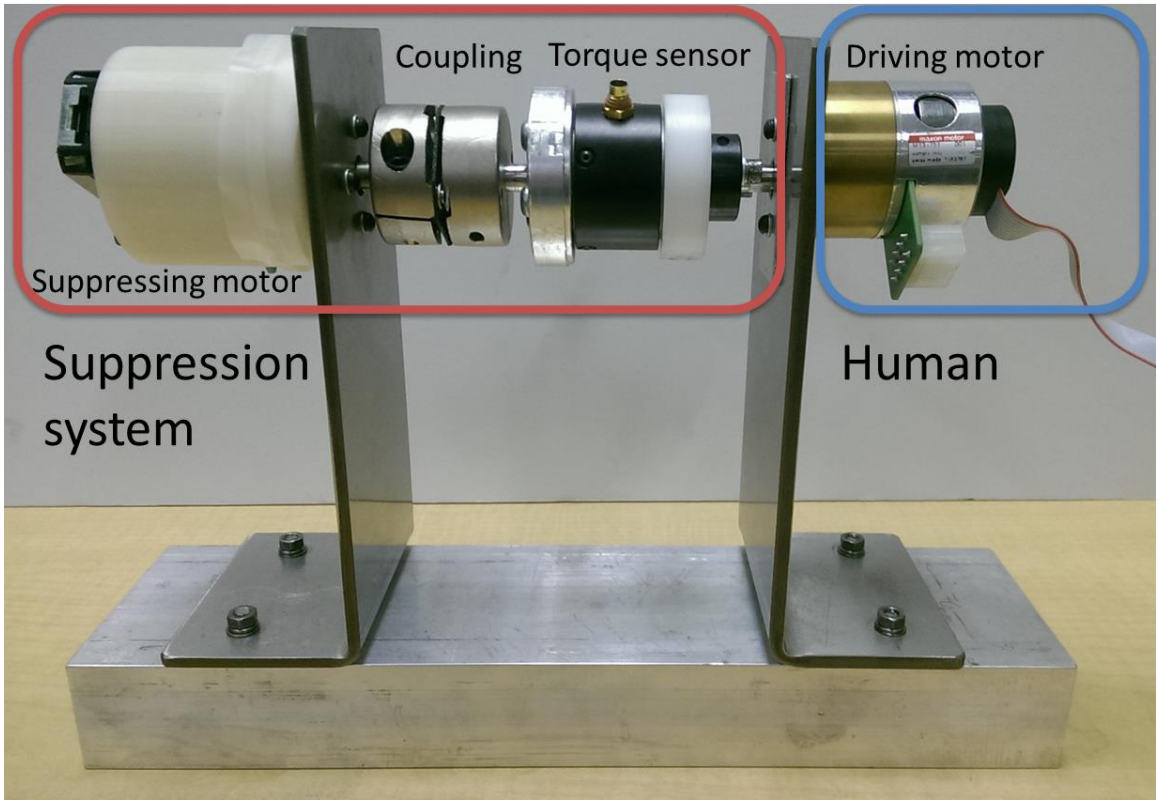

Figure 4.1 **Tremor Simulation Device (TSD). The Driving Motor (DM) represents the human input, and the Suppressing Motor (SM) and the torque sensor represent the suppression system.**

4.2. Stability and Performance Analysis

4.2.1. Feedback Stability

In order to analyse the stability of the feedback system for any human input, we formulated the Transfer Function (TF) between the human input T_L and the velocity output ω. For the purpose of the analysis, the plant $G(s)$ from **Figure 3.5** is expanded in **Figure 4.2**.

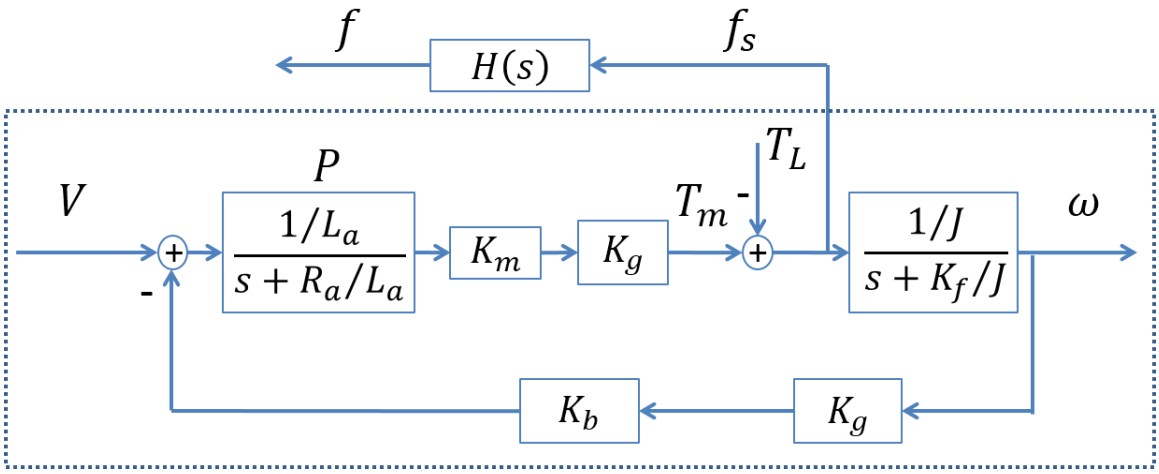

Figure 4.2 **Detailed plant G(s) diagram (encircled in dotted line) describing a BLDC motor with a gearbox. The suppression system consists of the plant G(s) and a force sensor H(s).**

The interaction force f in **Figure 4.2** can be described in the Laplace domain as follows:

$$f(s) = \big(T_m(s) - T_L(s)\big)H(s) \tag{19}$$

where $T_m(s)$ and $T_L(s)$ are the geared motor and human torques. The parameters in (19) can be expanded in terms of the human input $T_L(s)$ and the velocity $\omega(s)$ as follows:

$$f(s) = -\omega(s)R(s) - T_L(s)N(s) \tag{20}$$

where $R(s)$ and $N(s)$ are defined as (for clarity, the Laplace variable is dropped in the following formulations of this section):

$$R = \frac{YK_mK_gH}{1+WC_2K_mK_gH};\ N = \frac{H}{1+WC_2K_mK_gH} \tag{21}$$

where $Y(s), W(s)$ and $Z(s)$ are defined as

$$Y = \frac{(ZC_1+K_bK_g)P}{1+k_3C_1P};\ W = \frac{C_1P}{1+k_3C_1P};\ Z = 1 + k_2 + \frac{k_1}{s} \tag{22}$$

and $C_1(s), C_2(s), K_b, K_m, K_g$ stand for the PI and PID control blocks, back-EMF constant, torque constant, and the gear ratio respectively; $P(s)$ and $H(s)$ are the TF from the input

voltage to the resulting current, and the force sensor TF respectively (see **Figure 4.2**); $k_i, i = 1,2,3$ are the state feedback gains. The force sensor has a linear relationship between the force input and the voltage signal output. Additionally, the force sensor TF can be defined as a first order system $(1/\tau s + 1)$ [141]. Assuming the time constant τ to be much smaller than the response time of the suppression system, the sensor can be described as a constant. With the derivation for $f(s)$ in (20), the block diagram of **Figure 3.5** can be reorganized as in **Figure 4.3**. All the inner loops from **Figure 3.5**, with the exception of the $-i_a k_3$ feedback, are expressed in **Figure 4.3** as a single inner loop feedback. The SM current can be expressed as a function of both the velocity $\omega(s)$, and the interaction force $f(s)$. Thus, the feedback related to k_3 is observed in two separate paths in **Figure 4.3**, an inner loop and a feedforward (part of the outer loop). As shown in (20), the interaction force $f(s)$ can be expressed in terms of $\omega(s)$ and $T_L(s)$. Consequently, $f_{est}(s)$ is represented in **Figure 4.3** by the summation of the input path from $T_L(s)$ and the outer feedback loop.

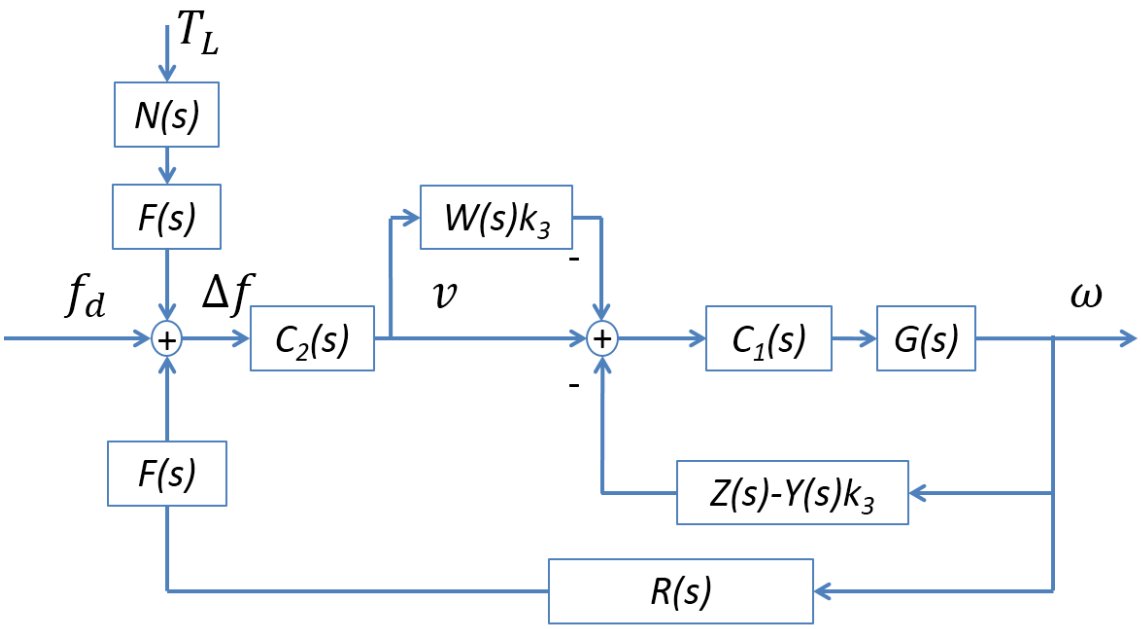

Figure 4.3 **Suppression system control diagram. The block diagram is similar to that of Figure 3.5 but organized to facilitate derivation of the TF from the human input to the velocity output.**

Based on the diagram of **Figure 4.3** it is straightforward to derive the TF from $T_L(s)$ to $\omega(s)$, remembering that $f_d = 0$. The resultant TF is

$$\frac{\omega}{T_L} = \frac{C_1 C_2 GNF(1 - Wk_3)}{1 + C_1 G(Z - Yk_3) - C_1 C_2 GRF(1 - Wk_3)} \tag{23}$$

where $G(s)$ is defined as follows:

$$G = \frac{K_g K_m}{JL_a s^2 + s(JR_a + K_f L_a) + K_f R_a + K_b K_g^2 K_m} \tag{24}$$

and $F(s)$ is simply the TF converted from the state space representation in (6) and (7). The parameters J, R_a, L_a, K_f are the total inertia, motor armature resistance, armature inductance, and the damping coefficient respectively.

The stability of the feedback system can be evaluated by examining the location of the eigenvalues or poles of the TF in (23). We first show the stability conditions for the equivalent internal system, comprising the speed and state feedback loops. Subsequently we analyse the outer admittance feedback loop stability with a PID controller. Since stability should be achieved regardless of the inclusion of a filter in the loop, the model for analysis is simplified, by excluding the KF block.

Internal Feedback System

Next the internal system is evaluated parametrically. The TF from desired velocity $v(s)$ to output velocity $\omega(s)$ is

$$\frac{\omega}{v} = \frac{C_1 G(1 - Wk_3)}{1 + C_1 G(Z - Yk_3)} \tag{25}$$

and can be obtained from (23) by substituting $C_2(s) = 1,\ N(s) = 1,\ F(s) = 1,\ R(s) = 0$. Substituting the corresponding transfer functions in (25) results in

$$\frac{\omega}{v} = \frac{K_m K_g(K_{vp} s^2 + K_{vi} s)}{a_{v4} s^4 + a_{v3} s^3 + a_{v2} s^2 + a_{v1} s + a_{v0}} \tag{26}$$

where $a_{vi}, i = 0,1,2,3,4$ are

$$a_{v4} = JL_a$$

$$a_{v3} = K_f L_a + JR_a + JK_{vp}k_3$$

$$a_{v2} = K_m K_g^2 K_b + K_{vp}K_m K_g + K_f R_a + JK_{vi}k_3 + K_f K_{vp}k_3 + K_m K_g K_{vp}k_2 \quad (27)$$

$$a_{v1} = K_{vi}K_m K_g + K_g K_m K_{vp}k_1 + K_f K_{vi}k_3 + K_m K_g K_{vi}k_2$$

$$a_{v0} = K_m K_g K_{vi}k_1$$

and $K_{v*}, * = p, i$ are the velocity PI gains. Using the Routh-Hurwitz Criterion [142], the elements of the first column of the Routh-Hurwitz table, $b_{v1} = (a_{v2}a_{v1} - a_{v3}a_{v0})/a_{v2}$, $c_{v1} = (b_{v1}a_{v1} - a_{v3}b_{v2})/b_{v1}$and $d_{v1} = a_{v0}$ are calculated. The conditions for LHP poles are then $b_{v1} > 0$, and $c_{v1} > 0$, which are a function of the system parameters and controller gains. Additionally, the system parameters are physical quantities that are positive by definition. Parameters and gains can be selected such that all stability conditions are met.

External Feedback System

The conditions for the PID admittance controller stability are developed next assuming stability has been achieved for the internal system. Substituting the respective transfer functions ($F(s) = 1; Z(s) = 0; k_i = 0, i = 1,2,3; C_1(s) = 1$) in (23) results in the following 3rd order parametric expression.

$$\frac{\omega}{T_L} = \frac{K_m K_g \left(K_{fp}s + K_{fd}s^2 + K_{fi}\right)}{a_{f3}s^3 + a_{f2}s^2 + a_{f1}s + a_{f0}} \quad (28)$$

where $a_{fi}, i = 0,1,2,3$ are

$$a_{f3} = J\left(L_a + K_{fd}K_m K_g\right)$$

$$a_{f2} = K_f L_a + JR_a + JK_{fp}K_m K_g + K_f K_{fd}K_m K_g \quad (29)$$

$$a_{f1} = K_f R_a + K_m K_g^2 K_b + JK_{fi}K_m K_g + K_f K_{fp}K_m K_g$$

$$a_{f0} = K_f K_{fi} K_m K_g$$

and $K_{f*}, * = p, d, i$ are the admittance controller PID gains. As mentioned, the parameters for the electromechanical system and of the controller in (28) are always positive. Calculating the elements of the first column of the Routh-Hurwitz table, $b_{f1} = \left(a_{f2}a_{f1} - a_{f3}a_{f0}\right)/a_{f2}$ and $c_{f1} = a_{f0}$, it can be shown the negative elements cancel out, and both b_{f1} and c_{f1} are always positive. No sign changes in the first column indicate no poles are in the RHP. Since there are no poles on the imaginary axis, the system is asymptotically (and bounded-input-bounded-output) stable. It should be noted, the external loop evaluated for stability is similar to that shown in **Figure 3.4**.

The parametric structure of the closed loop TF presented here could facilitate the design process of a tremor suppression system comprised of similar components. By taking into account the suppression system hardware parameters, desirable pole locations may be obtained, and thus the system performance may be tailored to specific requirements.

It may be of interest to examine the steady state error (Δf_{ss}) and the steady state response (ω_{ss}) to a unit step input (T_L).

$$\Delta f_{ss} = \left.\frac{s(\dots)}{a_{f3}s^3 + a_{f2}s^2 + a_{f1}s + a_{f0}}\right|_{s\to 0} = 0$$
$$\omega_{ss} = \frac{K_m K_g K_{fi}}{a_{f0}} = \frac{1}{K_f} \tag{30}$$

The former results in a zero error force while the latter in a constant velocity, inversely proportional to the damping coefficient, as shown in (30).

4.2.2. Controller Tuning

The Ziegler-Nichols method [143] can be used to obtain initial tuning of the admittance controller. We propose the following tuning approach. With the system as in **Figure 3.4** find the ultimate gain and period using the Ziegler-Nichols method, by introducing a small perturbation with the DM. The values obtained in the tuning of the

system of **Figure 3.4** can then be applied to the system in **Figure 3.5**. Further fine-tuning may be needed. Once the PID parameters are chosen, the state feedback can be added.

To obtain initial values for the state feedback gains, we first computed the poles of $G(s)$ using parameters from the components data sheets. Three poles for $G(s)$ were located; two were in the left half plane and one on the imaginary axis. Consequently, we calculated the required gains to move the imaginary pole to the left half plane. A placement of -0.1 was deemed suitable for the initial gains based on the TSD testing. The initial gains used were $k = [0.3679, 0.0092, 0.0025]$. Moving the imaginary pole further to the left resulted in too large gains and poor performance of the TSD. The state feedback gains used in our testing were $k = [0.185, 0.0092, 0.0025]$. It should be noted that the state feedback gains used effectively resulted in the position state feedback being the most significant, while rendering the velocity and current states feedback negligible. Setting a small gain for the velocity state also prevents redundancy with the inner velocity controller.

4.2.3. Step Response

To test the system with the designed parameters and to check that performance specification are met, a step response test was carried out. The DM step input was defined as a 2 rad/s step and is shown in **Figure 4.4**. The velocity input, associated with the case that the DM is disengaged from the SM (dashed blue line) serves as a reference to the TSD output velocity (solid red line). The interaction force (black line with circles) is also shown. The interaction force settles at around 0.08 Nm in steady state, close to the desired control goal. A first order LPF was used to smooth out the measured force. The step response results in a rise time of 200 ms, and a settling time of 1.06 s (for 8% of the final value). Additionally, there is about 20% velocity overshoot. The delay time, defined as the time between input and visible system response, was 80 ms [144], [145].

One of the main performance considerations for a system interfacing with a human is the response time achieved by the control system such that it would not be perceivable by the user. Findings by different researchers suggest delays between 100-700 ms are acceptable depending on the system tested and task performed [146]–[150].

A paper by Chen et al., reviewing human robot interaction performance, suggests negative effects to task performance can occur when delays are above 170 ms [151]. The time delay observed from our step response suggest our system achieves a performance that is suitable for a human interaction. It should be noted that such a delay could be substantially reduced with a real-time platform.

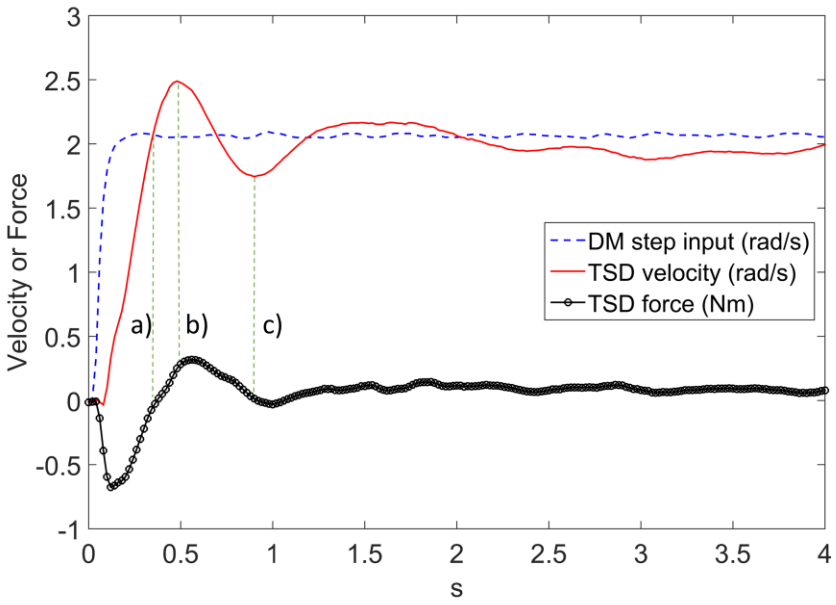

Figure 4.4 **Step response of the system in Figure 3.5. The blue dashed and red solid lines are the DM velocity input and TSD response respectively. The black line with circles is the TSD interaction force. The rise time and delay time are 200 and 220 ms respectively. The Settling time (within 8%) is 1.06 s.**

4.3. Experimental Results

The suppression approach described in **Chapter 3** was implemented with the TSD to assess its performance. The DM generated input was a superposition of both the voluntary and the tremor motion components. The DM driving input was constructed based on data recorded from a person with essential tremor (labelled et05) [152]. A sample acceleration data for et05, is shown in **Figure 4.5 A**, and the corresponding frequency spectrum is shown in **Figure 4.5 B**. The tremor data used for the simulation contained a principal tremor frequency at 4.3 Hz. Higher order harmonics can also be observed. Processing was done to convert the original data to angular velocity units

(**Figure 4.5 C**). Additionally, the original tremor data required resampling to match the simulation rate.

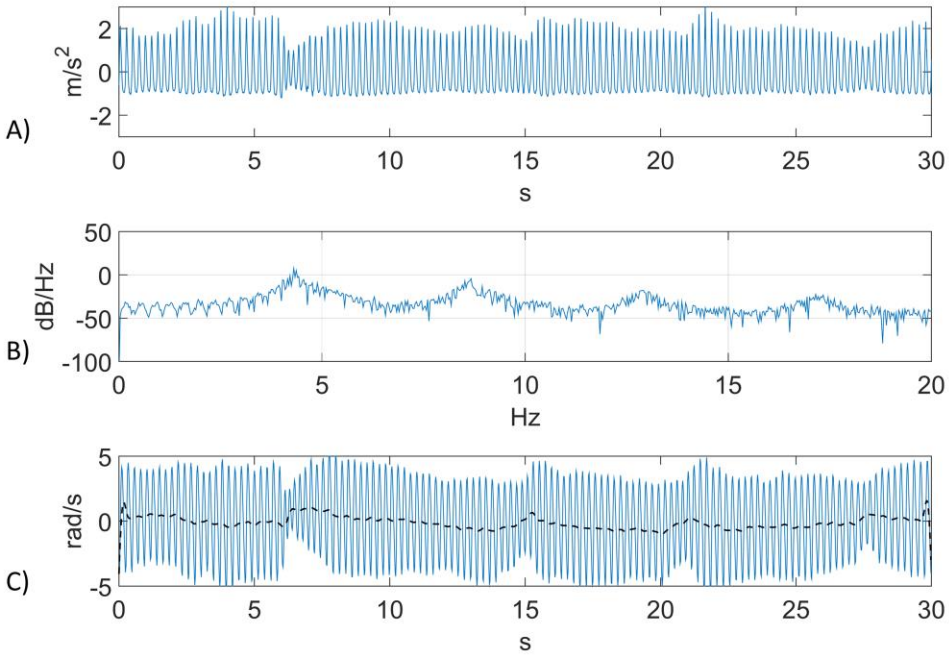

Figure 4.5 Tremor data of person et05 [152] **A) Linear acceleration data B) PSD C) Angular velocity and its zero-phase filtering.**

For the sake of clarity, we first consider the case where the tremor is not present, as discussed in section 3.3.1 and shown in **Figure 3.4**. The human input, produced by the DM, was defined as a velocity sinusoid having an amplitude of 2 rad/s and a frequency of 0.5 Hz representing a voluntary motion component [153], [154]. A force corresponding to (T_L) is associated with the above defined velocity human input. A first order LPF was used to smooth out the measured voluntary force. The results are provided in **Figure 4.6**, showing the velocity and interaction torque measured between the SM and the DM. The two lines shown in **Figure 4.6 A** are the input velocity signal, produced by the DM when disengaged from the SM, and the TSD output velocity signal produced with **Figure 3.4** control implemented. A tracking error and delay is observed between the two lines and is associated to software and mechanical time constants affecting the SM signal generation. Furthermore, the force associated with the DM input

velocity signal is relatively low, lending to the friction present in the system having a noticeable effect on the controller response. In particular, a recurrent error is observed around the peaks of the velocity signal. The recurrent error is caused when the force sensor output is close to zero. Additionally, in the above case, the SM is controlled in open loop velocity. The SM controller thus does not attempt to compensate for velocity lags.

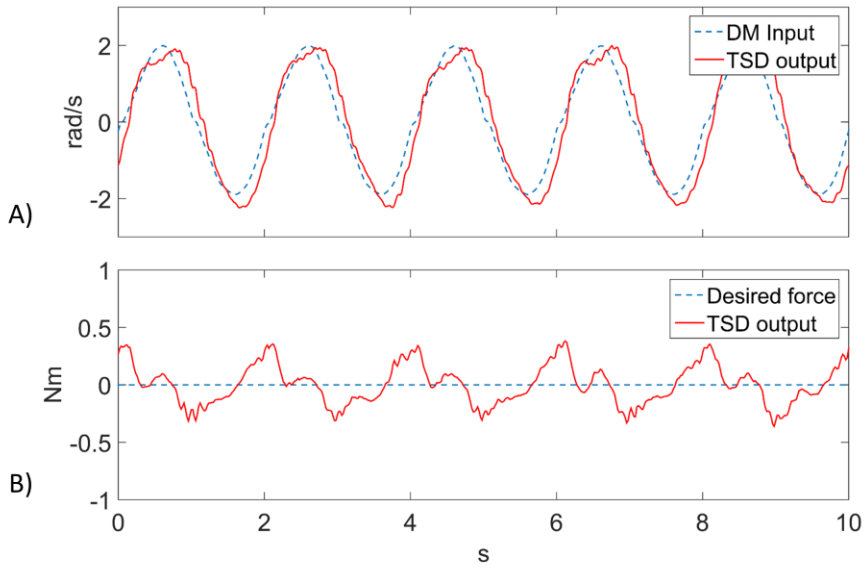

Figure 4.6 **Basic admittance control implementation. The TSD is controlled as in Figure 3.4. A) The input velocity produced by the DM when disengaged from the SM (blue dashed line) and output velocity of the TSD when engaged with the DM (red solid line). B) The measured interaction force (red solid line) and desired force (blue dashed line).**

The subsequent step involved implementing the tremor suppression control structure shown in **Figure 3.5**, with the results provided in **Figure 4.7**. In this case, the person's velocity data contained a relatively small ($< |1|$ rad/s) voluntary component amplitude that did not vary significantly, as shown in **Figure 4.5 B** and **C**. Consequently, a similar velocity signal to that used in **Figure 4.6 A** (frequency of 0.5 Hz and amplitude of 2 rad/s) was superimposed with the person's velocity data. The combined signal was

used as the DM velocity input. **Figure 4.7 A** shows three lines, the measured velocity when no suppression was present, its zero-phase LPF, representing the desired voluntary motion, and the SM suppression-on output.

It was necessary to obtain a reference signal to which the attenuated signal could be compared. The DM encounters resistance and friction loads caused by several components including its own gearing and bearing as well as the SM gearing and bearing, the latter likely representing a greater impact due to the reverse direction of the gearbox. Therefore, a signal with no suppression was obtained by physically disengaging the SM from the DM. Disconnecting the motors removed the resistance imposed on the DM by the SM. The desired voluntary velocity was obtained by offline zero-phase filtering of the suppression-off signal. The TSD suppression results were then compared relative to the desired velocity as shown in **Figure 4.7 A**. The maximum and RMS velocity error values are 1.33 and 0.57 rad/s respectively. The interaction forces between the DM and the SM are shown in **Figure 4.7 B**. The forces recorded indicate the SM was able to follow the DM, with the resistance remaining predominantly below 0.5 Nm. The maximum and RMS interaction forces recorded were 0.98 and 0.36 Nm respectively.

The suppression-on signal shows delay and tracking errors relative to the desired signal in **Figure 4.7 A**. Mechanical resistance in the system caused by friction, backlash, mostly in the gearboxes, and by assembly misalignment, contribute to tracking errors. Additionally, software delays as well as a slow build-up of DM force causes the controller to provide a slow velocity response relative to the suppression-off case. The largest velocity tracking errors are observed close to the velocity peaks (also zero acceleration) as shown in **Figure 4.7 A**. The same peak velocity tracking errors also correspond to the force DC crossing, i.e. near zero force as seen in **Figure 4.7 B**. In contrast, the largest forces are observed at the velocity zero crossings, where the forces also exhibit the most significant discontinuities. It is also interesting to note that the best tracking results are achieved at the velocity zero crossings.

To evaluate the level of signal attenuation, a PSD of the velocity signal was calculated. The signal power reduction was calculated as per (5) where P_{ON}^{f} and P_{OFF}^{f} are the total signal power in the suppression-on and suppression-off cases respectively. $PC\left(P_{ON}^{f}, P_{OFF}^{f}\right)$ was calculated separately for the voluntary and tremorous motions (and

respective frequencies). The 0-2 Hz frequency band was considered for the voluntary component [154]. It has been shown (for a position signal) that a large portion of the signal power is contained within the first two harmonics (above 94%) [68]. Therefore the 2-10 Hz frequency band, corresponding to the (1st and 2nd harmonics) was considered for the tremor component [7], [64], [68], [45]. A Hanning window was used in the PSD computation. **Figure 4.8** shows the logarithmic-scale PSD plot.

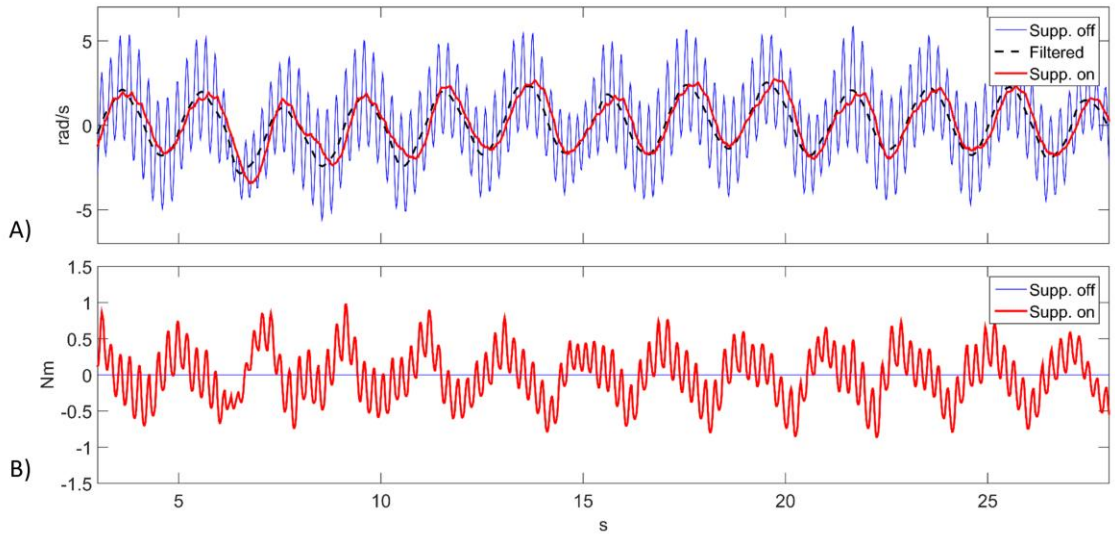

Figure 4.7 **Tremor suppression approach implementation. The TSD is controlled as in Fig. 3 A) Suppression-off (blue solid line), its zero-phase filtering (black dashed line) and suppression-on velocity (red solid line). B) The interaction force (red solid line) and desired force (blue solid line).**

In the frequency range associated with the involuntary movements above 2 Hz, a clear power attenuation to the first and second harmonics is observed, with above 99.9% power reduction of the 1st harmonic, 98.9% for the 2nd harmonic, and 99.8 for the combined harmonics. At the frequency of the voluntary velocity (around 0.5 Hz), the PSD active suppression overlaps closely with the suppression-off case as seen in **Figure 4.8**. The voluntary component power change resulted in 0.18% attenuation. With relation to the PSD results, the state feedback was significant in augmenting specifically the voluntary motion amplitude and thus to achieve a small reduction to the voluntary signal power in **Figure 4.8**.

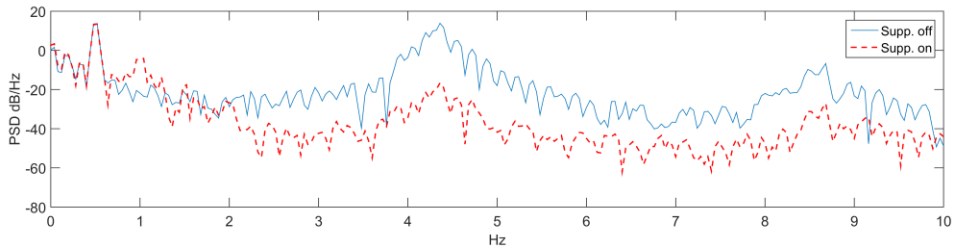

Figure 4.8 **PSD of the velocity signal. A clear difference can be observed between the suppression-off case (blue solid line) and the suppression-on case (red dashed line).**

4.4. Discussion

In reference to the step response test of **Figure 4.4**, we make several observations. First, it is noted that the velocity input generated by the DM (blue dashed line) is not an ideal step input, as it contains some delay in reaching the target value. Consequently the TSD velocity response (red solid line) is evaluated relative to the DM input rather than to an ideal step input. Second, the TSD response is driven by force and therefore influenced by the force that the DM is generating for the given velocity step. It is likely that a different electromechanical DM would have a different force profile when generating the same velocity step. In turn, the TSD would react differently. Third, the velocity variability observed after reaching the steady state is associated to low respective torques generated by the DM as seen in **Figure 4.4**. The above is also the motivation for selecting an 8% settling time range rather than the more standard 2 or 5%. Fourth, the velocity step response demonstrates a slightly underdamped system response with an overshoot of approximately 20%. The overshoots are again associated, to some degree, with the DM as it is slow to produce a substantive force that can guide the TSD to the desired velocity. Future research should focus on obtaining a more dampened response, in particular when implemented in a system involving a human interaction. Different filter implementations and PID tuning may help produce a more dampened response. Furthermore it is important to keep in mind that human movements typically follow a more gradual curve associated with lower frequencies such as shown in **Figure 4.6** and **Figure 4.7**. Fifth, the TSD interaction force (black line with circles) can be interpreted as follows. When the DM is actuated in order to generate the step profile, it encounters resistance by the SM. The first negative peak in the force, observed after the first five or so sample points, is associated to the resistance imposed by the SM. At this point the SM applies resistance acting in the opposite motion

direction, analogous to a friction resistance force. The interaction force starts to diminish once the TSD (SM+DM) begins the motion. The interaction force then becomes zero when the TSD velocity crosses the desired velocity as indicated by the vertical green dashed line a) in **Figure 4.4**. The TSD velocity then overshoots causing a resistance force, but this time with a positive sign. The interaction force sign has changed because the DM is slowing down in order to reach the desired velocity, as indicated by the middle green dashed line b). A similar pattern develops up to the vertical green dashed line c), after which the interaction force reaches its steady state. Factors contributing to the force steady state error (0.08 Nm) include calibration errors, the relatively large range of the sensor used 100 in-lb (11.3 Nm), and other mechanical disturbances. Therefore, the assumption made in section 3.3.1 concerning the slave and master impedances is reasonably satisfied in steady state. However, it should be noted that the above mentioned assumption refers to a theoretical condition, while in practice it may not be fully achieved [155]. The (master) impedance delivered to the user could nevertheless be mitigated by improving the electromechanical assembly and eliminating friction and mechanical disturbances.

Generally friction will have a significant influence at low velocities and at direction reversal [156], [157]. Yet in our testing results in **Figure 4.6** and **Figure 4.7**, the tracking errors observed that are associated to friction occur mostly at the velocity peaks. Consider the dynamic robot equation [158].

$$M(q)\ddot{q} + c(q,\dot{q})\dot{q} + g(q) = \tau - \tau_f \tag{31}$$

where *q* is the joint angle vector, *M* is the mass matrix, *C* is the Coriolis and centrifugal term, *g* is the gravity term and τ, τ_f are the applied and friction forces respectively. It is apparent from (31) that the significance of the friction forces will depend on their weight with respect to the other elements in the expression. Thus, assuming all the elements on the left hand side of (31) are fixed, then given a large driving torque τ, the friction force impact on the dynamic performance can be expected to be smaller compared to the case when the driving torque is small. In our testing, the acceleration and deceleration are largest at the velocity zero crossing. The acceleration is also proportional to the DM driving torque. Thus, the driving torques are largest at the velocity zero crossing, causing the friction forces to have less influence on the tracking performance. Conversely, the

smallest driving force values correspond to the velocity peaks (zero acceleration), which also coincide with the largest tracking errors. The above can account for the friction behaviour observed in our tests. Additionally, when generally referring to friction effects at low velocities there may be an implicit assumption that the driving forces are also low in conjunction with the low velocity [159].

As mentioned previously, the friction phenomenon is typically observed at low velocities. It should be considered that increased friction forces at lower velocities are indeed playing a role in the TSD testing results. The increased interaction forces observed during the velocity zero crossing might be evidence of the above. The large force discontinuities observed at the velocity zero crossing, particularly in **Figure 4.6 B**, are attributed to the DM direction change, resulting in an abrupt force drop. There is a transient velocity tracking error seen in **Figure 4.6 A** specifically associated to the force discontinuities.

It is interesting to note that the results in **Figure 4.6** and **Figure 4.7** display similar tracking patterns (e.g. largest errors at peaks) and not very dissimilar performance. Specifically, the maximum and RMS velocity error from the voluntary only implementation case (**Figure 4.6**) are 0.98 and 0.45 rad/s respectively (compare to 1.33 and 0.57 rad/s). The maximum and RMS interaction forces are 0.36 and 0.17 Nm respectively (compare to 0.98 and 0.36 Nm). Thus, the velocity tracking results are more comparable than the force results, where the voluntary case (**Figure 4.6**) outperforms the tremor case (**Figure 4.7**). The increased forces in the tremor case likely contribute to the larger maximum and RMS values observed in **Figure 4.7**. The above suggests that no significant artefacts or performance deterioration are introduced by the additional controller elements in **Figure 3.5** compared to **Figure 3.4**.

The tuning of the PID controller influences the tracking performance. Plant parameters are not explicitly required or utilized in the controller tuning. Nevertheless, improving the tuning further could lead to a reduction in the tracking delay observed in **Figure 4.6** and **Figure 4.7**. It should be noted that the limitations of linear controllers may prohibit overcoming disturbances and nonlinearities in the system. Employing a nonlinear controller or a linear controller synthesis based on an accurate plant modelling are potential ways to achieve superior tracking performance. Furthermore, improved

tracking as a consequence of controller adjustment will likely be associated to less impedance reflected by the master.

Taking a stepped approach in the implementation by first implementing the controller of **Figure 3.4** facilitated the verification of the feedback loop performance. Moreover, the tuning parameters of the PID admittance controller obtained for the schematic of **Figure 3.4** (see section **4.2.2**) were transferrable to the implementation of the controller of **Figure 3.5**, while requiring only minor adjustments.

Quantification methods evaluating suppression effectiveness haven't been standardized in the literature, making it difficult to compare systems' performances. A review of existing evaluation methods for tremor suppression is available in [7]. When evaluating the performance of a suppression system it is important to consider both spectral and temporal metrics. Additionally it is important to evaluate the forces perceived by a user of the suppression system. PSD is one common method used for evaluating tremor suppression in the frequency domain. For our PSD plots, we calculated the total signal power (over a 20 s period) for both the voluntary and the tremor frequency bands. For the time domain evaluation, we employed velocity tracking, calculating the error RMS. A summary of simulation systems for tremor suppression is provided in **Table 4.1**. Of the three systems presented, two represent rigidly actuated systems and one an FES system. Additionally, only the Repetitive Control of Functional Electrical Stimulation (RC-FES) system [73] had reported both frequency and time domain performance values related to the voluntary motion. The Tuned Vibration Absorber (TVA) [86] did report amplitude results for both the 1st and 2nd tremor harmonics, however only in dB. Thus, a tremor reduction in percentage of the full scale of the original signal power could not be attained. In contrast, both the RC-FES and the Torque Estimation Method (TEM) [68] provided percentage data for the tremor reduction. Our system achieves better reduction for both the 1st and 2nd harmonics. Finally, tracking errors were provided in both the RC-FES and TEM works for a position signal with an average error value of 8.4% and 2.09% respectively. Our system was controlled in velocity and achieved an RMS tracking error of 0.58 rad/s.

Table 4.1 Simulation Systems Review

Simulation System	DOF	Control Method	Amplitude/Power Reduction		Tracking Error
			Tremor (1st and 2nd harmonics)	Voluntary	
Tuned Vibration Absorber (TVA) [86]	2 [a]	Impedance control	1st: 14.27 dB and 13.93 dB 2nd: 9.7 dB and 4.95 dB	NA	NA
Repetitive Control of Functional Electrical Stimulation (RC-FES) [91]	1	Repetitive model-based controller	1st: 41.4%	12%	Position: $e_A = 8.4\%$ (11.098 deg)
Torque Estimation Method (TEM) [68]	1	Impedance control	1st: 35.78 dB (98.4%) 2nd: 12.24 dB (74.3%)	NA	Position: $e_A = 2.09\%$
Tremor Suppression Device (TSD)	1	Admittance and inner speed control	1st: 30.46 dB (99.9%) 2nd: 20.34 dB (98.9%)	0.3 dB (0.18%)	Velocity: $e_A = 4.17\%$ [b]. $e_M = 1.33$ and $e_{RMS} = 0.58$ rad/s.

NA indicates information wasn't available.

[a] Two joints attenuated with a single absorber.

[b] The % tracking error was calculated at each data point relative to the suppression-off signal and averaged. e_A, e_M, e_{RMS} refer to average %, maximum and RMS errors.

4.5. Limitations and Conclusion

The purpose of this chapter is to demonstrate the feasibility and working performance of the suggested tremor suppression approach. The next chapters will show the work done towards applying the approach to a system that can be validated with persons with tremor. This method can be easily realized in a multiple joint system. Because no musculoskeletal model of the arm is needed, distal and proximal joints can be treated independently to achieve separate attenuation. The above is particularly true when using a geared motor, which reduces nonlinearities and decouples joints [160].

One potential limitation for the TSD, in terms of mechanical integrity, relates to the force level of the unintentional motion. Data referring to tremor torque values is limited; however other researchers have restricted robotic actuated torques to approximately 3 Nm when testing with participants [64]. Specifically for the TSD, using a direct drive method, without gearing, and improving assembly alignment accuracy may

improve the velocity tracking performance. It should be noted that passive dampers (e.g. a brake) might not be suitable for the approach presented here, as they cannot produce a movement to track the desired human motion [161].

This chapter presented an approach to tremor suppression. The suppression controller employs an admittance feedback with an internal velocity feedback. The controller results in tracking of the voluntary motion while rejecting the tremorous motion. The obtained results are promising. In particular, a significant reduction to the tremor signal is observed (above 99%) while the volitional motion signal power is minimally affected (less than a 0.2%).

4.6. Related Publications

G. Herrnstadt and C. Menon, “Admittance based voluntary driven motion with speed controlled tremor rejection,” *IEEE/ASME Trans. Mechatronics*, pp. 1–1, 2016.

Chapter 5.

An Elbow Orthosis for Speed Controlled Voluntary Driven Tremor Suppression

5.1. Introduction

We have developed a one DOF elbow orthosis that could be worn by an individual with tremor. A speed controlled voluntary driven suppression approach is implemented with the orthosis. As mentioned in **Chapter 3**, typically tremor suppression methods estimate the tremor component of the signal and produce a canceling counterpart signal. The suggested approach, instead estimates the voluntary component of the motion. A controller then actuates the orthosis based on the voluntary signal while simultaneously rejecting the tremorous motion.

We tested the suppressive orthosis using a 1 DOF robotic system that simulates the human arm. Two different kinds of arm motion profiles, namely velocity and torque, were considered and consequently investigated to demonstrate the suppression approach can successfully attenuate tremor regardless of the type of profile the human arm is generating.

The suggested suppression approach does not require a model of the human arm. The orthosis forearm gravitational forces are considered as part of the disturbance to the suppression system along with the human input. Therefore the suppression system can be modeled linearly. Two cases are demonstrated for the compensation of the orthosis forearm gravitational forces involving compensation by the suppression system and by the human.

The electromechanical design of the orthosis is presented, and data from two patients having Essential Tremor and Parkinson's disease are used as the human input. Velocity tracking as well as PSD results for both the velocity and torque driven cases are presented.

5.2. Orthosis System

An orthosis system was developed in order to validate the suggested tremor suppression approach through experimental testing [162]. The orthosis, shown in **Figure 5.1**, is a 1 DOF system targeting the human elbow, composed of a SM, gearing, sensors that include a force transducer and an encoder, and upper and forearm braces. The SM gearing include an off the shelf spur gearbox with a reduction ratio of 26:1 and additional external spur gears with a reduction ratio of 120:72. The upper and forearm braces as well as the main body of the orthosis were 3D printed using an ABS plastic variant. An aluminum beam is used to connect the forearm brace to the main orthosis body. Several fit adjustments were incorporated into the orthosis design as shown in **Figure 5.1 A**. Adjustment for upper arm length is achieved through sliding of the top and bottom supports, while adjustment for the forearm is made possible through two passive intersecting joints (P1, P2) in the forearm brace as shown in **Figure 5.1 A**. The donned orthosis is demonstrated in **Figure 5.1 B**. The orthosis is all but symmetric. Adjustability for right or left arms is achieved by replacing only a single part (marked in **Figure 5.1 B**), and switching between the upper arm top and bottom sliding supports.

In this chapter, the tests are limited to the evaluation of a test-bench (no individuals with tremor are included) in order to evaluate the feasibility of the proposed approach and orthosis. For this purpose, a DM is added to the orthosis (see **Figure 5.1 A**) to simulate the tremorous input that could be provided by a human subject. Details of the orthosis components and performance are provided in **Table 5.1**.

Table 5.1 Orthosis system specifications.

Components		Performance	
Name	**Model #**	**Criteria**	**Value**
SM	Maxon EC 45 flat P/N 339286	Stall torque (Nm)	16.5
SM gearbox	26:1 Maxon Spur Gearhead GS 45 A P/N 301173	Continuous torque (Nm)	3
DM	Maxon EC 45 flat P/N 339287	Weight (g)[1]	1600
DM gearbox	18:1 Maxon Spur Gearhead GS 45A P/N 301175	Max speed (rpm)	109.1
Force Transducer	Transducer Techniques, TRT-100	Elbow range (°)	0 - 120
Force Amplifier	Transducer Techniques, TM0-1		

[1] DM not included in the measurement.

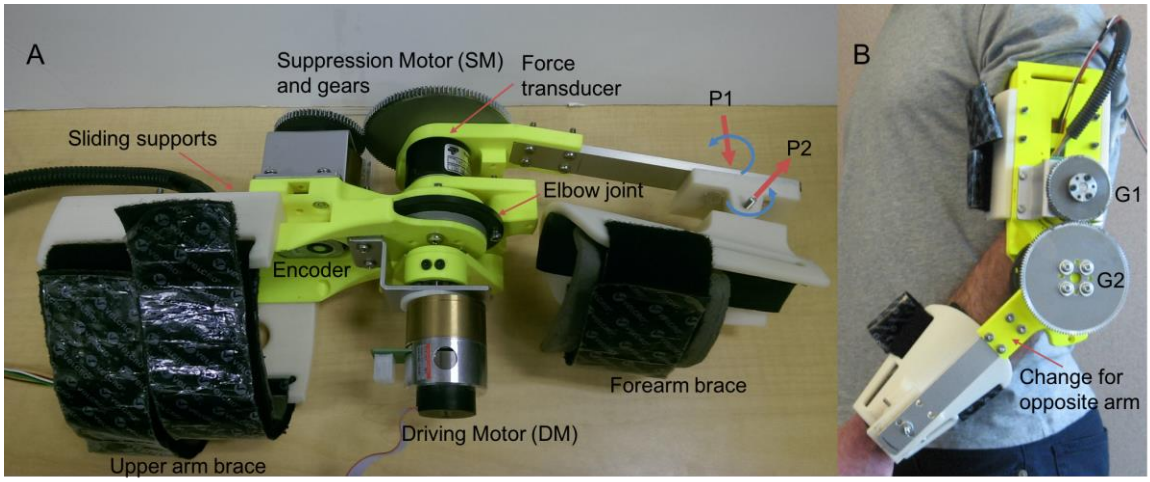

Figure 5.1 Orthosis system. A) The orthosis simulation system connected to the DM. P1 and P2 indicate the two passive wrist joints. B) The orthosis donned.

5.3. Orthosis Control

The control of the orthosis was implemented using the feedback loops shown in the block diagram of **Figure 5.2**. A PID force controller was used as the admittance block [155], and a PI controller was used as the speed controller corresponding to the elementary blocks of the approach presented in **Figure 3.1**. The filter block was

implemented with a KF (see section 3.3.2), a stochastic estimator that is often employed in both tremor suppression as well as non-tremor related applications [163], [164]. As mentioned in section 3.1, tremor and voluntary motion frequencies typically have little overlap. ET and PD frequencies are considered to be in the range of 4-12 Hz and 4-6 Hz respectively, while ADL tend to be in the range of 0-2 Hz [68], [133], [165]. The KF regards the tremor component as a stochastic noise and is therefore able to distinguish it from the voluntary component. Other filters may be used successfully, such as a g-h filter, or a LPF as shown in section 3.3.3. However, it should be noted that a chosen filter's performance is expected to influence the overall suppression system performance. $G(s)$ refers to the SM and gearbox model, that form part of the suppressive system along with the force sensor. A state feedback was also incorporated to improve the speed controller tracking. The controller in **Figure 5.2** is equivalent to that in **Figure 3.5**, shown to be stable, with the addition of a gravity feedback loop. Several saturations were implemented with both the speed controller, limiting the acceleration/deceleration of the SM (± 23077 rpm/s), and with the force controller, limiting its output velocity into the speed controller (± 115 rpm).

In this work, in addition to the human input labeled T_h, the disturbance to the suppressive system also includes the orthosis forearm gravitational forces (nonlinear dynamics) labeled T_g, as shown in **Figure 5.2**. The gravity disturbance component due to the orthosis forearm link can be approximately compensated with an additional loop as shown in the top loop such that the signal f_g and subsequently Δf entering into the admittance controller acts to counteract for the gravity component. The admittance controller can be represented as

$$\omega_c = K_{fp}\Delta f + K_{fd}\frac{d\Delta f}{dt} + K_{fi}\int_0^t \Delta f ds \qquad \textbf{(32)}$$

where K_{fp}, K_{fd}, K_{fi} are suitable PID gains, and ω_c is the controller velocity output. The input to the force controller is defined as

$$\Delta f = f_{est} + f_d - f_g \qquad \textbf{(33)}$$

where f_{est}, f_d, f_g are the estimated voluntary interaction force applied to the orthosis, the desired interaction force and the gravitational force respectively. It should be noted the orthosis forearm link physical parameters are predetermined and known; thus the gravity load is deterministically known and bounded. The gravity compensation is updated online as a function of the measured position [105], [166].

The suppression system is intended to be transparent to the user such that when pushed against, the orthosis moves away with minimum resistance (i.e. $f_d = 0$ in **(33)**) [134], [167]. Furthermore, it is assumed the human is capable of performing voluntary motions independently as well as counteracting the gravitational forces acting on their own limb unassisted. Therefore, compensation for the human arm by the suppression system is not incorporated.

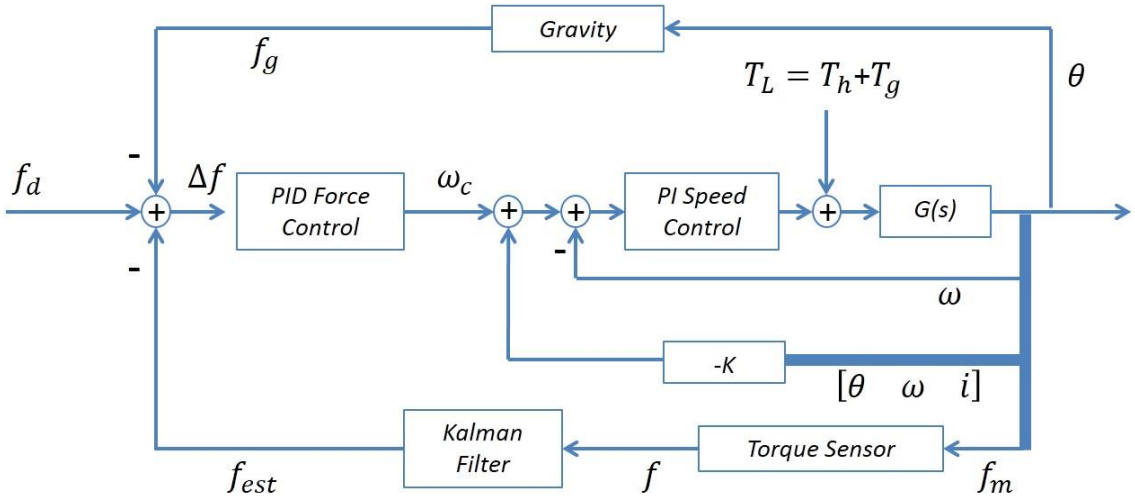

Figure 5.2 Orthosis control diagram. The controller includes a force feedback, with an inner speed controller and state feedback, as well as a gravity compensation loop.

5.4. Experimental Procedure

This work involved simulating the human input to the system with the DM. The purpose of the simulation is to validate the tremor suppression approach using the orthosis prior to testing with a human subject. Experimental simulations can help to optimize and debug the system, while promoting its safety. Data from two patients with ET and PD [152] was used as an input to the DM simulating the human motion. Additionally, two kinds of inputs were provided, namely a velocity profile input and a torque profile input. A human user of the proposed system may, when using the system,

provide an input that is constructed of either kind or of a combination of the two kinds of input profiles. The two inputs were used in order to demonstrate the system could perform successfully with either input type. The patients' raw data used in the experimental simulations was preprocessed to convert it (from linear acceleration units) to appropriate input signal units of velocity and torque.

Furthermore, two strategies for compensating the orthosis forearm gravity force were demonstrated. In one case the gravity was compensated by the suppression system while in the other case, the human compensated for the orthosis forearm gravity force. The former gravity compensation case was implemented in conjunction with the velocity driven input, while the latter was implemented with the torque driven input case. When implementing the gravity compensation loop as shown in **Figure 5.2**, the physical parameters of the orthosis forearm were used. The forearm link and cuff, of the prototype fabricated in our lab (**Figure 5.1**), have an equivalent moment arm and mass of approximately 117 mm and 290 g respectively.

The performance of the suppression-on case was evaluated relative to the unsuppressed case, representing the free human tremor without the effect of the suppressive system. As in section 4.3, the acquisition of the suppression-off signal was done with the DM physically disconnected from the suppression system. It should be noted that the reference velocity signal was obtained offline, from the suppression-off data, for the evaluation of the system and would not be available in a real application with a human user.

The admittance (PID) controller tuning was done heuristically, however, initial controller values can be found based on the Ziegler and Nichols method [143] as mentioned in section **4.2.2**. The ultimate gain and period procedure can be applied to the closed loop orthosis system. A small perturbation is provided with the DM and the proportional gain is increased until constant oscillations are achieved. The ultimate gain and period can then be extracted in order to obtain the initial controller gains.

As mentioned in section **5.3**, the control goal was defined as $f_d = 0$. However, it is noted that while fine-tuning the controller, the suppression-on velocity signal was also considered relative to the desired reference velocity (suppression-off). Some performance compromise between achieving a small interaction force and close velocity

tracking was required. Generally, the derivative gain contributed less to the overall performance, as is often the case in practice [168]. The state feedback was added once the PID tuning was obtained. The PI controller was pre-tuned by the manufacturer.

A PC and a data acquisition device (NI USB-6341) were used in the experiments to collect and process the signals. Programing and control algorithms were implemented in NI LabVIEW 2014 software. Additionally, MathWorks Matlab R2015b was used for offline processing and for producing plots.

5.5. Experimental Results

5.5.1. Velocity Based

The input provided by the user follows a velocity profile. The velocity input was constructed from data of an ET patient (et02). The original raw data and its PSD plot are shown in **Figure 5.3**. The patient data has a first harmonic tremor frequency at 4.3 Hz. Once the patient data was converted to angular velocity units, it was superimposed with a sinusoidal velocity signal having a frequency of 0.8 Hz and amplitude of 1 rad/s, representing the voluntary motion. The gravity compensation for the orthosis arm was performed by the suppression system as demonstrated in **Figure 5.2**. As mentioned in section **5.4**, the unsuppressed intentional velocity was acquired in order to serve as a reference for the suppression-on case. A velocity signal was recorded and zero-phase filtered while the DM was physically disengaged from the robot arm and the SM, representing the unsuppressed human motion containing the voluntary and tremor components. When activated, the suppression system should track the filtered velocity signal associated with the suppression-off case.

The velocity tracking and interaction forces obtained are shown in **Figure 5.4**. Velocity tracking errors are apparent at the peaks of the sinusoid motion in **Figure 5.4 A**. The velocity peaks correspond to the interaction force crossing the zero line. The forces, produced by the DM, around the zero crossing are less consistent and consequently are responsible for larger velocity tracking errors. The RMS values of the velocity tracking error and of the interaction force signals are 0.31 rad/s and 0.44 Nm respectively. The PSD of the suppression-off and suppression-on signals were also compared as shown in **Figure 5.5**. A clear power reduction can be observed in the tremor frequencies,

particularly above 2 Hz, while in the vicinity of the intentional motion frequency (0.8 Hz) the signals overlap, indicating a small impact to the voluntary component. The tremor power reduction for the 1st and 2nd harmonics was 99.8 and 99.1% respectively and 99.8% combined, while the intentional component power was increased by 0.15%.

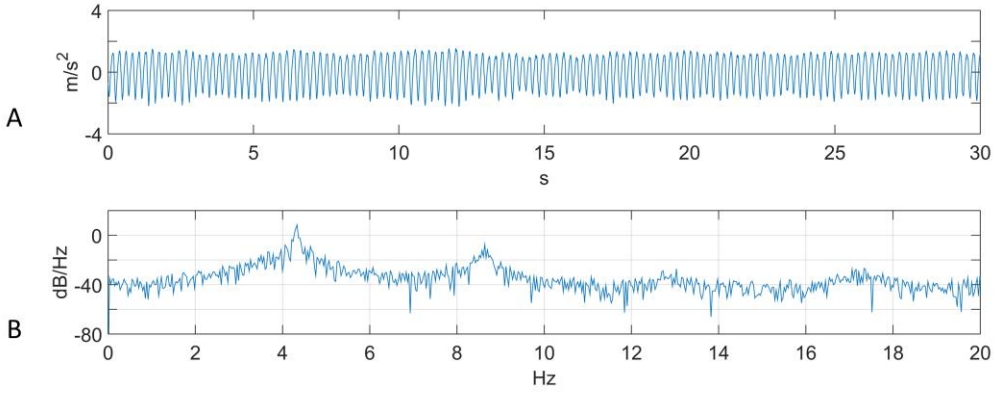

Figure 5.3 ET patient data (et02). A) Linear acceleration. B) PSD. A first harmonic tremor frequency is observed at 4.3 Hz.

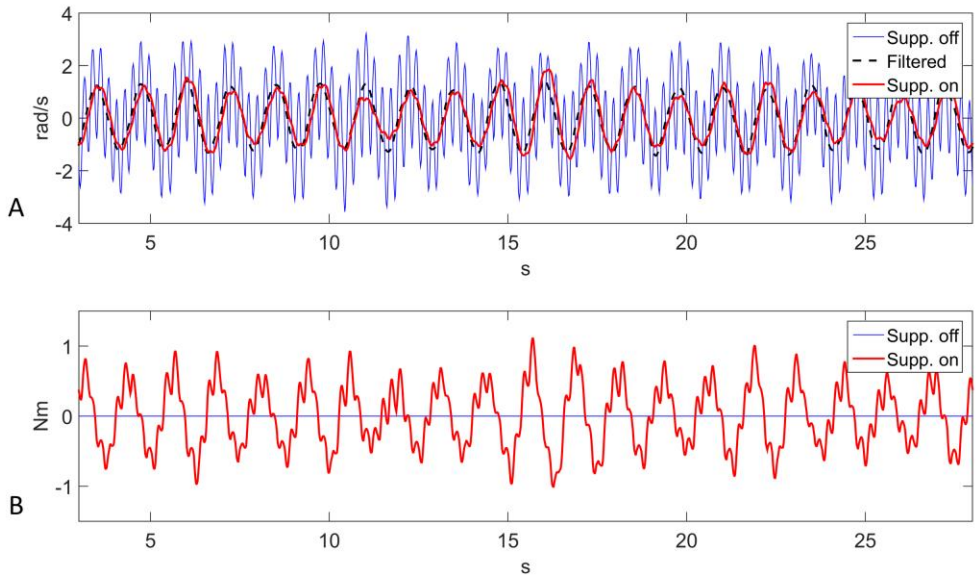

Figure 5.4 Velocity driven case suppression velocity and force tracking results. A) Velocity tracking B) Interaction force.

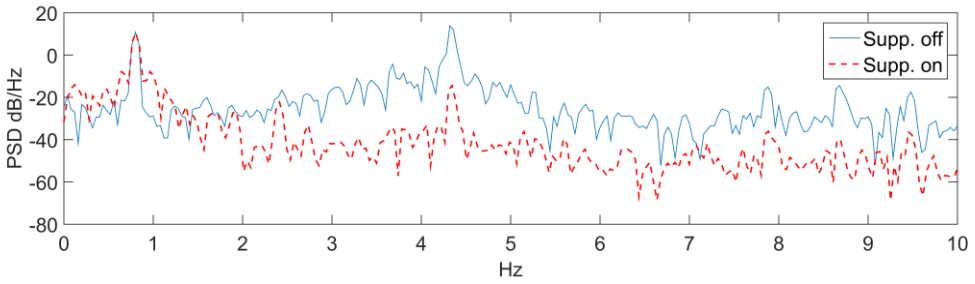

Figure 5.5 Velocity based input, PSD of suppression-on and -off cases.

5.5.2. Torque Based

In the torque driven case the input provided by the user follows a torque profile. The DM (user) in this case performed the gravity compensation for the orthosis arm, thus the control is as demonstrated in **Figure 5.2**, excluding the gravity (top) loop. It is assumed a user would be able to carry the load imposed by the orthosis arm. The torque input was constructed from data of a PD patient (park05). The original raw data and its PSD plot are shown in **Figure 5.6**. The tremor data from the patient has a first harmonic tremor frequency at 4.5 Hz, which was superimposed with a sinusoidal torque signal having a frequency of 0.8 Hz and amplitude of 0.3 Nm, representing the voluntary motion. As in the velocity driven case (section 5.5.1), the intentional velocity associated with the input torque signal was acquired in order to serve as a reference for the suppression-on case. The velocity signal was recorded while the DM was physically disengaged from the SM but with the robot arm attached, representing the unsuppressed human motion, containing the voluntary and tremor components. Consequently, zero-phase filtering of the suppression-off velocity resulted in the voluntary velocity component that would serve as the reference signal. When activated, the suppression system should track the filtered velocity signal associated with the suppression-off torque signal.

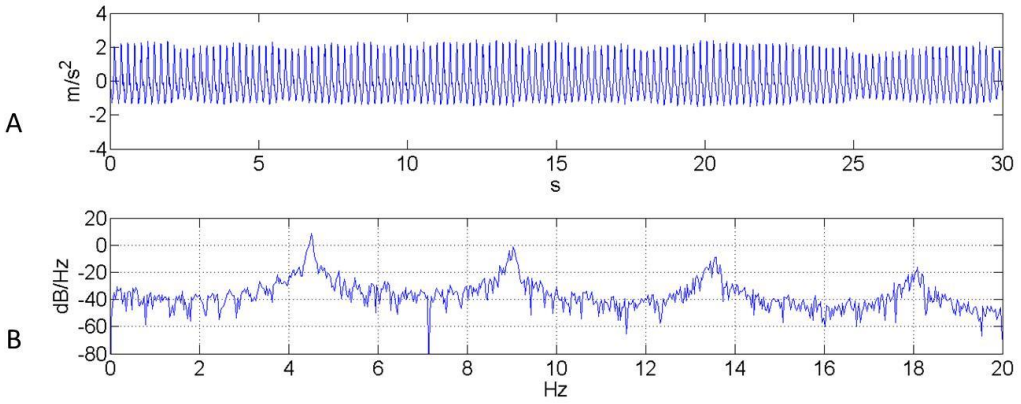

Figure 5.6 PD patient (park05) data. A) Linear acceleration. B) PSD. A first harmonic tremor frequency is observed at 4.5 Hz.

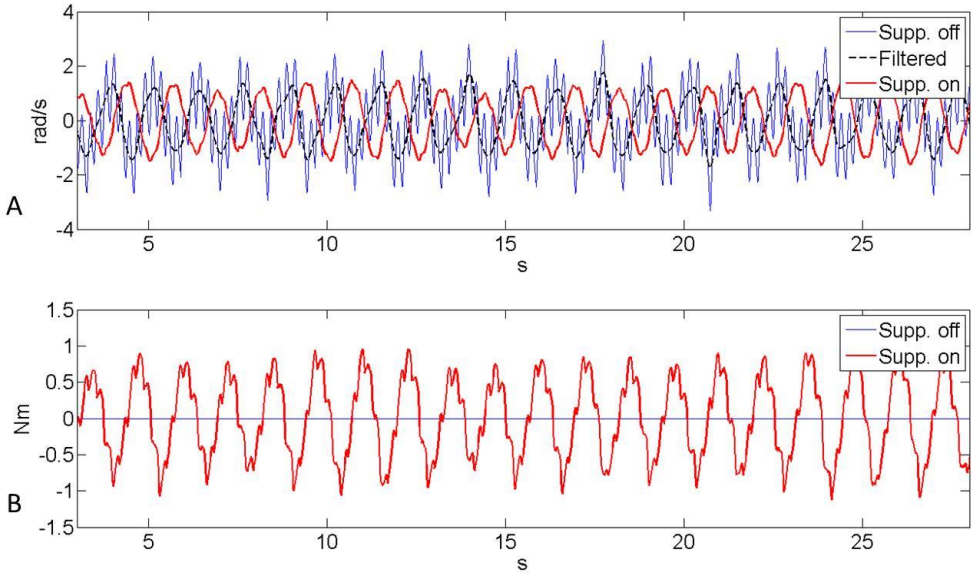

Figure 5.7 Torque driven case suppression velocity and force tracking results. A) Velocity tracking B) Interaction force.

The velocity tracking and interaction forces obtained are shown in **Figure 5.7** [169]. A delay of approximately 0.5 s is observed in the velocity-tracking signal. The delay is explained by the fact that the torque driven case does not define a specific velocity profile. Rather, the associated velocity profile amplitude and phase depend on the load. To demonstrate the aforementioned and to analyze the delay, a system is considered composed of an ideal torque generator representing the DM, and with inertial and damping loads resisting the motion. The system model is defined as

$$J\ddot{y} + B\dot{y} = L\sin(\lambda t) \tag{34}$$

where J, B and L are the inertia, damping, and input torque amplitude respectively. y is the dependent variable (in our case angular position) and $\lambda = 2\pi f$where f is the input signal frequency in Hz. The term on the right side in **(34)** represents the input torque generated by the DM, while the terms on the left side represent the loads resisting the DM. The expression in **(34)** is a second order Ordinary Differential Equation (ODE). The general solution to the ODE is composed of complimentary and particular solutions having the following forms

$$y = y_c + y_p$$

$$y_c = C_1 + C_2 e^{-\frac{B}{J}t} \tag{35}$$

$$y_p = \alpha\cos(\lambda t) + \beta\sin(\lambda t)$$

where C_1, C_2 are constants of the complementary solution y_c and t is the independent variable (time in our case). The particular solution y_p is a summation of a sine and cosine where α and β are functions of J, B, λ and L as follows

$$\alpha = -\frac{LB}{\lambda(J^2\lambda^2 + B^2)}$$

$$\beta = \frac{J\lambda}{B}\alpha \tag{36}$$

The particular solution can also be expressed as a sine function with a phase shift as follows

$$\alpha\cos(\lambda t) + \beta\sin(\lambda t) = \gamma\sin(\lambda t + \phi) \tag{37}$$

where γ and ϕ are defined as

$$\gamma^2 = \alpha^2 + \beta^2 \tag{38}$$

$$\phi = \tan^{-1}\left(\frac{\alpha}{\beta}\right)$$

Substituting **(36)** into the expression for ϕ in **(38)** results in the following

$$\phi = \tan^{-1}\left(\frac{B}{J\lambda}\right) \quad \textbf{(39)}$$

The expression in **(39)** describes the phase shift as a function of the load inertia and damping as well as of λ. The complimentary solution does not contribute to a phase change; instead the exponential in y_c is responsible to the decay of the signal. The above analysis provides a rationalization for the delay observed in the velocity tracking of the torque driven case. Furthermore, it suggests the delay is not directly related to the suppression system but rather is linked to how the DM is affected by any resistive loads acting on it.

To validate the above model **(34)**, the relationship between J and B From **(39)** is explicitly derived as a linear relationship where B is a function of J as follows

$$B = J\lambda \tan\phi \quad \textbf{(40)}$$

We can obtain the value for $\lambda = 5.0265$ rad/s from our experiment input frequency ($f = 0.8$ Hz). The time delay, and therefore the phase shift ϕ, can be obtained from the experiment results. Next, we find a value for the load inertia applied to the DM by the orthosis system. The expressions for the total inertia, reflected at the DM shaft, for the orthosis suppression-on and -off system configurations are calculated as

$$J_{ON} = J_m + J_{gdm} + \frac{\left(\left(\left(J_m + J_{gsm}\right)K_{gsm}^2 + J_{G1}\right)K_{ge}^2 + J_{G2} + J_l\right)}{K_{gdm}^2}$$

$$J_{OFF} = J_m + J_{gdm} + \frac{J_l}{K_{gdm}^2} \quad \textbf{(41)}$$

where $J_l, J_m, J_{gsm}, J_{gdm}$ are the orthosis arm, the SM (or DM), SM gearbox, and the DM gearbox moment of inertias respectively. $J_{Gi}, i = 1,2$ are the external gears moment of

inertias, and K_{gsm}, K_{gdm}, K_{ge} are the SM gearbox, DM gearbox, and external gear reductions respectively. Note that the free tremor motion (suppression-off) was recorded while the DM was connected to the robot arm. Substituting the orthosis system parameter values in **(41)** results in a total moment of inertia of $J_{OFF} = 3.2e-05$ Kgm^2 and $J_{ON} = 1.136e-04$ Kgm^2 for the suppression-off and suppression-on cases respectively. For the phase values (ϕ) we look at the phase shift between the input current (A) and the output position (rad). The time delays for the suppression-off and -on cases are 0.76 *s* and 1.32 *s* respectively, which converts to $\phi_{OFF} = 3.7824$ and $\phi_{ON} = 6.6978$ rad.

Consequently, substituting the above calculated inertia values from **(41)** and the values for λ and ϕ_{OFF}, ϕ_{ON} in **(40)**, we can find the respective damping coefficients $B_{OFF} = 1.2e-04$ Nm/(rad/s) and $B_{ON} = 2.514e-04$ Nm/(rad/s).

We can graphically analyse the delay observed in **Figure 5.7** by reviewing the Bode phase plot between the armature current and output position of the DM. The following TF describes the relationship between the DM input current and the output position

$$\frac{\theta(s)}{I(s)} = \frac{K_{gdm}K_t}{s(Js+B)} \quad \textbf{(42)}$$

where $\theta(s), I(s)$ and K_t are the output rotational position, the input current, and the DM torque constant respectively. The expression in **(42)** can be written in the time domain as a function of the angular position as follows

$$J\ddot{\theta} + B\dot{\theta} = K_{gdm}T_m \quad \textbf{(43)}$$

It is interesting to note the expression in **(43)** is equivalent to that in **(34)**, with the only difference being the term on the right side. In **(34)**, the right side term is expressed as a sinusoid multiplied by a constant, while in **(43)** it is expressed simply as the motor torque parameter T_m multiplied by a constant. Furthermore, we consider the following DM TF (from DM input voltage to output position)

$$\frac{\theta(s)}{V(s)} = \frac{K_{gdm}K_t}{s\left(JLs^2 + JRs + BR + K_eK_{gdm}^2K_t\right)} \quad \textbf{(44)}$$

where $V(s), L, R$ and K_e are the armature voltage, armature inductance, armature resistance, and the back EMF constant.

The Bode phase plots of the two DM transfer functions, **(42)** and **(44)**, are shown in **Figure 5.8**, where the former is represented by the red lines (torque driven case), and the latter is represented by the blue lines (velocity driven input case). Each case is plotted for two values of inertia and damping, namely suppression-off (solid line) and suppression-on (dashed line). In order to show both the suppression-on and –off cases on the Bode plot, the ϕ_{ON} was phase shifted by $-\pi$. Phase shifting does not affect the inertia and damping values calculations, and allows to see both angles within the Bode plot phase range of $\pi/2$ rad.

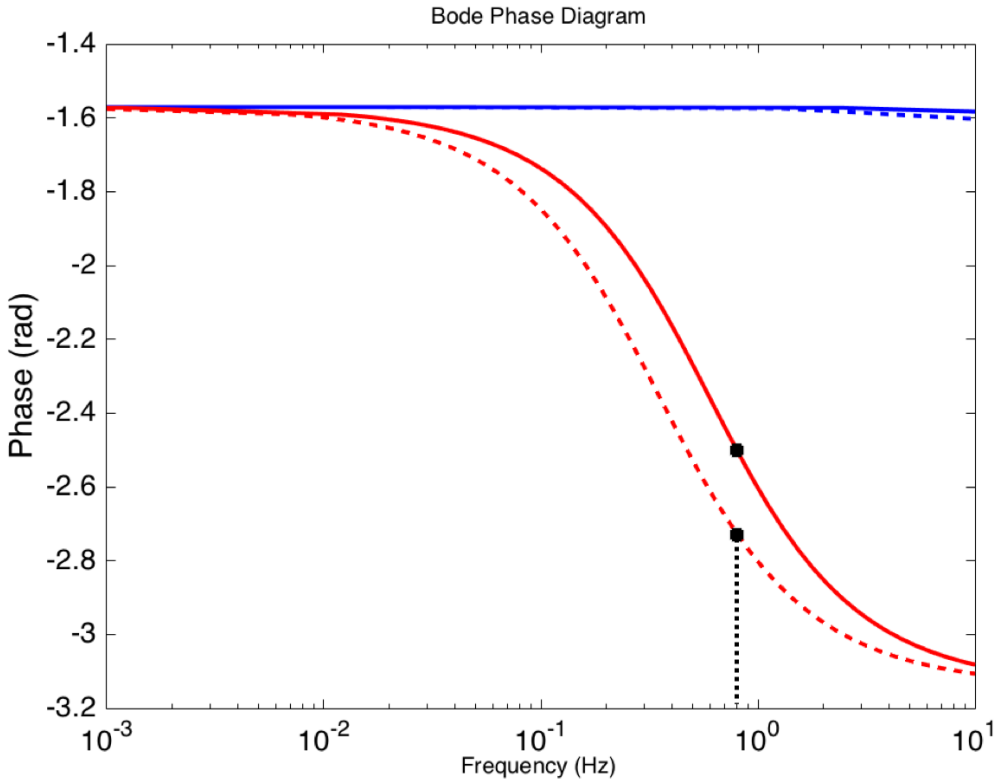

Figure 5.8 **Phase response of open loop torque (red lines) and velocity (blue lines) driven motor. The marked black squares and the vertical dashed line indicate the 0.8 Hz frequency intersection with the phase lines.**

The phase shift, between the suppression-on and -off that was calculated from the experimental results was $(6.6978 - \pi) - 3.7824 = -0.2262$ rad. The same phase shift is seen in **Figure 5.8** at the 0.8 Hz frequency between the suppression-on phase ($-2.73 + 2\pi = 3.55$ rad) and the suppression-off phase ($-2.5 + 2\pi = 3.78$ rad). It is interesting to note, at the 0.8 Hz frequency, minimal phase change is observed for the velocity driven case between the suppression-on and -off.

The PSD of the suppression-off and suppression-on signals were compared and are shown in **Figure 5.9**. A clear power reduction can be observed for the tremor frequencies (above 2 Hz), while in the vicinity of the intentional motion frequency (0.8 Hz) the signals overlap closely, indicating a small impact to the voluntary component power. The tremor power reduction for the 1st and 2nd harmonics was 99.4 and 90.4%

respectively and 99.4% when combined, while the intentional component power was decreased by 0.34%.

The lag in the velocity signal was corrected in order to calculate RMS errors. The calculated RMS values for the velocity tracking error and for the interaction force signals were 0.3 rad/s and 0.55 Nm respectively.

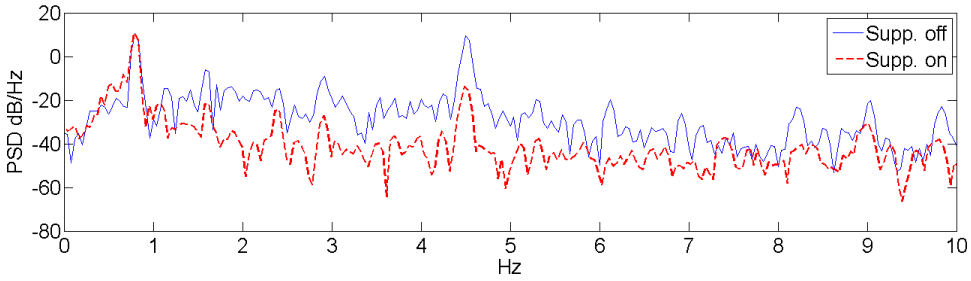

Figure 5.9 Torque based input, PSD of suppression-on and -off cases.

5.6. Discussion

In this work the performance with regard to both components of the motion, i.e. the tremorous and the intentional are emphasized. The time domain performance is evaluated by measuring the velocity and force tracking errors RMS, while the PSD is used to evaluate the spectral domain performance, as was done in Chapter **4** and in similar publications in the field. PSD for the voluntary, 1st and 2nd harmonics were calculated for the 0-2, 2-6 and 6-10 Hz frequency bands respectively.

The suggested approach considers the human input and the orthosis forearm link (in the velocity driven case) as disturbances to the suppression system. As was mentioned previously, this notion carries several benefits. Human arm parameters are not required for the controller tuning. Additionally, the controller design is simplified to a linear system case. Compensating for the gravitational effects on the human arm is also not needed.

We experimented with several variables in tandem as mentioned in section **5.4**. Most importantly, we tested two types of user inputs to the system, namely velocity and torque profile inputs. In addition in sections **5.5.1**, and **5.5.2**, we tested compensating the orthosis gravity force by either the suppression system or the user, as well as using data from two tremor patients having different pathologies (ET and PD). The TF associated

with **Figure 5.3** and **Figure 5.6** can be expressed as a second order system similar to that provided in [7], [83], [84], with the addition of a differentiator to obtain a velocity output. The associated TF describes the relationship between the human muscle torque and the associated output velocity. In our experiments instead, a motor (DM) is simulating the human input. The TF describing the implementation of **Figure 5.3**, similar to **(44)**, can be written as

$$G_{DM1}(s) = \frac{1}{M_h s^2 + C_h s + D_h}$$

$$M_h = {JL_a}/{K_g K_m}, C_h = {\left(JR_a + K_f L_a\right)}/{K_g K_m}, D_h = {K_f R_a + K_b K_g^2 K_m}/{K_g K_m} \quad \textbf{(45)}$$

and the TF describing the implementation of **Figure 5.6**, similar to **(42)**, is

$$G_{DM2}(s) = \frac{1}{s{J}/{K_m K_g} + {K_f}/{K_m K_g}} \quad \textbf{(46)}$$

where $J, R_a, L_a, K_f, K_m, K_g$ are the moment of inertia, motor armature resistance, armature inductance, motor damping coefficient, torque constant, and the gear ratio respectively. G_{DM1} refers to the velocity driven case with a TF from input voltage to output velocity, and G_{DM2} refers to the torque driven case with a TF from input current to output velocity. It is interesting to note that unlike the torque driven case, the velocity driven case has a similar TF structure as is often described in the literature for a human arm, with M_h, C_h, D_h representing the moment of inertia, damping, and stiffness of the arm joint.

Several observations can be made with regard to the analysis provided in section **5.5.2** and the value obtained for the damping coefficients. The values for the inertias are smaller than the damping values. However, the magnitude of the acceleration and velocity will determine the contribution of either to the total load force. Additionally, when the suppression system is active, large torques (currents) may be applied by the SM inversely related to the velocity (as revealed in **Figure 5.7**), in a comparable manner to viscous loads. From the DM perspective, the above may represent variable damping, based on the level of SM current activation. The damping value for the suppression-on

can be reflected at the DM gearbox shaft as $B_{ONgdm} = 0.069$ Nm/(rad/s). B_{ONgdm} can be physically interpreted as meaning that while in suppression-on, the system is applying a torque of 0.069 Nm for every 1 rad/s of velocity. The top velocity reached in our experiments (suppression on) was approximately 1.5 rad/s, which would have resulted in a maximum damping force of approximately 0.1 Nm applied to the DM; well within a range that the suppression system is capable of, and in fact, within the measured interaction force values, as seen in **Figure 5.7 B**.

The velocity tracking and PSD results indicate the system can successfully follow the desired motion profile while significantly reducing the tremor. The velocity signal delay observed in the torque driven case is the exception to the above. However, we have shown in **(34)** and in **(43)**, a model to explain the delay. It should be noted, the inertia and damping loads in **(34)** can exist unrelated to the suppression system (i.e. by any other mechanical element), therefore it is suggested the observed phase shift is attributed primarily to the DM. It is difficult to determine with certainty whether this phenomenon would carry over when testing with humans; the following chapter will address this question. It is, however, deemed to be unlikely as, in contrast to the DM (when driven in torque), the human motion involves feedback loops [170], [171] which can help regulate the desired motion. Furthermore, there is evidence that motor control for a body movement from one point to another follows a bell-shaped velocity profile [172], [173], which suggests the control goal to be velocity related.

A justification for testing in both velocity and torque mode emerges from the lack of certainty as to how a human motion is generated. It may be that depending on the activity and circumstances the input from the user will follow a position, velocity, a torque profile or a combination of the above.

A notable difference was observed in the PSD results of the torque driven case compared to the velocity driven case. Specifically, a lower attenuation of 90% was achieved for the 2nd tremor harmonic in the torque driven case as opposed to 99.1% in the velocity driven case. It is noted however, that the 2nd tremor harmonic was already relatively reduced in the suppression-off case (peak was approximately 5 dB less than in the velocity driven case) leaving less power to be attenuated. Furthermore, the power contained in the 2nd harmonic formed a relatively small portion of the total tremor power contained in the first two harmonics (0.3% in the torque driven case compared to 0.55%

in the velocity driven case). Unlike the velocity driven case, the orthosis arm and mechanical joint were connected to the DM in the torque driven suppression-off case. Consequently, the 2nd harmonic relatively low power may be due to the motion-inhibiting effect of the orthosis arm inertia in combination with the joint friction.

As far as compensating for the phase shift observed in section **5.5.2**, two approaches are considered, namely compensation by the suppression system or by the DM. The load parameters appear inside the DM transfer functions (velocity or torque driven), which suggests it may not be possible to compensate directly with the DM. Compensation then, should be done by the suppression system such that the DM transfer function parameters (inertia and damping) are unchanged between the unloaded (suppression-off) and loaded (suppression-on) cases. However, to successfully compensate, the SM may need to be controlled in torque. Compensation by the suppression system may be achieved by adding elements that cancel out with the inertia and damping in **(34)**. In practice, this entails using velocity and acceleration feedback loops to provide an equivalent torque command ($-J\ddot{y} - B\dot{y}$) to the left side of **(34)**. In our application however, the suppression system is driven in velocity and thus implementing an accurate torque command for the compensation would not be feasible.

It is interesting to note that a DC motor model, as in **(44)**, has a feedback loop (back EMF) when controlled in voltage, while in the case of the current control, as in **(42)**, it does not. The lack of feedback in the torque driven case may be a contributing factor to the lag that was observed, as is also evident in the Bode plot of **Figure 5.8**.

5.7. Summary and Conclusion

The steps taken in this chapter are aimed at demonstrating the feasibility of the approach in reducing pathological tremor, when implemented with an elbow orthosis. We obtained above 99% tremor power reduction while the effect on the voluntary signal power remained below 1% for both the velocity and torque driven cases. The system was able to track the desired velocity signal with an RMS error of 0.31 rad/s for the velocity driven case. A dynamic model was proposed to explain the delay observed in the torque driven case. The model matches standard models used in the literature (for a DC motor) and provides reasoning for the observed delay. Furthermore, we discuss how the delay can be accounted for in the system design in future development. The

interaction force RMS was 0.44 Nm and 0.55 Nm for the for velocity and torque driven cases respectively.

5.8. Related Publications

G. Herrnstadt and C. Menon, “Voluntary-Driven Elbow Orthosis with Speed-Controlled Tremor Suppression,” *Front. Bioeng. Biotechnol.*, vol. 4, no. March, pp. 1–10, 2016.

G. Herrnstadt and C. Menon, “Elbow Orthosis for Tremor Suppression - A Torque Based Input Case,” in *Lecture Notes in Computer Science*, Springer, 2017, pp. 292–302.

Chapter 6.

Following Elbow Volitional Movement with a Suppression Orthosis: Tests with Individuals with Pathological Tremor

6.1. Introduction

A voluntary-driven, speed-controlled tremor rejection approach was investigated using a robotic orthosis for suppression of pathological tremor at the elbow. Nine participants with either Essential Tremor (ET) or Parkinson's disease (PD) were recruited and tested off medication. The participants performed functional tasks of moving a cup and reaching an object, as well as computerized pursuit tracking tasks following a sinusoid and a random target. All tasks were performed both with and without the suppressive orthosis. Additionally, four aged matched healthy participants were recruited. The healthy participants performed pursuit tracking tasks only.

6.2. System Implementation

6.2.1. Suppression Approach and Elbow Orthoses

The implemented controller was based on an admittance-driven approach whereby the user's voluntary torque component is translated to a respective voluntary angular velocity, while a speed controller contributes to the tremor component rejection. The suggested suppression approach and control strategy were demonstrated using a preliminary engineered system in Chapter 3 and Chapter 4. Subsequently, an elbow orthosis prototype was developed and experimentally tested to validate the suppression approach in Chapter 5. In previous chapters the human input was robotically simulated. In this chapter, the objective of the work presented in this chapter is to validate the suppression approach. To this end, the previously developed orthosis is employed in the testing of individuals with tremor. Modifications to the controller implemented with the suppression approach, relative to previous chapters, are mentioned in section **6.2.2**. The finalized Tremor Suppression Orthosis (TSO) used with participants is shown in **Figure 6.1 a** embedded with a torque sensor and an encoder. To help keep the TSO in place

during the study and to distribute its weight more effectively, a shoulder sling was used (AliMed® Hemi Shoulder Sling). In addition, a Measurement Orthosis (MO) was used in the study to measure the free unobstructed motion (containing the tremor) of the tremor participants. The MO was composed of a lightweight brace and purposely implemented with an encoder, replicating the technology in the TSO, as shown in **Figure 6.1 b**. The TSO and MO weights were 1.7 Kg and 0.3 Kg respectively. Foam padding was used in both devices for the upper and forearm braces.

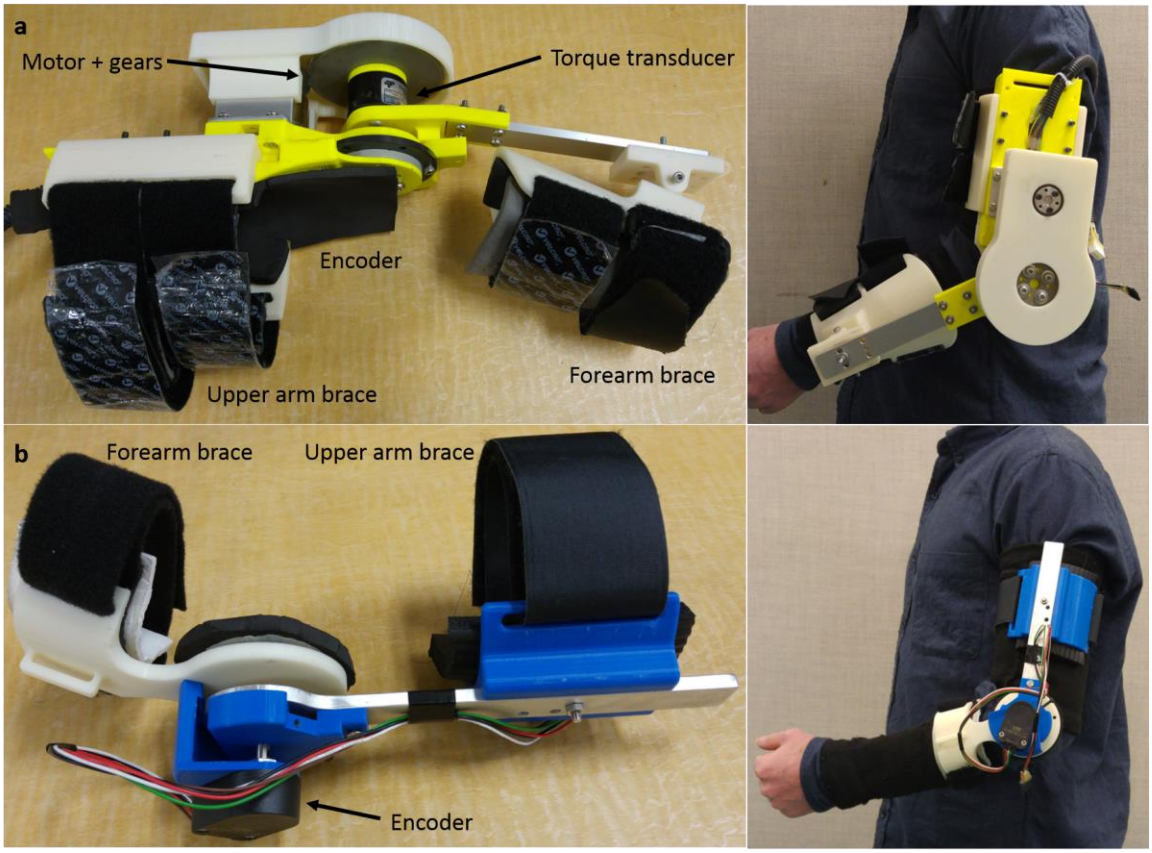

Figure 6.1 (a) TSO components and TSO donned. (b) MO components and MO donned.

6.2.2. Changes Relative to Previous Controller Implementation

Several changes relative to the previous control approach, presented in Chapter 3-Chapter 5, were implemented in this work. First, an Adaptive Band Pass Filter (ABPF) was implemented in NI LabView 2014 to separate the measured torque into its voluntary and tremor components [110], whereas previously a KF was used (see section **3.3.2**). The parameters used in the ABPF approach (elaborated below) were $\Delta f = 0.25\ Hz$, and

$\beta = 1$; in addition, a gain of 0.8 was used for the Band Pass Filter. f_{mod} was calculated individually for each participant as described in section **6.3**. The voluntary torque signal obtained following the ABPF was further LPF with a first order filter with a cut off frequency of 5 Hz, due to the presence of a ~9 Hz noise component. Second, based on the system response in Chapter 4, a need for additional dampness was identified. Consequently, a non-linear integral correction factor, utilizing a velocity feedback, was added to the admittance controller as follows

$$I_{cf} = \frac{1}{1 + 10\left({(1-v)^2}/{V^2}\right)}$$
$$v = {|v_m|}/{V}, v \leq 1 \quad (47)$$

where v_m, v and V are the measured velocity, the normalized velocity and the full scale velocity parameter, selected as 2 rad/s. The admittance integral gain K_{fi} was scaled by I_{cf}. The integral correction factor values ranged approximately between $0.28 \leq I_{cf} \leq 1$. At high velocities the integral gain remained unchanged ($I_{cf} = 1$), while for slow velocities it was reduced, resulting in a more damped response. The concept of the integral correction factor is similar to that of gain scheduling. The adaptive admittance control structure employed in the testing is shown in **Figure 6.2**. Third, the state feedback control loop was not necessary and therefore omitted. Lastly, the software sampling rate was doubled to 100 Hz resulting in a reduced loop latency of $0.01\ s$.

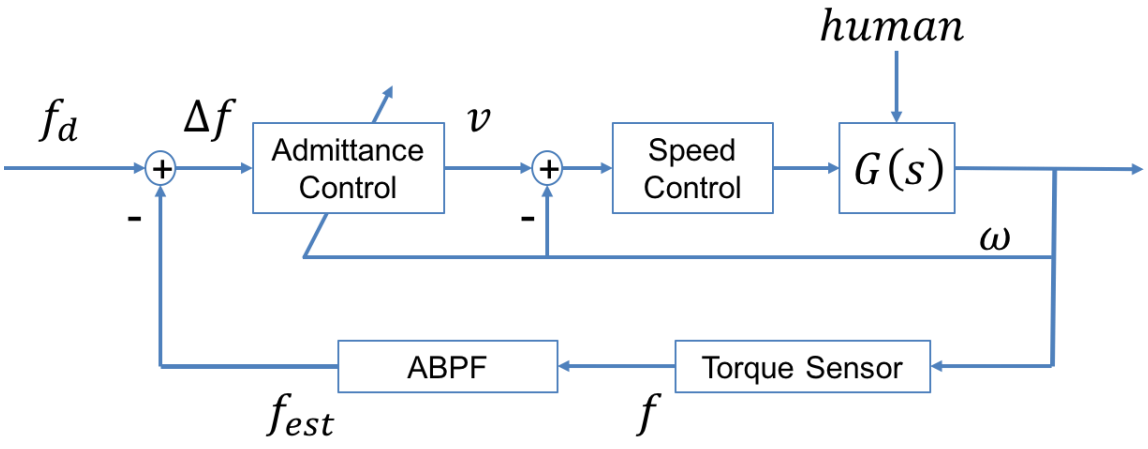

Figure 6.2 **Control structure employed during testing with indivduals with tremor.**

ABPF

The components involved in the ABPF method are shown as four blocks in **Figure 6.3**. The filter block is a Butterworth second order band pass filter with a center frequency that is adapted based on the feedback T_p (fundamental tremor frequency period). The filter block has the characteristic of zero-phase at the center frequency. The filter block outputs a signal with a tremor component only. The period block constantly measures the tremor half period in order for the filter to continuously adapt to the center frequency. To eliminate stochastic noise in the tremor frequency calculation a damping block is added, effectively limiting the rate at which the frequency can change. Finally a saturation like block is added in case the change in frequency following the damping block is greater than some specified limits $\pm f_{max}$.

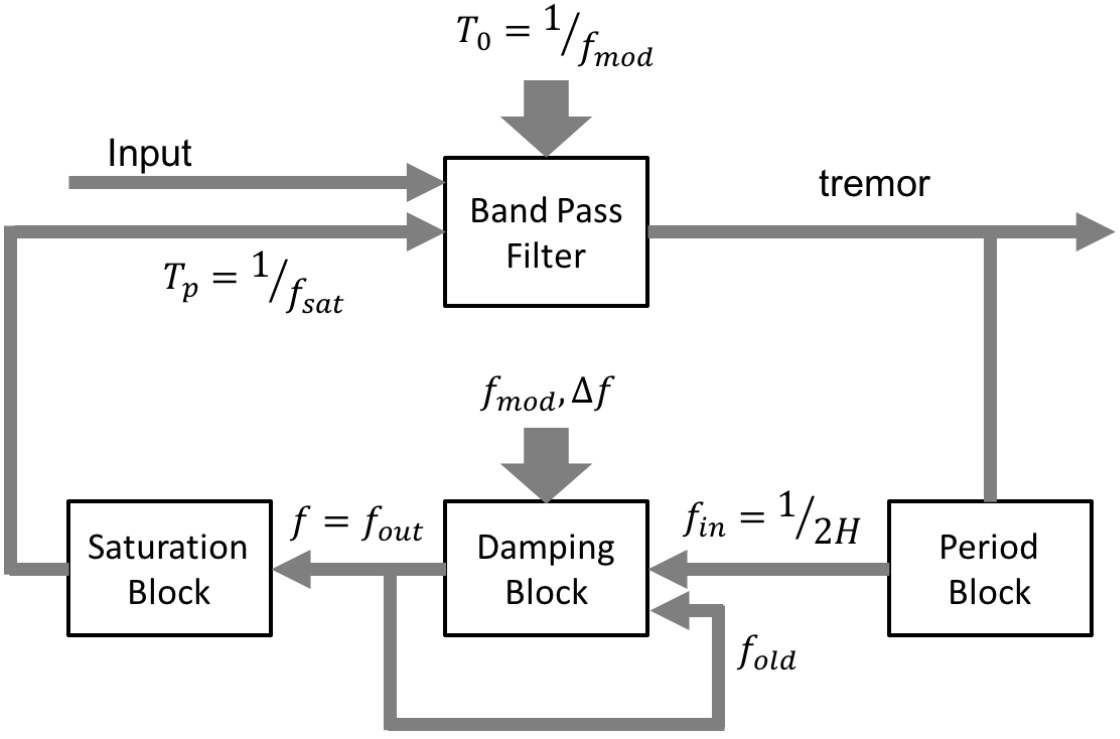

Figure 6.3 Adaptive Band Pass Filter Block Diagram [110]**.**

An RMSE comparison between the ABPF and KF was carried out with a velocity signal containing tremor and voluntary components. The tremor component was obtained from patient et05 [152]. For the voluntary component a sinusoid with an amplitude of 1 rad/s was used. Four sinusoid frequencies, between 0 and 1 Hz, were considered. The RMSE was calculated based on 10 s of data. The KF used was as described in section 3.3.2. For the ABPF, two β values were tested, one was $\beta = 1$ as mentioned above and the second was $\beta = 2.3$ as suggested in [110]. A third case involving the ABPF with $\beta = 1$ followed by a first order LPF with a cutoff at 4 Hz was also included in the comparison. As mentioned above a gain of 0.8 was used for the Band Pass Filter. The fundamental frequency for this patient's tremor signal is at 4.3 Hz; therefore f_{mod} was set to 4.3. Δf was 0.25 Hz. The obtained RMSE results are compared in **Table 6.1**.

Table 6.1 ABPF comparison

Voluntary frequency (Hz)	ABPF (β=1)	ABPF (β=2.3)	ABPF (β=1) with 4 Hz cutoff LPF	KF
0	0.200	0.139	0.130	0.145
0.1	0.199	0.142	0.135	0.157
0.5	0.209	0.200	0.200	0.516
1	0.238	0.305	0.325	0.689
0.5 (no tremor)	0.101	0.217	0.186	0.487

The ABPF with $\beta = 1$ and a LPF outperformed the KF in all voluntary frequencies and in particular at higher voluntary motion frequencies. The above results suggest the ABPF offers superior performance to the KF, for the application considered.

6.3. Participant Selection and Experimental Protocol

6.3.1. Individuals with Tremor

Nine participants were recruited to evaluate the tremor suppression orthosis. Individuals who have been diagnosed with mild to severe tremor were considered for the study. The following conditions were excluded: previous surgical operation or injuries to the arm, non-tremor related arm disability, and previous surgical intervention to treat tremor or a neurologic condition other than pathological tremor that affects the arms. Participants were recruited through the International Essential Tremor Foundation and the Movement Disorder Clinic, University of British Columbia Hospital. Participants were invited for up to two sessions. Each session lasted approximately two hours. Additionally, participants were asked to abstain from taking medications 12 hours prior to the study and advised to refrain from drinking alcohol 24 hours before the study. A tremor severity assessment was carried out at the end of each study session using the performance section (assessing the tremor severity) of The Essential Tremor Rating Assessment Scale (TETRAS) [40], [174]. The participants' details are provided in **Table 6.2**. Informed consent was obtained from all participants.

Table 6.2 Participant Data

Participant	Gender	Age	Disease Duration (y)	Handedness	More Severe Side[a]	TETRAS[b]	Diagnosis and Notes
T01	F	59	55	R	L	27.5	ET
T02	M	65	5	R	R	21	PD (tremor dominant)
T03	M	66	3	R	R	22.5	PD (also ET)
T04	M	69	4	R	R	24	ET
T05	M	56	53	R	R	26.5	ET (head injury)
T06	M	71	10	R	R	16	ET
T07	M	69	3	R	L	21	NA
T08	F	81	20	R	L	24.5	ET
T09	F	63	6	R	R	8	ET
Mean	-	66.6	17.7	-	-	21.2	-

[a] Based on the individual's testament and/or a neurologist assessment.
[b] The TETRAS performance section scale is scored out of a total of 64.
NA indicates information wasn't available.

The experimental protocol involved the following three tasks:

In *Task 1*, the participants were asked to move a cup on a table from one location to another and back. Tape marking on a table were used to specify the start and end locations.

In *Task 2*, the participants were asked to reach with their arm, in a horizontally suspended posture, and point to an object in the vicinity starting from rest position and maintaining the posture for a duration of 10 seconds.

In *Task 3*, participants viewed a target moving on a computer screen as shown in **Figure 6.4 a** and were able to follow the target by moving their forearm. The participants' elbow joint movement was translated to a cursor movement on the screen (filled orange circle in **Figure 6.4 a**). *Task 3* has the added value of distinguishing the intentional (the target

cursor) from the executed movement. Sinusoid target profiles (e.g. top of **Figure 6.4 b**) and pseudo-random target profiles (e.g. bottom of **Figure 6.4 b**) were used, and each were implemented with a slow and fast velocity. To that end, two frequencies (0.3 and 0.5 Hz) were defined for the sinusoid profile. For the pseudo-random profile, successive random position targets were defined and a ramp shape velocity profile was used (shown as a red dashed line at the bottom of **Figure 6.4 b**) in order to reach the target positions. Two (slow and fast) top-velocity and acceleration/deceleration values were selected. Consequently, the continuous target position associated with the random profile followed a parabolic shape, shown as a blue dashed line in the bottom of **Figure 6.4 b**. The study participants did not have any prior knowledge of the next pseudo-random target and were asked to follow the target cursor (i.e. match its current position and velocity). Two values (8 or 9 pixel/deg) were used for scaling between the participants' elbow angular motion and the target on screen pixel motion depending on the individual's Range of Motion (ROM). Throughout the study a fully extended elbow position was considered as the zero angle.

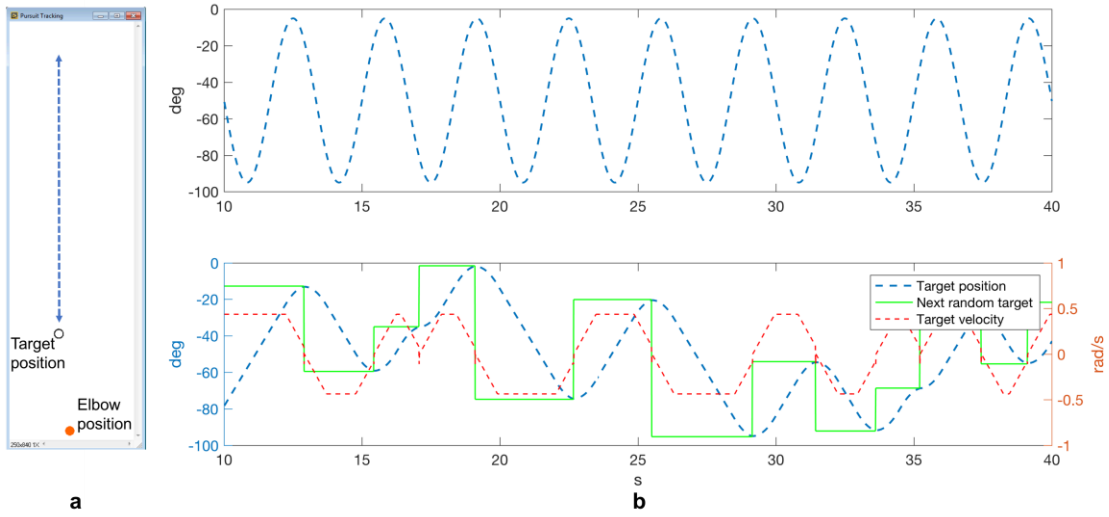

Figure 6.4 **Computer interface and illustrative pursuit target profiles (a) Graphical interface as seen by the study participants on a computer screen. The outlined circle indicates the position of the target on the screen. The dashed blue arrow is added for illustration of the target (vertical) motion direction. The filled orange circle indicates the participant's elbow cursor position. (b) Example of a sinusoid (top) and a pseudo-random (bottom) target position profiles. Target position and Next random target indicate the current target position and the random target position goal. Target velocity indicates the current target velcity. The zero degree angle refers to the fully extended elbow position as well as to the cursors being located at the bottom of the graphical interface window.**

The experimental protocol tasks, sequence, repetitions and velocity parameters are presented in **Table 6.3**. *Task 1* aims to induce intention tremor, a type of kinetic tremor, while *Task 2* a postural tremor. *Task 3* may also result in kinetic tremor; furthermore, its main benefit is the availability of the voluntary component of the motion (i.e. the target). Up to two training repetitions were offered for *Task 3* for each device and motion profile before its execution.

Table 6.3 **Protocol Summary**

Tasks		Repetitions	Tremor activation	Velocity Settings[a]
#	Description			
1	Moving an object/pick and place a cup	2	kinetic tremor	-

2	Suspended forearm/Pointing at an object		2	postural tremor	
3	Target pursuit	Sinusoid target	Slow	3	kinetic tremor	The top sinusoid target velocity was 720π×f pixels/sec with a frequency of f=0.3 and f=0.5 Hz in the slow and fast acceleration cases respectively (resulting in 1.316 and 2.19 rad/s for 9 pixel/deg scaling).
			Fast	3		
		Random target	Slow	3	Kinetic tremor and/or intention tremor	The random target slow and fast velocities were 2 and 4 pixels/loop-step (resulting in 0.387 and 0.872 rad/s for 9 pixel/deg scaling), while the time to reach the target velocities (acceleration/deceleration) was set to 80 and 60 loop-steps respectively.
			Fast	3		

All the tasks were repeated with both the MO and the TSO. Tasks 1-2 were recorded for approximately 10 s while Task 3 for 30-60 s.

[a] Converting from pixels/loop-step to rad/s was done by first dividing by the scale factor (resulting in deg/loop-step), then converting from deg to rad, and finally multiplying by the loop rate to obtain the value in rad/s.

Tuning of the ABPF filter implementation involved selecting a center tremor frequency f_{mod}. To this end, the following procedure was employed:

1. The MO was donned and the protocol tasks executed (see **Table 6.3**).
2. The 1st harmonic tremor frequency from the data obtained with the MO was calculated.
3. The calculated 1st harmonic frequency was fed to the ABPF algorithm as f_{mod}.
4. The TSO was donned and the protocol tasks executed.

6.3.2. Healthy Individuals

Healthy individuals, approximately age matched with the tremor participants, with no history of tremor were recruited. The healthy participants' details are provided in **Table 6.4**. The healthy participants only performed *Task 3* with the MO.

Table 6.4 Healthy Participant Data

Participant	Gender	Age	Handedness	Hand Tested
H01	M	65	R	R
H02	M	67	R	R
H03	M	58	R	R
H04	F	66	R	R
Mean	-	64.0	-	-

6.4. Data Processing and Expected Outcomes

As mentioned, the MO was incorporated in the protocol in order to record the free motion and serve as a reference for the TSO in both the spectral and time domains. Although the MO may introduce some motion attenuation through its joint friction and forearm brace inertia, it was considered negligible (approximately zero attenuation). In fact, the weight of the MO forearm brace with padding was 42.5 g, similar to a wrist watch. Position and velocity signals were available directly from the embedded encoders in the MO and TSO. A torque signal was available from the TSO.

6.4.1. Spectral Analysis

The data collected in *Tasks 1*, *Task 2* and *Task 3* was processed in order to assess the TSO tremor suppression. The PSD for both the TSO and MO was calculated in order to obtain the tremor component power change (i.e. $PC(P_{TSO}^{t}, P_{MO}^{t})$) as per **(5)**. The data of *Task 3* was also assessed for the effect the TSO had on the voluntary component. The PSD for the TSO, MO, and for the target signal was calculated in the voluntary motion frequency range in order to obtain the voluntary component power changes (i.e. $PC\left(P_{TSO}^{v}, P_{Target}^{v}\right)$ and $PC\left(P_{MO}^{v}, P_{Target}^{v}\right)$) as per **(5)**. The signal power change difference was defined as the difference between $PC\left(P_{TSO}^{v}, P_{Target}^{v}\right)$ and $PC\left(P_{MO}^{v}, P_{Target}^{v}\right)$.

The PSD of the MO was also used to obtain the participants' fundamental tremor frequency. The fundamental tremor frequency corresponded to the PSD peak amplitude in the 2-10 Hz range.

The spectral analysis in all the tasks was performed exclusively with the velocity signal, for which the tremor signal to noise ratio was more substantial than in the position signal. A large attenuation percentage is desirable for the tremor signal power change, namely $PC(P_{TSO}^{t}, P_{MO}^{t})$. Instead for the voluntary component a small signal power change, either positive or negative, between each device (MO and TSO) and the target signal is ideal. More importantly, the signal power change difference ($PC\left(P_{TSO}^{v}, P_{Target}^{v}\right) - PC\left(P_{MO}^{v}, P_{Target}^{v}\right)$) should be small indicating no additional interference is introduced by the TSO.

6.4.2. Temporal Analysis

In the time domain, processing of *Task 3* data involved voluntary motion tracking errors of both position and velocity signals. The respective motion errors between the TSO and the target, and between the MO and the target are defined as e_{TSO} and e_{MO}. A mathematical representation of the tracking error components is provided next.

The errors that can be expected when a participant with tremor uses the MO consist of the following

$$e_{MO} = e_{td} + e_{ti} + e_{h} \quad \textbf{(48)}$$

where e_h is an error due to normal human skill/ability, e_{ti} is the indirect error due to the tremor condition and e_{td} is the direct error due to the tremor motion. The error due to the tremor condition (e_{ti}) in **(48)** does not refer to an error caused by the actual tremor motion (as e_{td}), but instead to a voluntary tracking error induced indirectly by the existing tremor condition. Examples of errors that can be associated to e_{ti} include bradykinesia and rigidity in PD [6]. Some studies have identified impaired balance and gait in ET patients [175]. If such motor impairments exist in the upper limbs they may also contribute to the error referred to by e_{ti}. By performing a zero phase, Low Pass Filtering (LPF) of the MO signal (fMO) the direct tremor error can be removed resulting in

$$e_{fMO} = e_{ti} + e_{h} \quad \textbf{(49)}$$

Note an implicit assumption was made in **(49)** as to the frequency content of e_{ti} and e_h, namely that they consist of primarily low frequency content, similar to voluntary motion. The zero phase LPF was designed empirically based on a visual inspection and was fixed for all participants. The filtfilt Matlab function was used. The position signal pass and stop bands were 0.5 and 3 Hz, respectively, while the velocity signal pass and stop bands were 1.5 and 3 Hz, respectively.

An error in tracking the target motion is also expected when a participant with tremor uses the TSO. It was postulated that the tracking error might comprise of three subcomponents as follows

$$e_{TSO} = e_{ti} + e_d + e_h \quad \textbf{(50)}$$

where e_d is a device error due to the TSO. The error e_d is primarily associated to any system element (e.g. control loop and hardware latencies, modeling errors, etc.) leading to a reduction of orthosis transparency or to increased impedance experienced by the operator. Note that with the MO it was assumed no device error is present. The same normal human error e_h and indirect tremor error e_{ti} as with the MO (see **(48)**) are also expected to exist with the TSO. It should be noted the direct-tremor error was neglected $(e_{td} \cong 0)$ in **(50)**, supposing full tremor suppression is achieved by the TSO. If instead the aforementioned was not achieved, any residual direct-tremor error could still be considered to be part of the device error (e_d).

It is of particular interest to evaluate errors associated with the TSO. The inclusion of the MO in the protocol can facilitate distinguishing between the error subcomponents mentioned in **(50)**. The TSO device error e_d can then be obtained by subtracting **(49)** from **(50)**. In the time domain, an equal amount of tracking error with the TSO and with the fMO relative to the target would be desirable and would indicate no additional interference is introduced by the TSO.

Interaction torque between the user and the TSO is also measured in the time domain as well as used in the controller scheme. It is desirable that the measured interaction torques are small in order for the user to feel little resistance.

As for healthy individuals performing *Task 3* with the MO, the following errors can be expected:

$$e_{MO}^{h} = e_h \quad \textbf{(51)}$$

Thus, subtracting **(51)** from **(49)** yields the indirect error due to tremor and using **(48)** can result in the direct error.

6.4.3. Data Selection and Processing

As mentioned in **Table 6.3**, the data recorded in *Tasks 1* and *Task 2* was approximately 10 s long, while for *Task 3* was at least 30 s and up to a minute in duration. 5 s of data, from *Task 1* and *Task 2*, were selected heuristically based on visible tremor. Since, *Task 1* and *Task 2* didn't always induce enough tremor in the participants' elbow, only one case of each is included per participant.

Specifically for *Task 3*, the beginning of the pursuit task recordings often had irregularities when participants were asked to commence the task. There were also occasional discontinuities mid data due to participants' confusion or distraction resulting in their elbow motion being interrupted. Therefore, in order to be able to compare continuous and representative data from all participants, 20 continuous seconds were selected.

The selected 20 s of data time range were chosen based on the lowest normalized RMSE values of the fMO and TSO relative to the target signal. The procedure for selecting the 20 s of data time range essentially involved scanning the whole time range, in increments of 10 s. The position and velocity RMSE were normalized with 90 deg and 2 rad/s respectively, chosen as full scale values. As an example, for a data spanning 43 s long, the RMSE was calculated for the 10-30 s and 20-40 s time ranges with the smaller value being selected. In conflicting instances where, for example, the 10-30 s range had a smaller position RMSE while the 20-40 s time range had a smaller velocity RMSE, a normalization relative to full scale values was performed for each and the range with the smaller normalized value was used. Specifically, full scale normalization values were 90 deg and 2 rad/s for the position and velocity respectively. In the sinusoid target case, the fMO and TSO signal time ranges

were identified independently. For instance, the fMO data might have included a 10-30 s time range, while the TSO range might have included a 20-40 s range. These would have resulted in exactly the same target motion profile throughout the 20 s period, with no phase difference. For the pseudo-random target, 20 s of data for the TSO were selected first and then the same time range was used for the fMO, in order to compare identical motion profiles.

As shown in **Table 6.3**, the four motion cases of *Task 3*, i.e. sinusoid slow, sinusoid fast, random slow, and random fast were each performed three times. For each motion case repetition, an RMSE or signal power value was obtained in the time or spectral domains. The three repetitions were then averaged resulting in 4 values representing the four motion cases. These 4 values were further averaged, associating a spectral and time domain analysis value to each participant.

It should be noted that when a waveform of 20 s was selected from a participant's testing data, the same time range was used for both the spectral (e.g. P_{TSO}^{t}) and time (e.g. e_{TSO}) domain analyses. However, it is emphasized that P_{TSO}^{f} is the power in the TSO, not the error e_{TSO} signal.

6.5. Results

6.5.1. Tremor Motion Component

Figure 6.5 a shows the percentage tremor power reduction, of the TSO relative to MO, for each participant when performing *Task 1* and *Task 2*. Square and plus markers indicate the values from *Task 1* and *Task 2* respectively. The mean and Standard Deviation (SD) tremor power change (reduction) for the motions in *Tasks 1-2* for all participants was -92.9 (6.01)%. Note the lower attenuation values for participants T02, T06, T07 are primarily due to a small amount of tremor detected with the MO, in particular in the Suspended forearm task. Consequently, little power reduction could be achieved with the TSO.

The tremor power reduction in *Task 3* is shown in **Figure 6.5 b**, while the tremor fundamental frequency for *Task 3* is shown in **Figure 6.5 c**. As mentioned in section 6.4.1, the tremor frequency was obtained from the PSD calculation of the MO. Each scatter plot in **Figure 6.5 b** and **c** was composed of four markers associated with the

four motion cases of *Task 3* (see **Table 6.3**). An outlined circle, a filled circle, an outlined diamond and a filled diamond shape respectively correspond to the sine slow (ss), sine fast (sf), random slow (rs) and random fast (rf) cases. The mean (SD) tremor motion power change was -94.37 (4.06)% and the mean (SD) tremor frequency for all the participants was 4.45 (0.93) Hz. The mean power change and frequency across all the participants are shown as horizontal dotted lines in **Figure 6.5 a**, **b** and **c**.

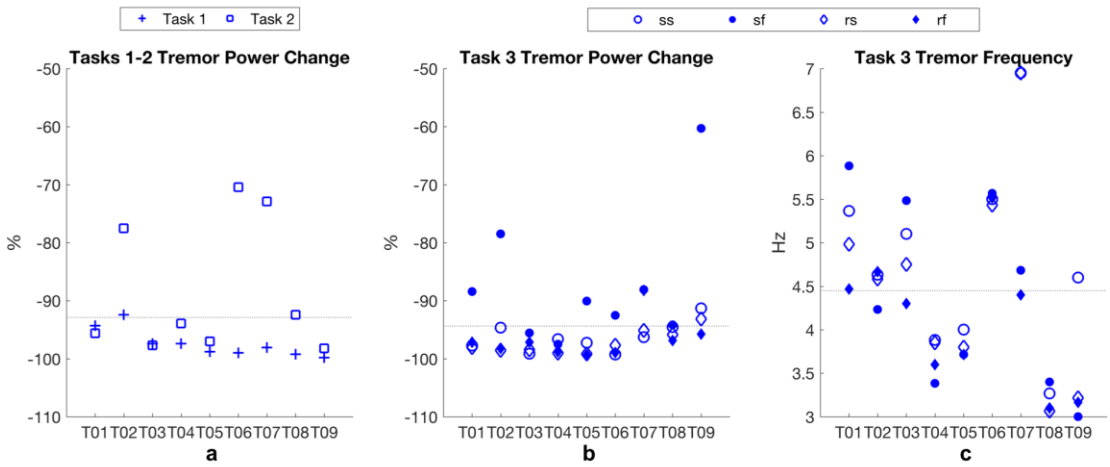

Figure 6.5 **Tremor motion related measures. (a) Tremor power change in *Tasks 1-2*. Square and plus markers indicate the values from Task 1 and Task 2 respectively. (b) Tremor power change in *Task 3*. (c) *Task 3* MO tremor fundamental frequency calculated based on PSD. The dotted horizontal lines in a-c indicate the participants' mean. The legend on the right refers to both b and c. The sine slow (ss), sine fast (sf), random slow (rs) and random fast (rf) motion cases are represented with outlined circle, filled circle, outlined diamond, and filled diamond shape markers, respectively.**

In order to confirm that the weight of the TSO is not a significant contributor to tremor suppression, the tracking tasks were recorded with the TSO with no power being supplied to the motor. Under such circumstances only the TSO inertia, friction and damping can lead to tremor suppression. If tremor is still evident then it is possible to exclude that the tremor suppression observed in **Figure 6.5** is caused by the mass of the TSO. The tracking tasks were therefore recorded with the TSO in power off mode with a subset of 5 participants (T02, T03, T04, T05, T06) performing only one repetition for each task case (see **Table 6.3**). The single repetition with the TSO in off mode was compared to the first repetition with the encoder. The tremor suppression for these

participants with the TSO in power off mode is shown in **Table 6.5** below. For simplicity, both the sinusoid and random motions, were assessed only in the 10-30 s time range.

Table 6.5 Tremor Suppression (%) with TSO in Off Mode

Target Profile	Participant				
	T02	T03	T04	T05	T06
Sinusoid	28.65	77.35	38.75	-10.45	58.2
Random	60.35	85.9	66.15	62.7	28.35
Mean	44.5	81.625	52.45	26.125	43.275

With the TSO in off mode, the mean tremor suppression for the five tested participants was 49.6%. The above results suggest the mass and friction in the TSO are a cause for some tremor reduction, however, significantly less than with the TSO in on mode. Incidentally, from the above it may be reasonable to infer that the weight of the MO would have little effect on the tremor.

6.5.2. Voluntary Motion Component

Representative tracking and PSD plots are shown for participant T06. **Figure 6.6** and **Figure 6.7** correspond to the sinusoid and random target motion cases respectively. Subfigure **a** refers to the slow target motion and subfigure **b** to the fast target motion. In both subfigures **a** and **b**, the top two subplots show the position and velocity associated to the target, the TSO and the MO. The velocity plot also shows the fMO velocity. In **Figure 6.7**, the next random target position goal is also shown. The bottom two subplots refer to the TSO interaction torque and the PSD obtained for both the TSO and MO. Since the suppression approach relies on a force transducer to track the voluntary motion [89], all interaction forces between the user and the device are recorded. The measured torque (Fm) represents the total motion composed of the voluntary and tremor components. The estimated torque (Fe) represents the voluntary component as a result of online filtering. It can be observed in the interaction torque subplots that Fm contains a high frequency component (tremor motion) which is not present in Fe. In the bottom PSD plots, it can be observed the TSO and MO curves overlap closely around the voluntary motion frequency (~0.5 Hz). Instead, in the higher frequencies of the tremor (~5-6 Hz) the TSO magnitude is reduced. As was shown in previous work by the authors, the implemented approach resulted in the peak sinusoid velocities being

associated with both larger tracking errors and lower interaction torques [162]. The above can be appreciated from the sinusoid profile velocity subplot in **Figure 6.6**.

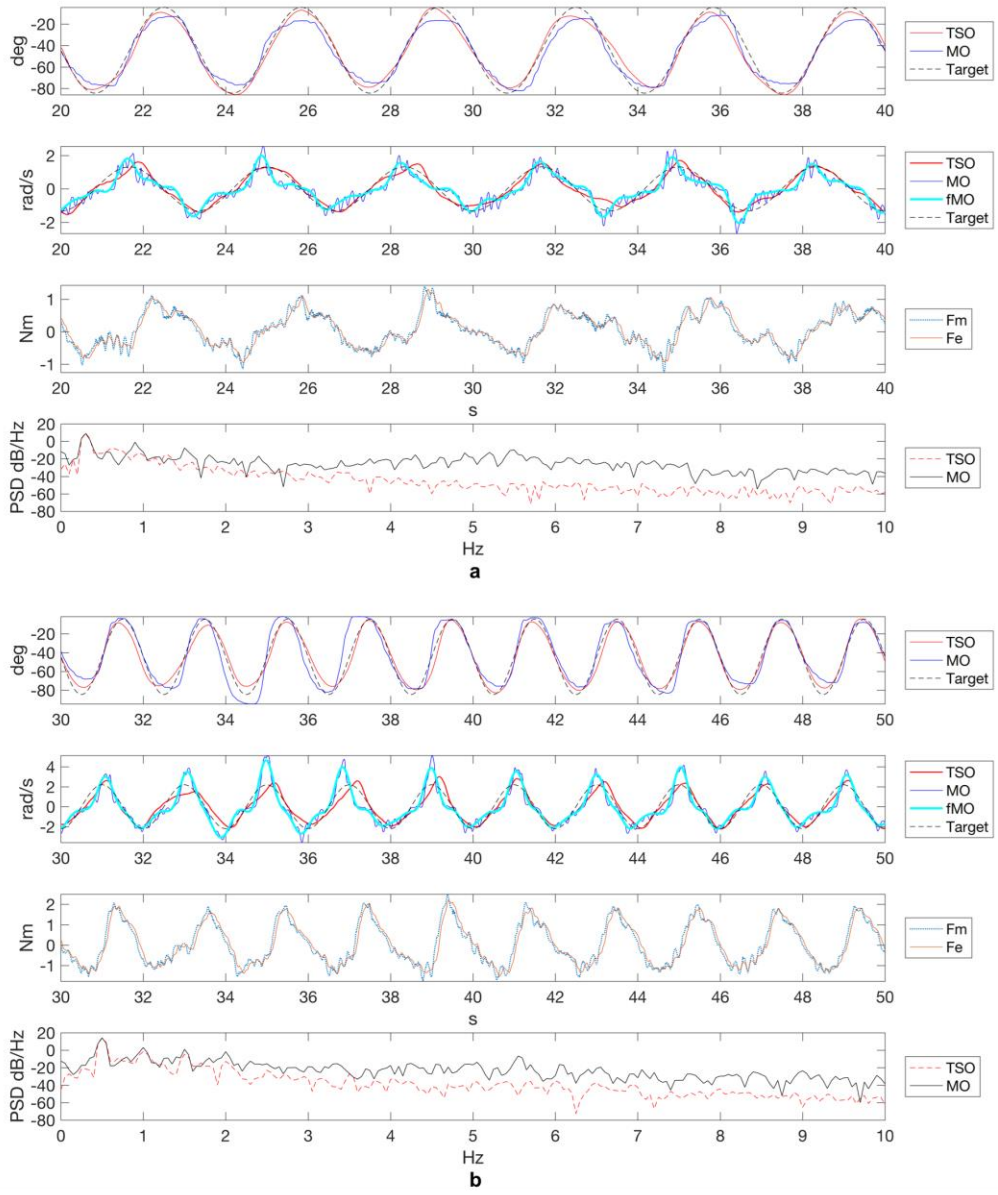

Figure 6.6 **Participant T06 sine target tasks (a) slow and (b) fast sinusoid target tasks. For both subfigures a and b, the subplots from top to bottom are position tracking (zero degree angle refers to a fully extended elbow position), velocity tracking, interaction torque, and PSD. TSO and MO refer to the Tremor Suppression Orthosis and Measurement Orthosis; Target refers to the target profile; fMO is the zero phase LPF of the MO; Fm is the measured torque and Fe is the estimated torque.**

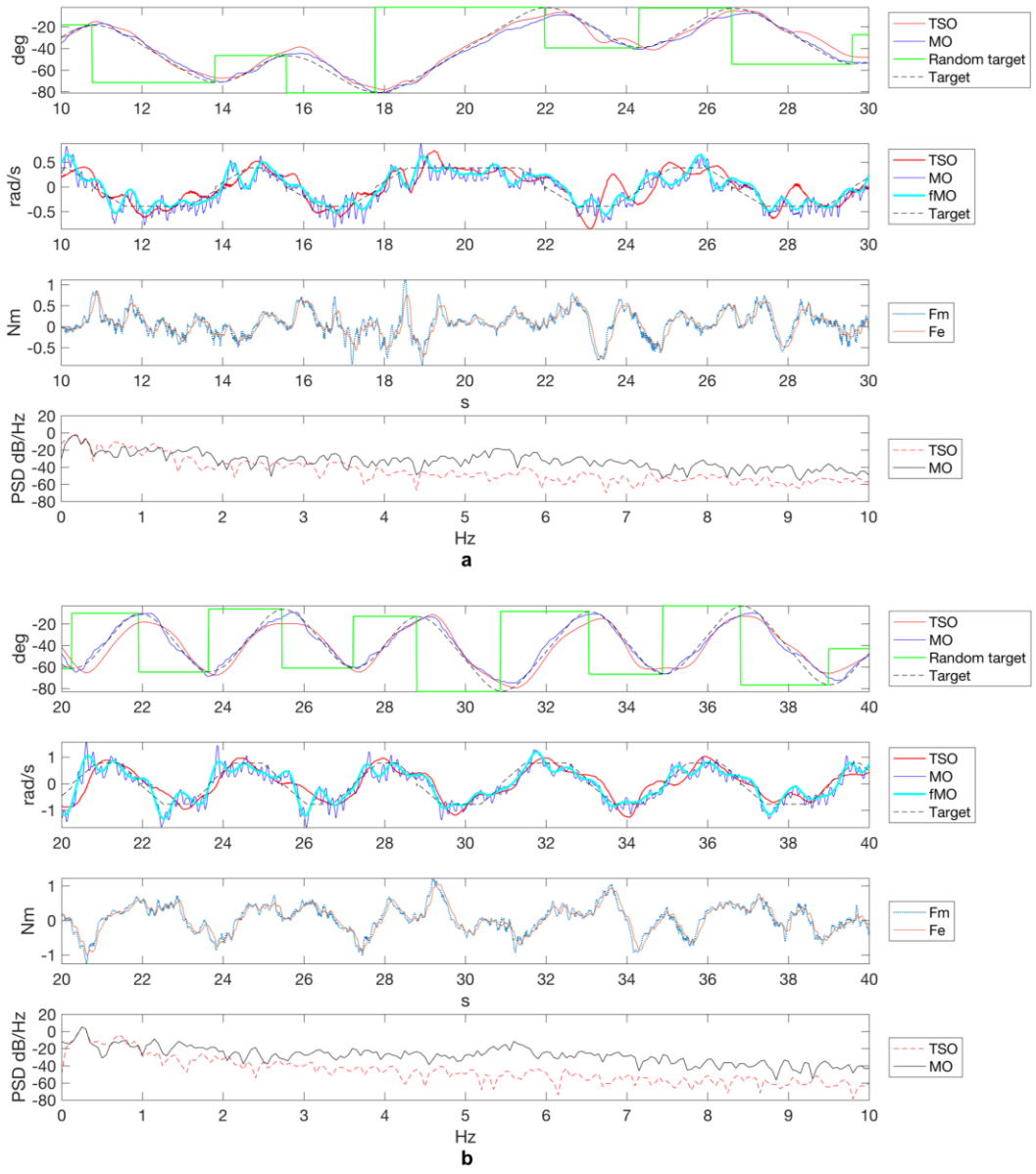

Figure 6.7 **Participant T06 pseudo-random target tasks. (a) slow and (b) fast pseudo-random target tasks. For both subfigures a and b, the subplots from top to bottom are position tracking (zero degree angle refers to a fully extended elbow position), velocity tracking, interaction torque, and PSD. Random target is the next random target position goal indicated by the solid green square wave line; TSO and MO refer to the Tremor Suppression Orthosis and Measurement Orthosis; Target refers to the target profile; fMO is the zero phase LPF of the MO; Fm is the measured torque and Fe is the estimated torque.**

The signal power change was also used to assess the voluntary motion (see section 6.4.1). The results for the voluntary assessment are shown in **Figure 6.8**. The voluntary component power changes for the MO ($PC\left(P_{MO}^{v}, P_{Target}^{v}\right)$) and the TSO ($PC\left(P_{TSO}^{v}, P_{Target}^{v}\right)$) are shown in **Figure 6.8 a**. The power change difference can be observed as the difference between the TSO and MO markers. The mean (SD) voluntary motion power change with the MO and with TSO were -4.32 (16.37)% and -10.96 (22.91)% respectively. Position and velocity tracking errors for all the participants are shown in **Figure 6.8 b** and **c**, respectively, comparing the fMO and the TSO. The mean (SD) position error with the fMO and with the TSO were 7.3 (1.9) deg and 8.2 (1.9) deg respectively. The mean (SD) velocity error with the fMO and with TSO were 0.39 (0.04) rad/s and 0.41 (0.07) rad/s respectively. **Figure 6.8 d** shows the RMS of the voluntary interaction torque (same as Fe in **Figure 6.6** and **Figure 6.7**) with the TSO. The mean (SD) interaction torque was 0.62 (0.04) Nm. The four data points in each of the scatter plots in **Figure 6.8 a-d** are demonstrated with different markers to distinguish between the four motion cases of *Task 3* (see **Table 6.3**). It is noted in **Figure 6.8 a**, positive or larger power change values are often associated with random motions while negative or smaller values with sinusoid motions. Conversely, in **Figure 6.8 b-d**, larger values are repeatedly associated with sinusoid motions while smaller values correspond to random motions.

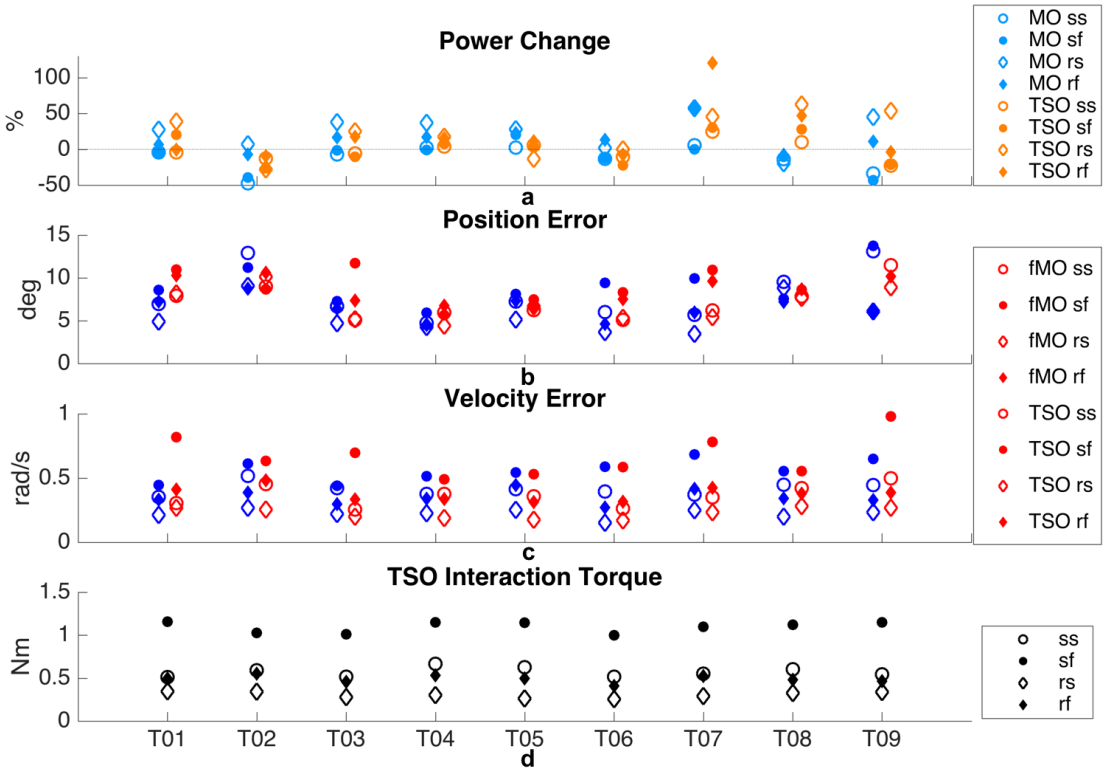

Figure 6.8 **Task 3 voluntary motion related measures. (a) Voluntary component power change for the MO, i.e. $PC\left(P^{v}_{MO}, P^{v}_{Target}\right)$ and the TSO, i.e. $PC\left(P^{v}_{TSO}, P^{v}_{Target}\right)$. Zero value is indicated by the horizontal dashed line. (b) Voluntary position pursuit tracking RMSE for the fMO and the TSO. (c) Voluntary velocity pursuit tracking RMSE for the fMO and the TSO. (d) Voluntary interaction torque RMS recorded with the TSO. For plots a-d, the sine slow (ss), sine fast (sf), random slow (rs) and random fast (rf) motion profiles are represented with outlined circle, filled circle, outlined diamond and filled diamond shapes, respectively.**

To corroborate the obtained results, statistical analyses were carried out for the tremor and voluntary motions. Specifically, we assessed whether the tremor reduction was significant, and whether the voluntary tracking errors and the voluntary power change between the fMO and TSO were different. All the data used in the statistical analysis was tested for normal distribution. In cases where a normal distribution was rejected, the Wilcoxon Signed Rank test was used [176].

The tremor reduction values (see **Figure 6.5 a**, **b**) obtained with the TSO were compared to no suppression (i.e. zero suppression). Due to the tremor suppression values distribution, in *Tasks 1-3*, not conforming normally as well as the small sample

size, the non-parametric Wilcoxon Signed Rank test was used [176]. The tremor reduction was deemed significant for *Task 1-2* ($p_{t12} < 0.005$) and *Task 3* ($p_{t3} < 0.005$).

For the voluntary motions, a statistical analysis was performed with a null hypothesis stating the mean tracking errors obtained with the fMO and the TSO are equal, for both position and velocity. Using a two-sided t-Test with a significance level of $\alpha = 0.05$, the null hypothesis was not rejected for neither position ($p_{vel} = 0.0501$) or velocity ($p_{vel} = 0.283$). A similar analysis was also carried out to test if the mean voluntary power changes (**Figure 6.8 a**) were equal. The hypothesis was also not rejected ($p_{PC} = 0.346$). Based on these tests, there is no evidence for statistically significant differences between the velocity errors as well as the voluntary power changes. It can be observed from **Figure 6.8 b** and **c** that generally faster motions resulted in larger errors. Consequently, it was interesting to re-assess the statistical analysis for the fast and slow motions profiles separately. Indeed, equivalency was not rejected for the slow motion profiles ($p_{posslow} = 0.586$, $p_{velslow} = 0.152$, $p_{PCslow} = 0.546$). Instead, for the fast motion profiles, both position and velocity errors were statistically different ($p_{posfast} = 0.0148$, $p_{velfast} = 0.0329$, $p_{PCfast} = 0.269$).

Looking at the tremor power change and the voluntary power change difference (between the TSO and MO), no clear relationship was observed as shown in **Figure 6.9 a** ($R^2 = 0.053, p = 0.55$). Importantly, the tremor reduction does not seem to depend significantly on the voluntary power change difference. Further analysis involving a linear regression between the tremor power change and the tremor severity (based on TETRAS) was performed and is shown in **Figure 6.9 b**. A linear trend is observed for a statistically significant regression model ($R^2 = 0.537, p = 0.025$). The participant with the lowest reduction of tremor also had the least amount of tremor, as measured by TETRAS. **Figure 6.9 c** shows the voluntary power change difference (y axis) against the difference in position RMSE between the TSO and fMO (x axis). **Figure 6.9 d** is similar to **c** but with velocity RMSE difference in the x axis. Two linear regressions are shown in **Figure 6.9 c** and **d**; one including the nine participants and one excluding T08 which may be considered an outlier. Based on the linear regression excluding T08 it is seen that a reduction in position or velocity tracking error difference is associated with a decrease in voluntary power change difference between the TSO and MO. In other words, when the tracking errors between the TSO and fMO are similar (i.e. the

difference is close to zero), so are the voluntary power changes between the two devices. It should be noted, the regressions in **Figure 6.9 c** and **d** were not statistically significant.

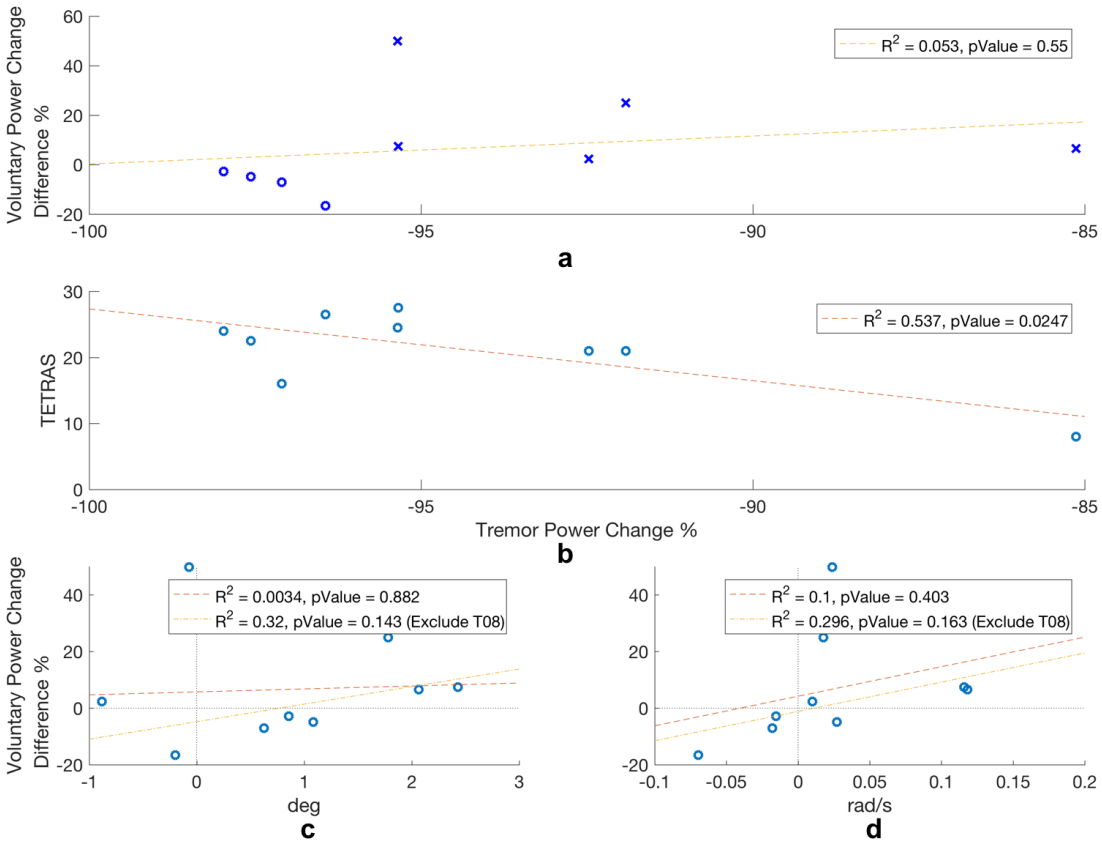

Figure 6.9 **Tremor, Voluntary and TETRAS Relations. (a) Tremor power change (reduction) vs the voluntary components power change difference (between TSO and MO). Circle and cross marker shapes indicate negative and positive voluntary power change differences, respectively. (b) Tremor power change vs tremor severity (TETRAS) for the nine participants. (c) Voluntary power change difference vs position RMSE difference (TSO-fMO). (d) Voluntary power change difference vs velocity RMSE difference (TSO-fMO).**

6.5.3. Motion Errors of Healthy Individuals

Task 3 position and velocity tracking errors for the healthy participants are shown in **Figure 6.10 a** and **b** respectively, obtained with the MO. The mean (SD) position error was 5.79 (1.2) deg. The mean (SD) velocity error was 0.373 (0.06) rad/s respectively.

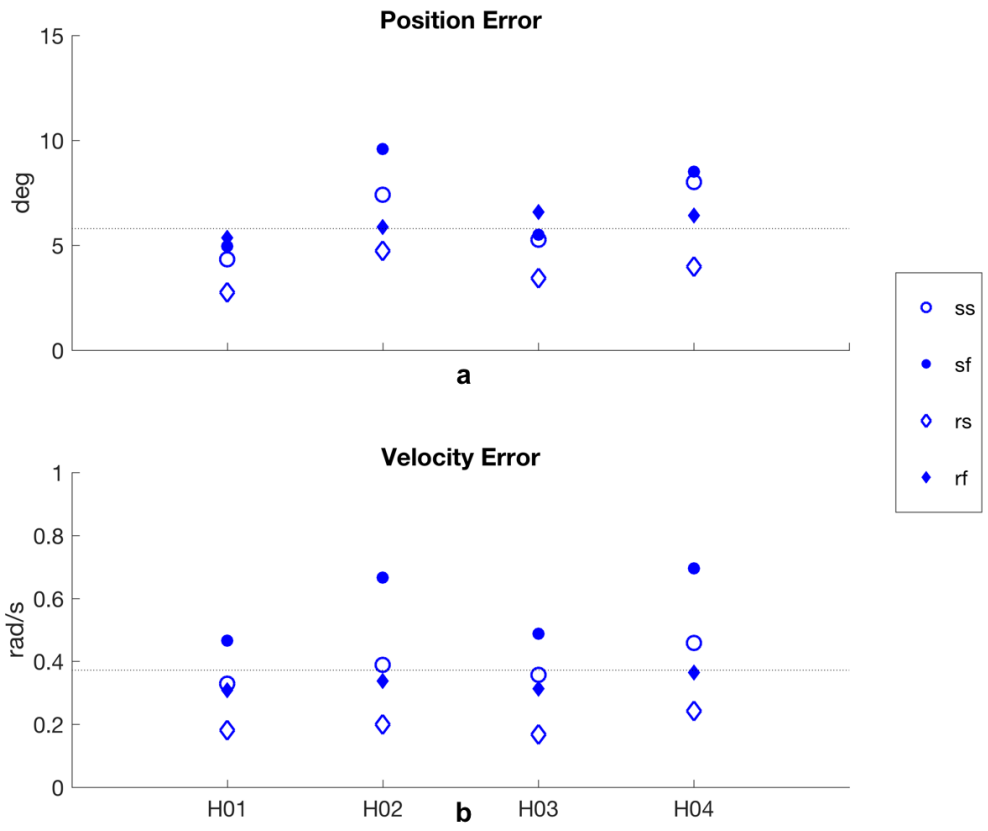

Figure 6.10 MO Voluntary motion related measures for healthy individuals. (a) Position pursuit tracking RMSE. (b) Velocity pursuit tracking RMSE. The dotted horizontal lines in a and b indicate the participants' mean. For plots a and b, the sine slow (ss), sine fast (sf), random slow (rs) and random fast (rf) motion profiles are represented with an outlined circle, a filled circle, an outlined diamond and a filled diamond shape respectively.

6.6. Discussion

We set out to demonstrate a voluntary-driven tremor suppression approach (employing a wearable technology) can effectively suppress pathological tremor while introducing little interference to the voluntary motion. The orthosis device was developed to target the elbow joint for this study. The elbow joint has been shown to be central to most activities of daily living [177], [178].

In previous chapters, the proposed tremor suppression approach and orthosis were demonstrated with an experimental setup involving a simulation of the human

input. Further improvements to the human simulating component, such as more accurate kinematics and dynamics could be made. Nevertheless, accurately emulating the human interaction, in particular someone with pathological tremor, may not be feasible. Therefore, it is reasonable to suggest that testing with tremor participants is needed in demonstrating proper operation of a suppression system. In section 5.5.2 it was pondered whether a phase difference would be observed also when testing with individuals with tremor. It is important to note that a similar phase change was not observed.

All participants in this study were right-handed. For all participants, other than T01, T07 and T08, the tremor was also more severe on the right side. All but one participant were tested on the side with the more severe tremor. The exception was T08 who was tested on the left side (and had worse tremor on the right side) due to a medical condition. It is interesting to note that in the literature there is conflicting evidence as to whether the more severe side is likely to be the dominant side [179], the non-dominant side [180], [181] or neither [49]. The reported discrepancy in the relation between severity and handedness may stem from the populations being investigated, e.g. community vs clinic-based studies, or due to the reporting method (self-report vs an objective assessment), as well as the tremor condition being investigated (PD vs ET). The adaptation of the TSO to either the left or right arm is straightforward requiring the replacement of a single component.

This study focuses primarily on the results of *Task 3*. Nevertheless, *Task 1* and *Task 2* are important as they demonstrate the TSO application to a more standard functional activity. These tasks results suggest the system could successfully suppress tremor not only in a target pursuit case, but also in a functional setting. The tremor suppression for *Task 1* and *Task 2* resulted in a mean power change (**Figure 6.5 a**) of -92.9%. Since the voluntary component of the motion was unknown, the effect to the voluntary signal power could not be evaluated.

Based on the results obtained in *Task 3*, we make several observations related to the tremor measures (**Figure 6.5 b** and **c**). There was a relatively large variation among the ET participants mean frequency (T01, T04, T05, T06, T08 and T09). Only two of the recruited participants were identified as PD (T02 and T03); therefore, it is difficult to determine if similar frequency variations would be observed among the PD

participants. The typical bandwidth for ET, however, is considered to be wider, overlapping below and above that of PD [4]. It is interesting to note that a large variance within a participant's frequency data was observed for (T01, T03, T07) as seen in **Figure 6.5 c**, of which only T01 had a confirmed diagnosis of ET. There were fewer instances of the attenuation being above -90% in the random pursuit targets (**Figure 6.5 b**). Expressed differently, there was generally more attenuation of tremor in the random target movements ($p < 0.05$). One suggested explanation may be that the uncertainty in the random target movement increased the cognitive load, perhaps activating an intention or goal-oriented component of the tremor [61] and leading to a more consistent elbow tremor, and thus, to a more evenly distributed signal power to be attenuated. Additionally, attenuation was overall higher for slower target motions ($p < 0.05$). A matching subjective observation with many of the participants was that it appeared tracking faster target motions was easier and induced less tremor. It is worth mentioning the effect of intention tremor is often seen in proximal more than in distal limb muscles [6], further corroborating the notion of intention (elbow) tremor in our testing.

Observations related to the voluntary measures in **Figure 6.8** are considered next. There were three participants (T02, T05, T08) for which the mean position RMSE improved (relative to the MO) when using the TSO and three participants (T04, T05, T06) for which the mean velocity RMSE improved (**Figure 6.8 b** and **c**). For five out of the nine participants (T02, T03, T04, T05, T09), the voluntary power change values obtained with the TSO had improved (i.e. were closer to zero) compared to the MO. Note that both the TSO and MO were measured relative to the target signal power (refer to section 6.4.1). T08 demonstrated the largest difference in the mean voluntary power change (49.88%) between the MO and the TSO. The large mean voluntary power change difference is likely related to the limited ROM the participant was achieving with the MO compared to the TSO. The difference in ROM may be due to device fitting issues. Alternatively, it may be that the TSO made it easier for this participant to reach a greater ROM due to its inherent actuation of the voluntary motion. For this participant, only two repetitions for the fast random movement were collected. The limited ROM achieved by T08 had more impact on the voluntary power change than on the tracking errors as seen in **Figure 6.8 b** and **c**. As previously mentioned in section 6.5.2, in relation to **Figure 6.8 a**, the random motion profiles were associated with larger power change values and lower tracking errors, while the opposite was observed for the

sinusoid motion profiles. The above is likely related to the lower speed of the random tasks, in comparison with the sinusoid tasks, and the gradual increase in motion range during the tasks. Likely, the random tasks required greater focus and cognitive load, as mentioned before, resulting in overall better tracking performance. As expected, the implemented admittance controller resulted in lower velocity motion profiles being associated with lower interaction torques as seen in **Figure 6.8 d**. The mean voluntary power change for the participants using the MO and TSO was approximately 4.32% and 10.96%, resulting in an increase of only 6.64%. When excluding T08, this increase is reduced to only 1.23%. As described in section 6.4, the TSO device error (e_d) can be obtained by subtracting **(49)** from **(50)**. Thus, from the results in **6.5.2**, the device position and velocity errors were $e_{dp} = 0.9$ deg and $e_{dv} = 0.02$ rad/s respectively. The full scale of the position and velocity motions performed in the tracking tasks were defined as 90 deg and 2 rad/s. Therefore, the impairment the TSO endows can be quantified by evaluating the respective RMSE increase relative to the full scale values resulting in 1% for both position and velocity errors. The statistical analysis did not demonstrate significant differences between the fMO and TSO mean tracking errors and voluntary power change. However, the rejected statistical equivalency for the fast-only motion tracking errors suggests high velocity is a dominant contributor to the overall errors. The above also highlights a potential limitation of the suppression approach and device, which should be mitigated in future work. The healthy subjects' position and velocity errors e_h are given in section **6.5.3**. Still referring to section 6.4.2, the mean position and velocity indirect tremor related errors e_{ti} can be estimated by subtracting **(51)** from **(49)**, resulting in $e_{tip} = 1.51$ deg and $e_{tiv} = 0.017$ rad/s. It is interesting to note that the resulting device position error is smaller than the indirect tremor position error. A larger sample of both healthy and tremor participants would be needed to discern with greater confidence the tracking errors as suggested in section **6.4** and estimated above.

As shown in **Figure 6.9 a**, no clear relationship was demonstrated between the power change of the tremor component and the voluntary components power change difference. However, it is interesting to note that positive voluntary power change differences tended to have lower tremor suppression values as observed by the cross markers. As noted in section 6.4, a positive difference in voluntary power change refers to an increase in the power when wearing the TSO relative to the MO. A simplified way to think of this is of having higher amplitude motions with the TSO relative to the MO.

Interestingly, a similar relation to that seen in **Figure 6.9 b** was reported in [64] and [182]. The trend observed seems to suggest the TSO effectiveness diminishes with tremor severity. Since other studies with completely different suppression systems revealed a similar trend between the tremor severity and its attenuation, it is worth considering that this relationship is independent of the suppression system. A potential limitation with regard to **Figure 6.9 b** is considered due to the TETRAS assessment performed post device testing and consequently being influenced by the testing. Performing the assessment prior to device testing may be a preferable protocol. Nevertheless, if indeed there is an effect due to fatigue and training, it may be assumed to affect all participants approximately equally. Furthermore, since this is an assistive device the assessment outcome is not crucial for the device's performance. Therefore, in this preliminary study, the implication of post testing is expected to be minor. Referring to **Figure 6.9 c** and **d**, the regression linear fit excluding participant T08 (considered as an outlier) is improved relative to the linear fit including all participants. Moreover, the linear fit excluding T08 suggests (albeit not statistically significant) that when the TSO tracking performance is equivalent to the MO, which is an ideal scenario, the voluntary power change will also show a close performance between the TSO and MO.

Pursuit tracking has been utilized by other researchers [61], [83], [91], [94]. The work by Freeman et al. also assessed the effect of the tremor suppression on the voluntary motion [91]. The voluntary amplitude reduction reported was between 0.2-32.1% for the different participants. It is expected that through practice with the TSO, the position and velocity error differences will diminish relative to the MO. Familiarity with the TSO interaction may play a part in the adaptation of the user and thus, contribute to a reduction in the voluntary tracking errors. In fact, when comparing the first and third repetition for each of the four motion cases of *Task 3* both in position and velocity (for all participants), there were 46 out of 72 instances (~64%) in which the tracking errors decreased. Instead, the tremor attenuation is expected to remain roughly unchanged or improve with increased TSO familiarity according to the relation observed in **Figure 6.9**.

Some limitations should be considered with regard to the testing protocol. Specifically, with regard to *Task 1* and *Task 2* protocol, a more rigorous and standardized approach to the design, recording and processing of functional tasks data should be considered in future work, more in line with *Task 3*. Perhaps more elaborate tasks can be considered that result in longer recording times and generate consistent

tremor. Protocol tasks should also better cater the study population by introducing activation conditions for different types of tremor. For instance, tasks designed to trigger rest tremor should be considered when PD participants are part of the study population. Tremor assessments should also cater to different tremor conditions such as PD. It should be noted, the TETRAS used in the study does not assess rest tremor. Additionally, as mentioned above, tremor assessments should be done prior to testing. Finally, a qualitative assessment should be planned and included in future work, e.g. thorough debriefing of patients. Clinicians and occupational therapists may be consulted in addressing the above points.

It should be considered that either the suppression of the tremorous movement or perturbation of the voluntary movement, due to software and hardware latencies in the orthosis response time, may elicit a stretch reflex [183], [184]. Reflex response time can take between 50-100 ms [185]. A response delay of approximately 80 ms was demonstrated in a simulation system used for validation of the suppression approach [89]. Several software related changes have been made to the system used in the participant testing as mentioned in **section 6.2.2**, which may contribute to a reduction of delay. Further delay reduction can be achieved by simply decreasing the software step time. Thus, triggering of stretch reflex may be avoided. Nevertheless, in future work the implication of stretch reflex may be explored. It is interesting to note that there is evidence of the tremor in ET at least in part being derived by reflex loops [21].

One of the potential drawbacks of the RMSE metric is that it is impacted by any phase difference between a target and a measured signal. When it is desirable to calculate errors between two signals with less emphasis on any existing phase shift, a spectral coherence can be used to calculate the frequency similarity between the signals [94]. In this study, we are interested in the error change between the two cases (without and with the TSO). Therefore, the use of RMSE is deemed suitable as a phase difference exists in both cases and thus, cancels out when compared. It is actually desirable to account for any additional phase errors that may be introduced by the TSO when compared to the MO.

A few participants commented they noticed a favourable effect of the suppression on their tremor and some expressed interest in such a device if the size and weight were reduced. Participants' comments also suggested they could "feel" the

device when performing motions. This can be interpreted as though participants felt the resistance or delay induced by the device. Acceptable fit and comfort were attained by adjusting the straps tightness according to each participant's feedback. Additional sleeved paddings were donned on the upper arm and forearm when necessary. There were no major complaints related to soft tissue contact. However, in some instances the device was readjusted on the arm mid testing due to slippage. Other studies also reported some migration of tremor to nearby joints [182]. A similar phenomenon was not observed in this study. It is interesting to note that even for participant T09, who had the mildest tremor condition (their tremor was barely visible), the proposed system successfully reduced their tremor by 85%. Therefore, the suppression system has demonstrated a significant tremor reduction for two different pathologies with a large variance in severity.

Due to looseness and play between the orthosis and the human arm as well as within the TSO mechanism, some backlash exists, which is not detected by the TSO. It is important to consider this limitation as it results in some of the tremor not being detected. It may be unreasonable to expect a complete elimination of backlash altogether in a rigid wearable device. However, modification of the system to reduce the backlash can in turn increase the signal to noise ratio and therefore lead to enhanced tremor suppression. Incidentally, backlash is not an issue with FES based solutions. Only one parameter (fundamental tremor frequency for the ABPF) required calibration in the proposed system, making the approach less sensitive to different users or neurophysiological changes – an advantage over current FES system.

6.7. Summary and Conclusion

This work aims to demonstrate the capability of a recently developed tremor suppression method and orthosis prototype, tested with participants with pathological tremor. An overall tremor reduction of more than 90% was achieved for all participants, whose tremor severity varied from 8 to 27.5 on the TETRAS performance scale. The device's effect to the voluntary motion was explicitly addressed and quantified, different from most tremor studies. The impact the TSO had on the voluntary motion was evaluated by conducting a comparison of voluntary tracking and voluntary signal power change. The TSO associated position and velocity tracking errors were only about 1 deg and 0.02 rad/s, respectively, while the participants' voluntary signal power with the TSO

increased by 6.6% relative to the MO. The demonstrated results for both the tremor and voluntary components suggest the tremor suppression approach can be beneficial for people affected by tremor.

6.8. Related Publications

A paper titled “Controlling an orthosis to follow elbow volitional movement in individuals with pathological tremor” is currently under review at the journal of Movement Disorders.

Chapter 7.

Conclusion and Future Work

7.1. Summary and Conclusion

As an isolated goal, suppressing human tremor may be perceived as a rudimentary task requiring only that the tremorous body part be constrained such that all motion is confined and absorbed. It is obvious, however, such a solution would not be adequate or desirable for individuals living with tremor. As such, the work presented in this thesis was aimed at developing a novel tremor suppression solution that not only rejects the tremor but also tracks the voluntary motion. Consequently, four objectives were defined as follows:

1. Propose a novel tremor suppression approach.
2. Validate the proposed approach via a hardware simulator.
3. Design a tremor suppression orthosis implemented with the proposed approach.
4. Test the suppression approach and orthosis on individuals with tremor.

The first objective was therefore to propose a suppression approach such that not only a substantial tremor reduction is achieved but also the impediment to the voluntary motion is quantifiably small. In **Chapter 3** the suppression approach is described in a generic and modular form such that different implementations may be feasible. The proposed approach relies on an admittance controller to track the voluntary motion and a velocity controller to reject the tremor. Implementation and controller structure are identified and suggested. Two important benefits are associated to the proposed approach; first, knowledge of the mechanical properties of the human limb interfacing with the suppression system is not required for successful tuning of the controller. Second, as discussed in section **3.4**, tremor can be sensed (and therefore attenuated) even when no existing tremor motion is allowed. Thus a lack of tremor motion is not a limitation to the approach. In fact, more tremor attenuation can lead to better SNR used in the decomposition of the voluntary and tremor components (i.e. ‘filter’ step in **Figure 3.1**).

In order to address the second objective, a suppression approach validation system was required. Subsequently, a proof-of-concept system was developed and demonstrated in **Chapter 4** that both simulates and suppresses the tremor. The two subsystems are independent such that the suppression subsystem has no prior knowledge of the tremor produced by the tremor simulation subsystem. Once the validation system hardware was designated, its stability was analyzed parametrically followed by a step response assessment of the performance. The spectral domain analysis of the results demonstrated a tremor reduction of 99.8%, while the voluntary motion change was only 0.18%. The time domain velocity error and interaction force RMS resulted in 0.57 rad/s, and 0.36 Nm respectively.

The next step, addressing the third objective, was to evaluate the performance of the suppression approach implemented with an orthosis. An elbow orthosis was subsequently developed as described in **Chapter 5**. A tremor simulation subsystem was also incorporated to validate and tune the orthosis and controller before proceeding to test with individuals with tremor. In addition to velocity, a second tremor profile was simulated based on torque. The motivation to test two different simulated inputs was to account for different scenarios when testing with individuals with tremor due to uncertainty as to how a human motion is generated. The disparities between the results from the two inputs were analysed and discussed with respect to potential implications when testing with individuals with tremor. Moreover, phase compensation methods are suggested for the torque based input. The results in the spectral domain showed reductions of 99.8% and 99.4% for the velocity and torque driven cases respectively. The voluntary motion instead was increased by 0.15% and decreased by 0.34% in the velocity and torque driven cases. In the velocity driven case, velocity tracking error and interaction force RMS were 0.31 rad/s and 0.44 Nm, respectively.

The natural evolution at this stage was to invite individuals with tremor and test the suppression approach using the developed orthosis, thus fulfilling the fourth and final objective. Several technical adaptations were made to the final systems as detailed in section **6.2.2** in order to improve performance and reliability. Nine individuals with pathological tremor were recruited with varying degrees of tremor severity. A standard tremor assessment scale was used to quantify the tremor severity. The key protocol task involved pursuit tracking with a target cursor moving on a computer screen. The participants' motion was represented with a second cursor. In the spectral domain, mean

tremor was reduced by 94.4%, while the mean intentional motion was increased by only 6.6%. Time domain mean tracking errors with both the MO and TSO were similar at 7.3 deg and 8.2 deg for the position, and 0.39 rad/s and 0.41 rad/s for the velocity. Using a non-parametric test (sign test) no statistical difference was observed between the tracking errors. The mean interaction force was 0.62 Nm. The participants' error in tracking the target was postulated to be composed of three main elements, i.e. normal human error, tremor movement disorder error, and error due the device (TSO). Recording of the pursuit tracking tasks with four healthy individuals was carried out to obtain an exploratory sense of magnitude for the error elements. In particular, the device error contribution was estimated at 0.9 deg and 0.02 rad/s for the position and velocity errors.

7.2. Thesis Scientific Contributions

The following peer reviewed contributions, related to the thesis topic, have been published or accepted for publication.

7.2.1. Refereed Journal Papers

1. Herrnstadt, G, Menon C (2016) Admittance based voluntary driven motion with speed controlled tremor rejection, IEEE/ASME Transactions on Mechatronics, DOI: 10.1109/TMECH.2016.2555811

2. Herrnstadt, G, Menon, C (2016) Voluntary-driven elbow orthosis with speed-controlled tremor suppression, Frontiers in Bioengineering and Biotechnology, Vol.4, No.29,10pp.

3. Herrnstadt G, Menon C (2013) On-off tremor suppression orthosis with electromagnetic brake, International Journal of Mechanical Engineering and Mechatronics, Vol. 1, No. 2, pp 7-14

7.2.2. Refereed Conference Papers

1. Herrnstadt, G, Menon*, C (2017) Elbow orthosis for tremor suppression – a torque based input case, 5th International Work-Conference on Bioinformatics and Biomedical Engineering, Granada, Spain. Published in Lecture Notes in Bioinformatics, Subseries of Lecture Notes in Computer Science, Springer, DOI: 10.1007/978-3-319-56148-6.

2. Sheikholeslami, S, Elnady, AM, Herrnstadt, G, and Menon C. Towards the Design of a pronation/supination orthosis for Essential Tremor

Assessment and Suppression (Wrist Supination and Pronation) The 37th Canadian Medical and Biological Engineering Conference, May 20 - 24, 2014, Vancouver, BC Canada.

7.2.3. Abstract Refereed Conference Papers

1. Herrnstadt, G, Menon, C. A tremor suppression simulation system: towards an assistive device. 24th John K. Friesen conference, 2015 Vancouver, Canada.

7.3. Other Scientific Contributions

The following peer reviewed contributions have been published or accepted for publication, however, are not considered part of the thesis.

7.3.1. Refereed Journal Papers

1. Herrnstadt, G, Alavi, N, Randhawa, B, Boyd, L, Menon, C (2015) Bimanual elbow robotic orthoses: preliminary investigations on an impairment force feedback rehabilitation method, Frontiers in Human Neuroscience, DOI: 10.3389/fnhum.2015.00169

7.3.2. Refereed Conference Papers

1. Herrnstadt, G, Alavi, N, Neva, J, Boyd, LA, Menon, C (2016) Preliminary results for a force feedback bimanual rehabilitation system, IEEE RAS/EMBS International Conference on Biomedical Robotics and Biomechatronics, Singapore.

2. Alavi, N, Herrnstadt, G, Randhawa, B, Boyd, A L, Menon C. Bimanual Elbow Exoskeleton: Force Based Protocol and Rehabilitation Quantification, 37th IEEE International Conference of the Engineering in Medicine and Biology Society, August 25 – 29, 2015, Milan, Italy

3. Webb, J, Herrnstadt, G, Xiao, ZG, and Menon, C. A portable 3D printed 2DOF arm Exoskeleton for Rehabilitation. The 37th Canadian Medical and Biological Engineering Conference, May 20 - 24, 2014, Vancouver, BC Canada.

4. Webb, J, Xiao, ZG, Aschenbrenner, KP, Herrnstadt, G, and Menon C, Towards a Portable Assistive Arm Exoskeleton for Stroke Patient Rehabilitation Controlled Through a Brain Computer Interface, IEEE International Conference on Biomedical Robotics and Biomechatronics June 24-28, 2012 Roma, Italy

7.3.3. Abstract Refereed Conference Papers

1. Herrnstadt, G, Alavi, N, Randhawa, BK, Boyd, LA, Menon, C, Bimanual elbow orthoses force feedback rehabilitation method, IEEE International Conference on Robotics and Automation May 26 - 30, 2015, Seattle, USA.

7.4. Future Work

Future research paths may involve investigating advances specific to the method proposed in this work. Alternatively, non-approach specific related modifications may be pursued.

A limitation related to the first fundamental assumption (see section 3.1.2) is identified. The more overlap there is between the tremor and voluntary frequencies, the less effective the suppression approach can be expected to be. In that case it is increasingly difficult to separate the intentional form tremor motions. Future work could explore avenues to bypass this limitation. One potential approach may involve looking at volitional and tremor motions synergies and motor primitives. It may be possible to then decompose the voluntary motion based on an activated joint space that matches either a healthy or pathological motion. A fundamental question can be directed at the second fundamental assumption in this work. Namely, whether tremor and volitional motions can be regarded as independent. Potential ways to test this assumption may involve performing voluntary movements at different velocities and looking at the tremor frequency and phase. Then, observing if any changes occur and if they correlate with the voluntary motion.

Another implicit assumption in this work involves the linear modeling of the suppression system and consequently the use of a linear controller. Similar one DOF rotational systems are often modeled linearly [186]. Nevertheless, future work should take into account the accuracy of the linearity assumption. For example, backlash may contribute to errors between the linear model and the real system. The above can be verified my simulating the model of the system and comparing its response to the hardware system for different inputs.

Since tracking of the voluntary motion is at the core of the proposed tremor suppression method, it stands to reason that obstruction to the voluntary motion should

be limited as much as possible. It is therefore desirable to provide a transparent response and interaction between the user and the system. Steps to reduce the interaction forces while maintaining or improving the tracking errors as shown in the results of **Chapter 4**, and **Chapter 5** should be taken in future work. Moreover, in **Chapter 6**, it has been shown that high velocities are a major contributor to larger forces and increased errors. A transparent system should naturally provide a low impedance to the user while avoiding an underdamped response. A combination of mechanical and software elements would likely need to be explored towards achieving such an improvement. For example, the use of a direct drive motor without gearing, and improving assembly alignment accuracy may help obtain better tracking performance. On the software side, a feedforward or controller compensation for the delay (e.g. smith predictor) can be used to reduce response delay time and thus improve transparency.

The implication of stretch reflex responses on the performance shown in Chapter **6** is not known. The aforementioned could be explored in future work. It is conceivable that improved transparency may positively affect stretch reflex responses and in so doing improve overall human-robot interaction performance.

The elbow is a relatively simple joint in the upper extremity lending itself for the development and testing of novel wearable technology. Future research can focus on developing an orthosis device for other joints of the upper limb such as wrist and shoulder. In particular, simultaneous suppression in multiple joints could be explored. The long term effects of suppressing tremor are unknown and may be an important research avenue. It is conceivable that neuroplasticity may lead to a residual tremor reduction even once the suppressive device is doffed. Alternatively, long term adaptation to the suppressive device may lead to worsening of tremor when the device is off. It is also important to consider the orthosis fit and size in future work. Further advancements considered include improving soft tissue contact to allow comfortable yet tight interface with limited slippage. The above is also linked to the backlash between the device and body part. Obviously the device size and weight plays a major factor here. Additionally, the scaling down of the device and its components could be investigated. One opportunity to simplifying the orthosis structure as well as reducing its size and weight may be via the use of alternate sensors. For instance, EMG can be used instead of a torque sensor while IMU’s can replace the encoders. A question still remains as to how

an EMG signal compares with that of a torque sensor for the differentiation of volitional and tremor motions.

It would be instructional to attempt to implement tremor suppression methods suggested by other researchers, with the TSO (e.g. [64], [68]). Such direct comparisons between leading suppression methods have not been demonstrated. Additionally, the results may uncover important information about the specific suppression approaches as well as the TSO.

A pertinent question concerning the approach proposed here is whether it is intuitive for a user to have the resulting orthosis velocity be related to the interaction torque. It is conceivable that instead a more intuitive manipulation approach may be to control the orthosis in torque/acceleration. Implementing such a solution, may also allow addressing the delay observed in the torque driven case in section **5.5.2**.

References

[1] J. Benito-León and E. D. Louis, “Essential tremor: emerging views of a common disorder.,” *Nat. Clin. Pract. Neurol.*, vol. 2, no. 12, p. 666–678; quiz 2p following 691, 2006.

[2] D. Hirtz, D. J. Thurman, K. Gwinn-Hardy, M. Mohamed, a. R. Chaudhuri, and R. Zalutsky, “How common are the ‘common’ neurologic disorders?,” *Neurology*, vol. 68, no. 5, pp. 326–337, 2007.

[3] E. D. Louis and J. J. Ferreira, “How common is the most common adult movement disorder? Update on the worldwide prevalence of essential tremor,” *Mov. Disord.*, vol. 25, no. 5, pp. 534–541, 2010.

[4] G. Deuschl, P. Bain, and M. Brin, “Consensus statement of the Movement Disorder Society on Tremor. Ad Hoc Scientific Committee.,” *Mov. Disord.*, vol. 13 Suppl 3, no. S3, pp. 2–23, Oct. 1998.

[5] A. Dalvi and A. Premkumar, “Tremor: etiology, phenomenology, and clinical features.,” *Dis. Mon.*, vol. 57, no. 3, pp. 109–26, Mar. 2011.

[6] R. J. Elble, “Tremor: clinical features, pathophysiology, and treatment.,” *Neurol. Clin.*, vol. 27, no. 3, pp. 679–95, v–vi, Aug. 2009.

[7] E. Rocon and J. Belda-Lois, “Pathological tremor management: Modelling, compensatory technology and evaluation,” *Technol. Disabil.*, vol. 16, pp. 3–18, 2004.

[8] A. R. Lanfranco, A. E. Castellanos, J. P. Desai, and W. C. Meyers, “Robotic Surgery,” *Ann. Surg.*, vol. 239, no. 1, pp. 14–21, 2004.

[9] G. T. Sung and I. S. Gill, “Robotic laparoscopic surgery: A comparison of the da Vinci and Zeus systems,” *Urology*, vol. 58, no. 6, pp. 893–898, 2001.

[10] M. Hallett, “Overview of human tremor physiology.,” *Mov. Disord.*, vol. 13 Suppl 3, pp. 43–48, 1998.

[11] R. J. Elble, “Origins of tremor.,” *Lancet*, vol. 355, no. 9210, pp. 1113–1114, 2000.

[12] D. E. Haines and E. Dietrichs, “The cerebellum – structure and connections,” in *Handbook of Clinical Neurology*, A. D. Sankara H. Subramony, Ed. Elsevier B.V., 2012, pp. 3–36.

[13] S. G. Massaquoi, “Physiology of clinical dysfunction of the cerebellum,” in *Handbook of Clinical Neurology*, A. D. Sankara H. Subramony, Ed. Elsevier B.V., 2012, pp. 37–62.

[14] P. Filip, O. V. Lungu, M.-U. Manto, and M. Bares, “Linking Essential Tremor to the Cerebellum: Physiological Evidence,” *The Cerebellum*, vol. 15, no. 6, pp. 774–780, Dec. 2016.

[15] J. Benito-Leon and A. Labiano-Fontcuberta, “Linking Essential Tremor to the Cerebellum: Clinical Evidence,” *The Cerebellum*, vol. 15, no. 3, pp. 253–262, Jun. 2016.

[16] A. Cerasa and A. Quattrone, “Linking Essential Tremor to the Cerebellum-Neuroimaging Evidence,” *Cerebellum*, vol. 15, no. 3, pp. 263–275, 2016.

[17] E. D. Louis, “Linking Essential Tremor to the Cerebellum: Neuropathological Evidence,” *Cerebellum*, vol. 15, no. 3, pp. 235–242, 2016.

[18] O. C. J. Lippold, “Physiological tremor,” *Sci. Am.*, vol. 224, no. 3, pp. 65–73, 1971.

[19] R. B. Stein and M. N. Oğuztöreli, “Tremor and other oscillations in neuromuscular systems.,” *Biol. Cybern.*, vol. 22, no. 3, pp. 147–157, 1976.

[20] V. Hömberg, H. Hefter, K. Reiners, and H. J. Freund, “Differential effects of changes in mechanical limb properties on physiological and pathological tremor.,” *J. Neurol. Neurosurg. Psychiatry*, vol. 50, no. 5, pp. 568–579, 1987.

[21] J. H. McAuley and C. D. Marsden, “Physiological and pathological tremors and rhythmic central motor control.,” *Brain*, vol. 123 (Pt 8, pp. 1545–1567, 2000.

[22] J. a. Burne, T. Blanche, and J. J. Morris, “Muscle loading as a method to isolate the underlying tremor components in essential tremor and Parkinson’s disease,” *Muscle and Nerve*, vol. 30, no. 3, pp. 347–355, 2004.

[23] R. Elble and G. Deuschl, “Milestones in tremor research,” *Movement Disorders*, vol. 26, no. 6. pp. 1096–1105, May-2011.

[24] R. J. Elble, “Characteristics of physiologic tremor in young and elderly adults,” *Clin. Neurophysiol.*, vol. 114, no. 4, pp. 624–635, Apr. 2003.

[25] E. Bizzi and V. C. K. Cheung, “The neural origin of muscle synergies,” *Front. Comput. Neurosci.*, vol. 7, no. April, pp. 1–6, 2013.

[26] M. Santello and C. E. Lang, “Are Movement Disorders and Sensorimotor Injuries Pathologic Synergies? When Normal Multi-Joint Movement Synergies Become Pathologic,” *Front. Hum. Neurosci.*, vol. 8, no. January, pp. 1–13, 2015.

[27] A. d’Avella, M. Giese, Y. P. Ivanenko, T. Schack, and T. Flash, “Editorial: Modularity in motor control: from muscle synergies to cognitive action representation,” *Front. Comput. Neurosci.*, vol. 9, no. October, pp. 1–6, 2015.

[28] S. Beck and M. Hallett, “Surround inhibition in the motor system,” *Exp. Brain Res.*, vol. 210, no. 2, pp. 165–172, 2011.

[29] A. Quartarone and M. Hallett, “Emerging concepts in the physiological basis of dystonia,” *Mov. Disord.*, vol. 28, no. 7, pp. 958–967, 2013.

[30] S. Morrison and K. M. Newell, “Postural and resting tremor in the upper limb,” *Clin. Neurophysiol.*, vol. 111, no. 4, pp. 651–663, 2000.

[31] B. Carignan, J. F. Daneault, and C. Duval, “Quantifying the importance of high frequency components on the amplitude of physiological tremor,” *Exp. Brain Res.*, vol. 202, no. 2, pp. 299–306, 2010.

[32] B. Carignan, J. F. Daneault, and C. Duval, “The organization of upper limb physiological tremor,” *Eur. J. Appl. Physiol.*, vol. 112, no. 4, pp. 1269–1284, 2012.

[33] K. T. Wyne, “A comprehensive review of tremor.,” *JAAPA*, vol. 18, no. 12, pp. 43-50-58, 2005.

[34] R. Zimmermann, G. Deuschl, A. Hornig, J. Schulte-Mönting, G. Fuchs, and C. H. Lücking, “Tremors in Parkinson’s disease: symptom analysis and rating.,” *Clin. Neuropharmacol.*, vol. 17, no. 4, pp. 303–14, Aug. 1994.

[35] T. Mds, C. G. Goetz, W. Poewe, O. Rascol, and S. Christina, “The Unified Parkinson’s Disease Rating Scale (UPDRS): Status and recommendations,” *Mov. Disord.*, vol. 18, no. 7, pp. 738–750, Jul. 2003.

[36] P. Bain, “A combined clinical and neurophysiological approach to the study of patients with tremor.,” *J. Neurol. Neurosurg. Psychiatry*, vol. 56, pp. 839–844, 1993.

[37] P. G. Bain, L. J. Findley, P. Atchison, M. Behari, M. Vidailhet, M. Gresty, J. C. Rothwell, P. D. Thompson, and C. D. Marsden, “Assessing tremor severity.,” *J. Neurol. Neurosurg. Psychiatry*, vol. 56, pp. 868–873, 1993.

[38] P. G. Bain, J. Mally, M. Gresty, and L. J. Findley, “Assessing the impact of essential tremor on upper limb function.,” *J. Neurol.*, vol. 241, no. 1, pp. 54–61, 1993.

[39] C. W. Hess and S. L. Pullman, “Tremor: clinical phenomenology and assessment techniques.,” *Tremor Other Hyperkinet. Mov. (N. Y).*, vol. 2, pp. 1–15, 2012.

[40] R. Elble, P. Bain, M. João Forjaz, D. Haubenberger, C. Testa, C. G. Goetz, A. F. G. Leentjens, P. Martinez-Martin, A. Pavy-Le Traon, B. Post, C. Sampaio, G. T. Stebbins, D. Weintraub, and A. Schrag, “Task force report: Scales for screening and evaluating tremor: Critique and recommendations,” *Mov. Disord.*, vol. 28, no. 13, pp. 1793–1800, 2013.

[41] G. K. Wenning, S. Kiechl, K. Seppi, J. Müller, B. Högl, M. Saletu, G. Rungger, A. Gasperi, J. Willeit, and W. Poewe, “Prevalence of movement disorders in men and women aged 50-89 years (Bruneck Study cohort): A population-based study,” *Lancet Neurol.*, vol. 4, no. 12, pp. 815–820, 2005.

[42] J. Shahed and J. Jankovic, “Exploring the relationship between essential tremor and Parkinson’s disease.,” *Parkinsonism Relat. Disord.*, vol. 13, no. 2, pp. 67–76, 2007.

[43] W. Tse, L. S. Libow, R. Neufeld, G. Lesser, J. Frank, S. Dolan, C. Tarshish, J. M. Gracies, C. W. Olanow, W. C. Koller, and T. D. Hälbig, “Prevalence of movement disorders in an elderly nursing home population,” *Arch. Gerontol. Geriatr.*, vol. 46, no. 3, pp. 359–366, 2008.

[44] M. T. Barbosa, P. Caramelli, M. C. Q. Cunningham, D. P. Maia, M. F. F. Lima-Costa, and F. Cardoso, “Prevalence and clinical classification of tremor in elderly-A community-based survey in Brazil,” *Mov. Disord.*, vol. 28, no. 5, pp. 640–646, 2013.

[45] E. D. Louis, “Essential Tremor,” *New England Journal of Medicine*, vol. 345, no. 12. pp. 887–891, 2001.

[46] G. Deuschl, J. Raethjen, H. Hellriegel, and R. Elble, “Treatment of patients with essential tremor.,” *Lancet. Neurol.*, vol. 10, no. 2, pp. 148–61, Feb. 2011.

[47] E. D. Louis, “Essential tremor.,” *Lancet. Neurol.*, vol. 4, no. 2, pp. 100–10, 2005.

[48] L. M. L. de Lau and M. M. B. Breteler, “Epidemiology of Parkinson’s disease.,” *Lancet. Neurol.*, vol. 5, no. June, pp. 525–535, 2006.

[49] Z. Farkas, A. Csillik, I. Szirmai, and A. Kamondi, “Asymmetry of tremor intensity and frequency in Parkinson’s disease and essential tremor,” *Park. Relat. Disord.*, vol. 12, no. 1, pp. 49–55, 2006.

[50] T. a Zesiewicz, R. Elble, E. D. Louis, R. A. Hauser, K. L. Sullivan, R. B. Dewey, W. G. Ondo, G. S. Gronseth, and W. J. Weiner, “Practice parameter: Therapies for essential tremor: Report of the quality standards subcommittee of the American Academy of Neurology,” *Neurology*, vol. 64, no. 12. pp. 2008–2020, 2005.

[51] B. J. Robottom, L. M. Shulman, and W. J. Weiner, “Drug-induced movement

disorders: Emergencies and management," *Neurol. Clin.*, vol. 30, no. 1, pp. 310–320, 2012.

[52] W. J. Elias, D. Huss, T. Voss, J. Loomba, M. Khaled, E. Zadicario, R. C. Frysinger, S. a Sperling, S. Wylie, S. J. Monteith, J. Druzgal, B. B. Shah, M. Harrison, and M. Wintermark, "A pilot study of focused ultrasound thalamotomy for essential tremor.," *N. Engl. J. Med.*, vol. 369, no. 7, pp. 640–8, Aug. 2013.

[53] K. E. Lyons, R. Pahwa, C. L. Comella, M. S. Eisa, R. J. Elble, S. Fahn, J. Jankovic, J. L. Juncos, W. C. Koller, W. G. Ondo, K. D. Sethi, M. B. Stern, C. M. Tanner, R. Tintner, and R. L. Watts, "Benefits and risks of pharmacological treatments for essential tremor," *Drug Saf.*, vol. 26, no. 7, pp. 461–481, 2003.

[54] W. S. Chang, H. H. Jung, E. J. Kweon, E. Zadicario, I. Rachmilevitch, and J. W. Chang, "Unilateral magnetic resonance guided focused ultrasound thalamotomy for essential tremor: practices and clinicoradiological outcomes," *J. Neurol. Neurosurg. Psychiatry*, vol. 86, no. 3, pp. 257–264, Mar. 2015.

[55] N. Lipsman, M. L. Schwartz, Y. Huang, L. Lee, T. Sankar, M. Chapman, K. Hynynen, and A. M. Lozano, "MR-guided focused ultrasound thalamotomy for essential tremor: A proof-of-concept study," *Lancet Neurol.*, vol. 12, no. 5, pp. 462–468, 2013.

[56] W. J. Elias, N. Lipsman, W. G. Ondo, P. Ghanouni, Y. G. Kim, W. Lee, M. Schwartz, K. Hynynen, A. M. Lozano, B. B. Shah, D. Huss, R. F. Dallapiazza, R. Gwinn, J. Witt, S. Ro, H. M. Eisenberg, P. S. Fishman, D. Gandhi, C. H. Halpern, R. Chuang, K. Butts Pauly, T. S. Tierney, M. T. Hayes, G. R. Cosgrove, T. Yamaguchi, K. Abe, T. Taira, and J. W. Chang, "A Randomized Trial of Focused Ultrasound Thalamotomy for Essential Tremor," *N. Engl. J. Med.*, vol. 375, no. 8, pp. 730–739, 2016.

[57] M. Manto, M. Topping, M. Soede, J. Sanchez-Lacuesta, W. Harwin, J. Pons, J. Williams, S. Skaarup, and L. Normie, "Dynamically responsive intervention for tremor suppression," *IEEE Eng. Med. Biol. Mag.*, vol. 22, no. 3, pp. 120–132, May 2003.

[58] E. Rocon, M. Manto, J. Pons, S. Camut, and J. M. Belda, “Mechanical suppression of essential tremor.,” *Cerebellum*, vol. 6, no. 1, pp. 73–8, Jan. 2007.

[59] J. Hendriks, M. Rosen, N. Berube, and M. Aisen, “A second-generation joystick for people disabled by tremor.,” in *RESNA 91, proceedings of the 14th Annual Conference*, 1991, pp. 248–250.

[60] M. L. Aisen, A. Arnold, I. Baiges, S. Maxwell, and M. Rosen, “The effect of mechanical damping loads on disabling action tremor.,” *Neurology*, vol. 43, no. 7, pp. 1346–50, Jul. 1993.

[61] M. J. Rosen, a S. Arnold, I. J. Baiges, M. L. Aisen, and S. R. Eglowstein, “Design of a controlled-energy-dissipation orthosis (CEDO) for functional suppression of intention tremors.,” *J. Rehabil. Res. Dev.*, vol. 32, no. 1, pp. 1–16, Feb. 1995.

[62] J. Kotovsky and M. J. Rosen, “A wearable tremor-suppression orthosis.,” *J. Rehabil. Res. Dev.*, vol. 35, no. 4, pp. 373–87, Oct. 1998.

[63] R. Loureiro, Juan M. Belda-Lois, E. R. Lima, J. L. Pons, J. J. Sanchez-Lacuesta, and W. S. Harwin, “Upper Limb Tremor Suppression in ADL Via an Orthosis Incorporating a Controllable Double Viscous Beam Actuator,” in *9th International Conference on Rehabilitation Robotics, 2005. ICORR 2005.*, 2005, pp. 119–122.

[64] E. Rocon, J. M. Belda-Lois, a F. Ruiz, M. Manto, J. C. Moreno, and J. L. Pons, “Design and validation of a rehabilitation robotic exoskeleton for tremor assessment and suppression.,” *IEEE Trans. Neural Syst. Rehabil. Eng.*, vol. 15, no. 3, pp. 367–78, Sep. 2007.

[65] T. Ando and M. Watanabe, “Myoelectric-Controlled Exoskeletal Elbow Robot to Suppress Essential Tremor: Extraction of Elbow Flexion Movement Using STFTs and TDNN,” *J. Robot. Mechatronics*, vol. 24, no. 1, pp. 141–149, Feb. 2012.

[66] E. Ohara, K. Yano, S. Horihata, T. Aoki, and Y. Nishimoto, “Tremor suppression control of Meal-Assist Robot with adaptive filter,” *2009 IEEE Int. Conf. Rehabil. Robot.*, pp. 498–503, Jun. 2009.

[67] K. Kiguchi, Y. Hayashi, and T. Asami, “An upper-limb power-assist robot with tremor suppression control,” in *2011 IEEE International Conference on Rehabilitation Robotics*, 2011, vol. 2011, pp. 1–4.

[68] B. Taheri, D. Case, and E. Richer, “Adaptive Suppression of Severe Pathological Tremor by Torque Estimation Method,” *IEEE/ASME Trans. Mechatronics*, vol. 20, no. 2, pp. 717–727, Apr. 2015.

[69] F. Widjaja, C. Y. Shee, W. T. Latt, W. L. Au, P. Poignet, and W. T. Ang, “Kalman filtering of accelerometer and electromyography (EMG) data in pathological tremor sensing system,” *2008 IEEE Int. Conf. Robot. Autom.*, pp. 3250–3255, May 2008.

[70] S. Skaarup, L. Bay, and K. West, “Polypyrrole actuators working at 2–30Hz,” *Synth. Met.*, vol. 157, no. 6–7, pp. 323–326, Apr. 2007.

[71] L. Swallow and E. Siores, “Tremor Suppression Using Smart Textile Fibre Systems,” *J. Fiber Bioeng. Informatics*, vol. 1, no. 4, pp. 261–266, Mar. 2009.

[72] D. Zhang, P. Poignet, F. Widjaja, and W. Tech Ang, “Neural oscillator based control for pathological tremor suppression via functional electrical stimulation,” *Control Eng. Pract.*, vol. 19, no. 1, pp. 74–88, 2011.

[73] L. Popović Maneski, N. Jorgovanović, V. Ilić, S. Došen, T. Keller, M. B. Popović, and D. B. Popović, “Electrical stimulation for the suppression of pathological tremor,” *Med. Biol. Eng. Comput.*, vol. 49, no. 10, pp. 1187–1193, Oct. 2011.

[74] S. Dosen, S. Muceli, J. Dideriksen, J. Romero, E. Rocon, J. Pons, and D. Farina, “Online Tremor Suppression Using Electromyography and Low Level Electrical Stimulation.,” *IEEE Trans. Neural Syst. Rehabil. Eng.*, vol. 4320, no. c, pp. 1–11, 2014.

[75] A. P. L. Bó, C. Azevedo-Coste, C. Geny, P. Poignet, and C. Fattal, “On the Use of Fixed-Intensity Functional Electrical Stimulation for Attenuating Essential Tremor,” *Artif. Organs*, vol. 38, no. 11, pp. 984–991, Nov. 2014.

[76] A. Fasano and G. Deuschl, “Therapeutic advances in tremor,” *Mov. Disord.*, vol. 30, no. 11, pp. 1557–1565, 2015.

[77] M. J. Edwards, P. Talelli, and J. C. Rothwell, “Clinical applications of transcranial magnetic stimulation in patients with movement disorders,” *Lancet Neurol.*, vol. 7, no. 9, pp. 827–840, 2008.

[78] T. Popa, M. Russo, M. Vidailhet, E. Roze, S. Lehéricy, C. Bonnet, E. Apartis, A. P. Legrand, L. Marais, S. Meunier, and C. Gallea, “Cerebellar rTMS stimulation may induce prolonged clinical benefits in essential tremor, and subjacent changes in functional connectivity: An open label trial,” *Brain Stimul.*, vol. 6, no. 2, pp. 175–179, 2013.

[79] M. Picillo, E. Moro, M. Edwards, V. Di Lazzaro, A. M. Lozano, and A. Fasano, “Subdural continuous theta burst stimulation of the motor cortex in essential tremor,” *Brain Stimul.*, vol. 8, no. 4, pp. 840–842, 2015.

[80] J.-P. Lefaucheur, A. Antal, S. S. Ayache, D. H. Benninger, J. Brunelin, F. Cogiamanian, M. Cotelli, D. De Ridder, R. Ferrucci, B. Langguth, P. Marangolo, V. Mylius, M. A. Nitsche, F. Padberg, U. Palm, E. Poulet, A. Priori, S. Rossi, M. Schecklmann, S. Vanneste, U. Ziemann, L. Garcia-Larrea, and W. Paulus, “Evidence-based guidelines on the therapeutic use of transcranial direct current stimulation (tDCS),” *Clin. Neurophysiol.*, vol. 128, no. 1, pp. 56–92, 2017.

[81] A. Gironell, S. Martínez-Horta, S. Aguilar, V. Torres, J. Pagonabarraga, B. Pascual-Sedano, and R. Ribosa-Nogué, “Transcranial direct current stimulation of the cerebellum in essential tremor: A controlled study,” *Brain Stimul.*, vol. 7, no. 3, pp. 491–492, 2014.

[82] J. S. Brittain, P. Probert-Smith, T. Z. Aziz, and P. Brown, “Tremor suppression by rhythmic transcranial current stimulation,” *Curr. Biol.*, vol. 23, no. 5, pp. 436–440, 2013.

[83] S. Pledgie, K. E. Barner, S. K. Agrawal, and T. Rahman, “Tremor suppression through impedance control.,” *IEEE Trans. Rehabil. Eng.*, vol. 8, no. 1, pp. 53–9,

Mar. 2000.

[84] B. Taheri, D. Case, and E. Richer, “Active Tremor Estimation and Suppression in Human Elbow Joint,” in *ASME 2011 Dynamic Systems and Control Conference and Bath/ASME Symposium on Fluid Power and Motion Control, Volume 2*, 2011, pp. 115–120.

[85] N. Hogan, “Impedance Control: An Approach to Manipulation: Parts I, II and III,” *J. Dyn. Syst. Meas. Control*, vol. 107, no. 1, p. 8, 1985.

[86] S. M. Hashemi, M. F. Golnaraghi, and A. E. Patla, “Tuned vibration absorber for suppression of rest tremor in Parkinson’s disease,” *Med. Biol. Eng. Comput.*, vol. 42, no. 1, pp. 61–70, Jan. 2004.

[87] B. Taheri, D. Case, and E. Richer, “Design and Development of a Human Arm Joint Simulator for Evaluation of Active Assistive Devices Control Algorithms,” in *Volume 1: Adaptive Control; Advanced Vehicle Propulsion Systems; Aerospace Systems; Autonomous Systems; Battery Modeling; Biochemical Systems; Control Over Networks; Control Systems Design; Cooperativ*, 2012, pp. 707–714.

[88] J. Chuanasa and S. Songschon, “Essential tremor suppression by a novel self-balancing device.,” *Prosthet. Orthot. Int.*, vol. 39, no. 3, pp. 219–25, Jun. 2014.

[89] G. Herrnstadt and C. Menon, “Admittance based voluntary driven motion with speed controlled tremor rejection,” *IEEE/ASME Trans. Mechatronics*, pp. 1–1, 2016.

[90] E. H. Copur, C. Freeman, B. Chu, and D. S. Laila, “FES based tremor suppression using repetitive control,” in *2015 54th IEEE Conference on Decision and Control (CDC)*, 2015, no. Cdc, pp. 6023–6028.

[91] C. T. Freeman, P. Sampson, J. H. Burridge, and A.-M. Hughes, “Repetitive control of functional electrical stimulation for induced tremor suppression,” *Mechatronics*, vol. 32, pp. 79–87, 2015.

[92] C. N. Riviere and N. V. Thakor, “Modeling and canceling tremor in human-

machine interfaces," *IEEE Eng. Med. Biol. Mag.*, vol. 15, no. 3, pp. 29–36, 1996.

[93] C. N. Riviere, R. S. Rader, and N. V Thakor, "Adaptive canceling of physiological tremor for improved precision in microsurgery.," *IEEE Trans. Biomed. Eng.*, vol. 45, no. 7, pp. 839–46, Jul. 1998.

[94] J. G. Gonzalez, E. a. Heredia, T. Rahman, K. E. Barner, and G. R. Arce, "Optimal digital filtering for tremor suppression," *IEEE Trans. Biomed. Eng.*, vol. 47, no. 5, pp. 664–673, 2000.

[95] J. Michaelis, "Introducing the neater eater.," *Action Res*, vol. 6, no. 1, pp. 2–3, 1988.

[96] N. Hogan, H. I. Krebs, J. Charnnarong, P. Srikrishna, and a Sharon, "MIT - MANUS : A Workstation for Manual Therapy and Training," *IEEE Int. Work. Robot Hum. Commun.*, pp. 161–165, 1992.

[97] M. Topping, "An overview of the development of handy 1, a rehabilitation robot to assist the severely disabled," *J. Intell. Robot. Syst. Theory Appl.*, vol. 34, pp. 253–263, 2002.

[98] M. Hillman, "2 Rehabilitation Robotics from Past to Present – A Historical Perspective," *Rehabilitation*, pp. 25–44, 2004.

[99] R. Soyama, S. Ishii, and A. Fukase, "Selectable Operating Interfaces of the Meal-Assistance Device ``My Spoon''," *Rehabilitation*, pp. 155–163, 2004.

[100] K. Yano, K. Nishiwaki, and S. Hiramatsu, "Tremor suppression control for a meal-assist robot," in *Lecture Notes in Computer Science (including subseries Lecture Notes in Artificial Intelligence and Lecture Notes in Bioinformatics)*, 2010, vol. 6191 LNCS, no. PART 1, pp. 354–359.

[101] A. Kumar and M. F. Phillips, "Use of powered mobile arm supports by people with neuromuscular conditions.," *J. Rehabil. Res. Dev.*, vol. 50, no. 1, pp. 61–70, 2013.

[102] A. Pathak, J. a. Redmond, M. Allen, and K. L. Chou, "A noninvasive handheld

assistive device to accommodate essential tremor: A pilot study," *Mov. Disord.*, vol. 29, no. 6, pp. 838–842, 2014.

[103] "READI-STEADI® ANTI-TREMOR ORTHOTIC GLOVE SYSTEM." [Online]. Available: https://www.readi-steadi.com/.

[104] "GyroGlove." [Online]. Available: https://gyrogear.co/.

[105] P. Artemiadis, *Neuro-Robotics*, vol. 2. Dordrecht: Springer Netherlands, 2014.

[106] R. J. L. M. Verstappen, C. T. Freeman, E. Rogers, T. Sampson, and J. H. Burridge, "Robust higher order repetitive control applied to human tremor suppression," *2012 IEEE Int. Symp. Intell. Control*, pp. 1214–1219, Oct. 2012.

[107] B. Taheri, D. Case, and E. Richer, "Robust controller for tremor suppression at musculoskeletal level in human wrist.," *IEEE Trans. Neural Syst. Rehabil. Eng.*, vol. 22, no. 2, pp. 379–88, Mar. 2014.

[108] K. C. C. Veluvolu, W. T. T. Latt, and W. T. T. Ang, "Double adaptive bandlimited multiple Fourier linear combiner for real-time estimation/filtering of physiological tremor," *Biomed. Signal Process. Control*, vol. 5, no. 1, pp. 37–44, 2010.

[109] S. Wang, Y. Gao, J. Zhao, and H. Cai, "Adaptive sliding bandlimited multiple fourier linear combiner for estimation of pathological tremor," *Biomed. Signal Process. Control*, vol. 10, no. 1, pp. 260–274, 2014.

[110] L. Z. Popović, T. B. Sekara, and M. B. Popović, "Adaptive band-pass filter (ABPF) for tremor extraction from inertial sensor data.," *Comput. Methods Programs Biomed.*, vol. 99, no. 3, pp. 298–305, Sep. 2010.

[111] R. E. Kalman and R. S. Bucy, "New Results in Linear Filtering and Prediction Theory," *J. Basic Eng.*, vol. 83, no. 1, p. 95, 1961.

[112] E. Rocon and J. L. Pons, *Exoskeletons in Rehabilitation Robotics*, vol. 69. Springer Berlin Heidelberg, 2011.

[113] E. Brookner, *Tracking and Kalman Filtering Made Easy*, vol. 1. New York, USA: John Wiley & Sons, Inc., 1998.

[114] K. C. Veluvolu and W. T. Ang, “Estimation of physiological tremor from accelerometers for real-time applications.,” *Sensors (Basel).*, vol. 11, no. 3, pp. 3020–36, Jan. 2011.

[115] A. P. L. Bó, P. Poignet, and C. Geny, “Pathological tremor and voluntary motion modeling and online estimation for active compensation,” *IEEE Trans. Neural Syst. Rehabil. Eng.*, vol. 19, no. 2, pp. 177–185, 2011.

[116] S. Tatinati, K. C. Veluvolu, S. M. Hong, W. T. Latt, and W. T. Ang, “Physiological tremor estimation with autoregressive (AR) model and kalman filter for robotics applications,” *IEEE Sens. J.*, vol. 13, no. 12, pp. 4977–4985, 2013.

[117] G. Zeng and A. Hemami, “An overview of robot force control,” *Robotica*, vol. 15, no. 5, pp. 473–482, 1997.

[118] S. Chiaverini and L. Sciavicco, “The Parallel Approach to Force/Position Control of Robotic Manipulators,” *IEEE Trans. Robot. Autom.*, vol. 9, no. 4, pp. 361–373, 1993.

[119] T. Yoshikawa, “Force control of robot manipulators,” *Proc. 2000 ICRA Millenn. Conf. IEEE Int. Conf. Robot. Autom. Symp. Proc. Cat No00CH37065*, vol. 1, no. April, pp. 220–226, 2000.

[120] A. Gupta, M. K. O’Malley, V. Patoglu, and C. Burgar, “Design, Control and Performance of *RiceWrist:* A Force Feedback Wrist Exoskeleton for Rehabilitation and Training,” *Int. J. Rob. Res.*, vol. 27, no. 2, pp. 233–251, 2008.

[121] P. R. Culmer, A. E. Jackson, S. Makower, R. Richardson, J. A. Cozens, M. C. Levesley, and B. B. Bhakta, “A control strategy for upper limb robotic rehabilitation with a dual robot system,” *IEEE/ASME Trans. Mechatronics*, vol. 15, no. 4, pp. 575–585, 2010.

[122] W. Meng, Q. Liu, Z. Zhou, Q. Ai, B. Sheng, and S. S. Xie, “Recent development of

mechanisms and control strategies for robot-assisted lower limb rehabilitation," *Mechatronics*, vol. 31, pp. 132–145, 2015.

[123] C. Ott, R. Mukherjee, and Y. Nakamura, "A Hybrid System Framework for Unified Impedance and Admittance Control," *J. Intell. Robot. Syst. Theory Appl.*, vol. 78, no. 3–4, pp. 359–375, 2015.

[124] R. Volpe and P. Khosla, "A theoretical and experimental investigation of explicit force control strategies for manipulators," *IEEE Trans. Automat. Contr.*, vol. 38, no. 11, pp. 1634–1650, 1993.

[125] J. De Schutter, H. Bruyninckx, W.-H. Zhu, and W. Mark, "Force control: a bird's eye view," *Lect. Notes Control Inf. Sci.*, vol. 230, pp. 1–17, 1998.

[126] G. C. Joyce and P. M. Rack, "The effects of load and force on tremor at the normal human elbow joint.," *J. Physiol.*, vol. 240, no. 2, pp. 375–396, 1974.

[127] P. M. Rack and H. F. Ross, "The role of reflexes in the resting tremor of Parkinson's disease.," *Brain*, vol. 109 (Pt 1, pp. 115–141, 1986.

[128] M. E. Héroux, G. Pari, and K. E. Norman, "The effect of inertial loading on wrist postural tremor in essential tremor," *Clin. Neurophysiol.*, vol. 120, no. 5, pp. 1020–1029, 2009.

[129] J. Buchli, F. Stulp, E. Theodorou, and S. Schaal, "Learning variable impedance control," *Int. J. Rob. Res.*, vol. 30, no. 7, pp. 820–833, 2011.

[130] S. Hussain, S. Q. Xie, and P. K. Jamwal, "Adaptive impedance control of a robotic orthosis for gait rehabilitation.," *IEEE Trans. Cybern.*, vol. 43, no. 3, pp. 1025–34, 2013.

[131] E. Perreault, L. Hargrove, D. Ludvig, H. Lee, and J. Sensinger, *Neuro-Robotics*, vol. 2. Dordrecht: Springer Netherlands, 2014.

[132] M. J. Roberts, *Signals and Systems - Analysis using Transform Methods and MATLAB, 2nd_edition,* 1st ed. Boston: McGraw-Hill, 2004.

[133] K. a Mann, F. W. Werner, and a K. Palmer, “Frequency spectrum analysis of wrist motion for activities of daily living.,” *J. Orthop. Res.*, vol. 7, no. 2, pp. 304–306, 1989.

[134] V. Duchaine, B. Mayer St.-Onge, and C. Gosselin, “Stable and Intuitive Control of an Intelligent Assist Device,” *IEEE Trans. Haptics*, vol. 5, no. 2, pp. 148–159, Apr. 2012.

[135] D. A. Lawrence, “Stability and transparency in bilateral teleoperation,” *IEEE Trans. Robot. Autom.*, vol. 9, no. 5, pp. 624–637, 1993.

[136] S. E. Salcudean, “Transparent Bilateral Teleoperation under Position and Rate Control,” *The International Journal of Robotics Research*, vol. 19, no. 12. pp. 1185–1202, 01-Dec-2000.

[137] Wen Yu, J. Rosen, and Xiaoou Li, “PID admittance control for an upper limb exoskeleton,” in *Proceedings of the 2011 American Control Conference*, 2011, pp. 1124–1129.

[138] F. L. Lewis, L. Xie, and D. Popa, *Optimal and robust estimation: with an introduction to stochastic control theory*. Boca Raton: CRC Press, 2008.

[139] A. H. Sayed, *Adaptive Filters*. Hoboken, NJ, USA: John Wiley & Sons, Inc., 2008.

[140] C. N. Riviere, S. G. Reich, and N. V Thakor, “Adaptive Fourier modeling for quantification of tremor.,” *J. Neurosci. Methods*, vol. 74, no. 1, pp. 77–87, Jun. 1997.

[141] H. Asaka, Kinji, Okuzaki, *Soft Actuators*. Tokyo: Springer Japan, 2014.

[142] Norman S. Nise, *Control Systems Engineering*. 2010.

[143] A. B. Corripio, *Tuning of Industrial Control Systems*. NC, USA: ISA—The Instrumentation, Systems, and Automation Society, 2001.

[144] N. S. Nise, *Control Systems Engineering*, 6th ed. Hoboken, NJ, USA: John Wiley

& Sons, Inc., 2010.

[145] I. S. MacKenzie and C. Ware, “Lag as a determinant of human performance in interactive systems,” *Proc. SIGCHI Conf. Hum. factors Comput. Syst. - CHI ’93*, pp. 488–493, 1993.

[146] M. D. Fabrizio, B. R. Lee, D. Y. Chan, D. Stoianovici, T. W. Jarrett, C. Yang, and L. R. Kavoussi, “Effect of time delay on surgical performance during telesurgical manipulation.,” *J. Endourol.*, vol. 14, no. 2, pp. 133–8, Mar. 2000.

[147] K. Englehart and B. Hudgins, “A robust, real-time control scheme for multifunction myoelectric control,” *IEEE Trans. Biomed. Eng.*, vol. 50, no. 7, pp. 848–54, 2003.

[148] T. R. Farrell and R. F. Weir, “The optimal controller delay for myoelectric prostheses,” *IEEE Trans. Neural Syst. Rehabil. Eng.*, vol. 15, no. 1, pp. 111–118, 2007.

[149] N. Gordon, D. Salmond, and A. Smith, “Novel approch to nonlinear/non-Gaussian Bayessian state estimate,” *IEE Proc. F (Radar Signal …*, vol. 140, pp. 107–113, 1993.

[150] L. H. Smith, L. J. Hargrove, B. A. Lock, and T. A. Kuiken, “Determining the Optimal Window Length for Pattern Recognition-Based Myoelectric Control,” *Neural Syst. Rehabil. Eng. {IEEE} Trans.*, vol. 19, no. 2, pp. 186–192, 2011.

[151] J. Y. C. Chen, E. C. Haas, and M. J. Barnes, “Human performance issues and user interface design for teleoperated robots,” *Syst. Man, Cybern. Part C Appl. Rev. IEEE Trans.*, vol. 37, no. 6, pp. 1231–1245, 2007.

[152] J. Timmer, S. Haussler, M. Lauk, and C.-H. Lucking, “Pathological tremors: Deterministic chaos or nonlinear stochastic oscillators?,” *Chaos*, vol. 10, no. 1, pp. 278–288, Mar. 2000.

[153] J. Rosen, J. C. Perry, N. Manning, S. Burns, and B. Hannaford, “The human arm kinematics and dynamics during daily activities - toward a 7 DOF upper limb powered exoskeleton,” *ICAR ’05. Proceedings., 12th Int. Conf. Adv. Robot. 2005.*,

pp. 532–539, 2005.

[154] F. Rahimi, Q. J. Almeida, D. Wang, and F. Janabi-Sharifi, “Tremor suppression orthoses for Parkinson’s patients: A frequency range perspective,” in *Proceedings of the 31st Annual International Conference of the IEEE Engineering in Medicine and Biology Society: Engineering the Future of Biomedicine, EMBC 2009*, 2009, pp. 1565–1568.

[155] N. Vitiello and T. Lenzi, “NEUROExos: A powered elbow exoskeleton for physical rehabilitation,” *Robot. IEEE …*, vol. 29, no. 1, pp. 220–235, 2013.

[156] C. Canudas de Wit, H. Olsson, K. J. Astrom, and P. Lischinsky, “A new model for control of systems with friction,” *IEEE Trans. Automat. Contr.*, vol. 40, no. 3, pp. 419–425, Mar. 1995.

[157] K. Menon and K. Krishnamurthy, “Control of low velocity friction and gear backlash in a machine tool feed drive system,” *Mechatronics*, vol. 9, no. 1, pp. 33–52, 1999.

[158] M. R. Kermani, R. V. Patel, and M. Moallem, “Friction identification and compensation in robotic manipulators,” *IEEE Trans. Instrum. Meas.*, vol. 56, no. 6, pp. 2346–2353, 2007.

[159] B. Armstrong-Hélouvry, P. Dupont, and C. C. De Wit, “A survey of models, analysis tools and compensation methods for the control of machines with friction,” *Automatica*, vol. 30, no. 7, pp. 1083–1138, Jul. 1994.

[160] B. Siciliano, L. Sciavicco, L. Villani, and G. Oriolo, *Robotics*. London: Springer London, 2009.

[161] G. Herrnstadt and C. Menon, “On-Off Tremor Suppression Orthosis with Electromagnetic Brake,” *Int. J. Mech. Eng. Mechatronics*, vol. 1, no. 2, 2013.

[162] G. Herrnstadt and C. Menon, “Voluntary-Driven Elbow Orthosis with Speed-Controlled Tremor Suppression,” *Front. Bioeng. Biotechnol.*, vol. 4, no. March, pp. 1–10, 2016.

[163] J. a. Gallego, E. Rocon, J. O. Roa, J. C. Moreno, a. D. Koutsou, and J. L. Pons, “On the use of inertial measurement units for real-time quantification of pathological tremor amplitude and frequency,” *Procedia Chem.*, vol. 1, no. 1, pp. 1219–1222, Sep. 2009.

[164] E. W. Kamen and J. K. Su, “Kalman Filter Applications,” 1999, pp. 225–267.

[165] K. T. Wyne, “A comprehensive review of tremor,” *J. Am. Acad. Physician Assist.*, vol. 18, no. 12, pp. 43–50, Dec. 2005.

[166] Le Tien Dung, Hee-Jun Kang, and Young-Shick Ro, “Robot manipulator modeling in Matlab-SimMechanics with PD control and online gravity compensation,” in *International Forum on Strategic Technology 2010*, 2010, no. 1, pp. 446–449.

[167] A. Gupta and M. O’Malley, “Design of a haptic arm exoskeleton for training and rehabilitation,” *Mechatronics, IEEE/ASME …*, vol. 11, no. 3, pp. 280–289, 2006.

[168] K. H. Ang, G. Chong, and Y. Li, “PID control system analysis, design, and technology,” *IEEE Trans. Control Syst. Technol.*, vol. 13, no. 4, pp. 559–576, 2005.

[169] G. Herrnstadt and C. Menon, “Elbow Orthosis for Tremor Suppression - A Torque Based Input Case,” in *Lecture Notes in Computer Science*, Springer, 2017, pp. 292–302.

[170] W. Mugge, J. Schuurmans, A. C. Schouten, and F. C. T. van der Helm, “Sensory Weighting of Force and Position Feedback in Human Motor Control Tasks,” *J. Neurosci.*, vol. 29, no. 17, pp. 5476–5482, 2009.

[171] R. Shadmehr, M. a Smith, and J. W. Krakauer, “Error correction, sensory prediction, and adaptation in motor control.,” *Annu. Rev. Neurosci.*, vol. 33, pp. 89–108, 2010.

[172] C. G. Atkeson and J. M. Hollerbach, “Kinematic Features of Unrestrained Vertical Arm Movements,” *J. Neurosci.*, vol. 5, no. 9, pp. 2318–2330, 1985.

[173] U. Rokni and H. Sompolinsky, “How the Brain Generates Movement,” *Neural Comput.*, vol. 24, no. 2, pp. 289–331, 2012.

[174] R. Elble, “The essential tremor rating assessment scale,” *J. Neurol. Neuromedicine*, pp. 34–38, 2016.

[175] E. D. Louis and M. S. Okun, “It is time to remove the ‘benign’ from the essential tremor label,” *Park. Relat. Disord.*, vol. 17, no. 7, pp. 516–520, 2011.

[176] E. Whitley and J. Ball, “Statistics review 6: Nonparametric methods,” *Crit. Care*, vol. 6, no. 6, p. 509, Dec. 2002.

[177] B. F. Morrey, L. J. Askew, and E. Y. Chao, “A biomechanical study of normal functional elbow motion.,” *J. Bone Joint Surg. Am.*, vol. 63, no. 6, pp. 872–877, 1981.

[178] J. Aizawa, T. Masuda, T. Koyama, K. Nakamaru, K. Isozaki, A. Okawa, and S. Morita, “Three-dimensional motion of the upper extremity joints during various activities of daily living,” *J. Biomech.*, vol. 43, no. 15, pp. 2915–2922, 2010.

[179] N. Biary and W. Koller, “Handedness and essential tremor.,” *Arch. Neurol.*, vol. 42, no. 11, pp. 1082–3, 1985.

[180] A. Machowska-Majchrzak, K. Pierzchała, S. Pietraszek, and B. Łabuz-Roszak, “Essential tremor – assessment of tremor accelerometric parameters’ symmetry and the relationship between hand dominance and severity of tremor,” *Neurol. Neurochir. Pol.*, vol. 45, no. 2, pp. 121–127, May 2011.

[181] E. D. Louis, K. J. Wendt, S. L. Pullman, and B. Ford, “Is Essential Tremor Symmetric?,” *Arch. Neurol.*, vol. 55, no. 12, p. 1553, 1998.

[182] J. Á. Gallego, E. Rocon, J. M. Belda-Lois, and J. L. Pons, “A neuroprosthesis for tremor management through the control of muscle co-contraction.,” *J. Neuroeng. Rehabil.*, vol. 10, no. 36, pp. 1–13, 2013.

[183] K. Darton, O. C. Lippold, M. Shahani, and U. Shahani, “Long-latency spinal

reflexes in humans," *J. Neurophysiol.*, vol. 53, no. 6, pp. 1604–1618, 1985.

[184] K. Nakazawa, S. I. Yamamoto, and H. Yano, "Short- and long-latency reflex responses during different motor tasks in elbow flexor muscles," *Exp. Brain Res.*, vol. 116, no. 1, pp. 20–28, 1997.

[185] J. Ramos, A. Wang, and S. Kim, "A Balance Feedback Human Machine Interface for humanoid teleoperation in dynamic tasks," in *2015 IEEE/RSJ International Conference on Intelligent Robots and Systems (IROS)*, 2015, pp. 4229–4235.

[186] S. Zak, *Systems and control*. New York: Oxford University Press, 2003.